Aus dem Zentrum für Medizinische Forschung
der Medizinischen Fakultät Mannheim
Direktor: Prof. Dr. med. Norbert Gretz
(Aufgelöst zum 16.04.2020)

Development of a new device to measure different aspects of kidney function

Inauguraldissertation
zur Erlangung des akademischen Grades
Doctor scientiarum humanarum (Dr. sc. hum)
der
Medizinischen Fakultät Mannheim
der Ruprecht-Karls-Universität
zu
Heidelberg

vorgelegt von
Mohammed Mohiuddin Yusuf
aus
Indien
2024

Dekan: Prof. Dr. med. Sergij Goerdt

Referentin: Prof. Dr. rer. nat. Karen Bieback

TABLE OF CONTENTS

ABBREVIATIONS

ADC	Analog to Digital Converter
AKI	Acute Kidney Injury
BW	Body Weight
CKD	Chronic Kidney Disease
FITC-S	Fluorescein Isothiocyanate Sinistrin
GFR	Glomerular Filtration Rate
IR	Infra-Red
LED	Light Emitting Diode
MRI	Magnetic Resonance Imaging
NIR	Near Infra-Red
PD	Photodiode
USB	Universal Serial Bus

1 INTRODUCTION

Kidneys play a crucial role in balancing the homeostasis of the body by filtering blood and regulating various electrolytes. Glomerular Filtration Rate (GFR), secretion, and reabsorption are key parameters that reflect the kidney's functional status [1]. Particularly GFR is a crucial indicator of renal function, representing the rate at which plasma is filtered by the glomeruli in the kidneys. Measuring GFR accurately is essential for diagnosing and monitoring various kidney disorders, such as CKD (Chronic Kidney Disease) and AKI (Acute Kidney Injury).

Conventional GFR assessment methods are accurate but invasive and extensively time consuming [2]. Researchers have explored various non-invasive transcutaneous methods for kidney function measurement (see section 1.2). This thesis proposes the design and the functionality of a novel transcutaneous device to measure GFR, secretion and reabsorption, offering a safer and comparatively more convenient approach to assess renal function. Among the miniaturized transcutaneous devices that are available for various physiological applications, it is observed that the reliability of the recorded signal relies on the layout of the various light sources and detectors [3].

Such use of LEDs as light sources and a photodiode as detector is a very common design choice for over the skin sensors, for instance in oximeters as they detect the haemoglobin in the blood by illuminating it eventually detecting the reflected light after absorption [4]. In case of GFR estimation, the biomarker absorbs the LED illuminations and emits light which the sensor detects. Similarly, in oximeters the haemoglobin absorbs a percentage of light depending on the oxygen content, and the remaining light is detected by the photodiode. Hence, the principle of sensing and detection is essentially the same for such devices.

1.1 The kidney anatomy and functions

The kidneys are the two vital organs (shaped like ‘beans’) located in the back of the abdomen [5, 6]. They are crucial in filtering waste and maintaining homeostasis in the

body. The kidneys are responsible for filtering the blood to remove toxins and waste products from the body, controlling the body's balance of electrolytes, regulating blood pressure, and producing hormones that help maintain the production of blood. A large quantity of blood is filtered by the kidneys which has been calculated to constitute around 20% of the total cardiac output [7]. Kidney dysfunction can lead to a variety of health problems, including electrolyte imbalances, hypertension, fluid overload, and eventual organ failure.

As shown in Figure 1, each kidney contains an outer layer called the renal cortex, and an inner renal medulla [5]. The renal cortex is composed of glomeruli, which are small clusters of capillaries that filter blood, and tubules, which are tiny tubes that help regulate the body's water balance and excrete waste products.

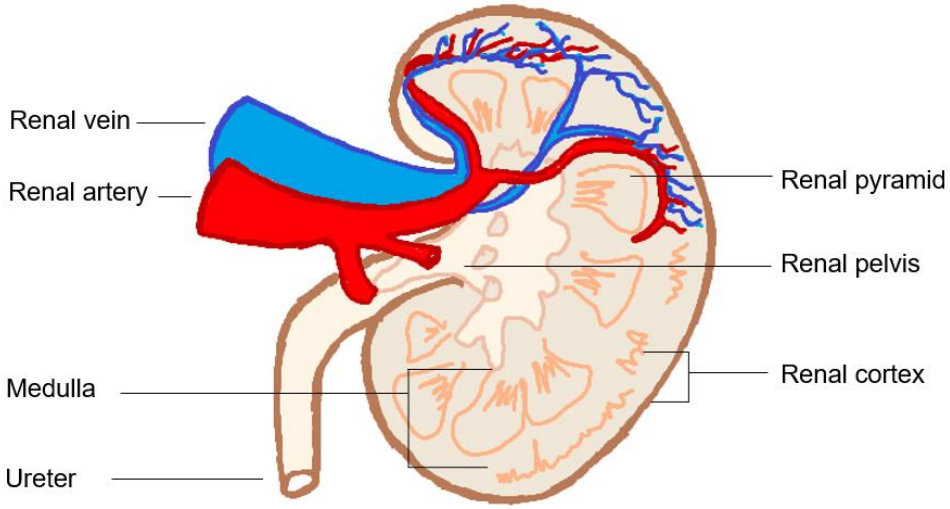

Figure 1: Parts of a kidney

(modification of figure from course 'Biology' at OpenStax [8])

The renal medulla is composed of pyramid-shaped regions called renal pyramids, which are made up of tubules and blood vessels that help filter and reabsorb substances from the blood. Since the filtration of the blood happens in the kidneys, the kidney comprises of a complex arrangement of arteries and veins which are responsible for transport of blood to and from the kidneys. The kidneys ensure that the body

can rid itself of toxins and waste, regulate water balance and electrolytes, and produce hormones that help control blood pressure and other body vitals [9].

Nephrons are the functional units of the kidney [10, 11]. Each nephron consists of a filtering unit that cleanses the blood and reabsorbs useful substances, and a tubule that produces urine. Nephrons are highly specialized structures that filter the blood and regulate the body's water balance, electrolyte balance, and acid-base balance. They are also responsible for removing toxins, drugs, and other potentially harmful substances. It is comprised of a renal corpuscle, tubule, and collecting duct (Figure 2) (modification of figure from course 'Biology' at OpenStax [8]). Typically, a mouse kidney consists of nephrons on the order of 12 to 16 thousand [12].

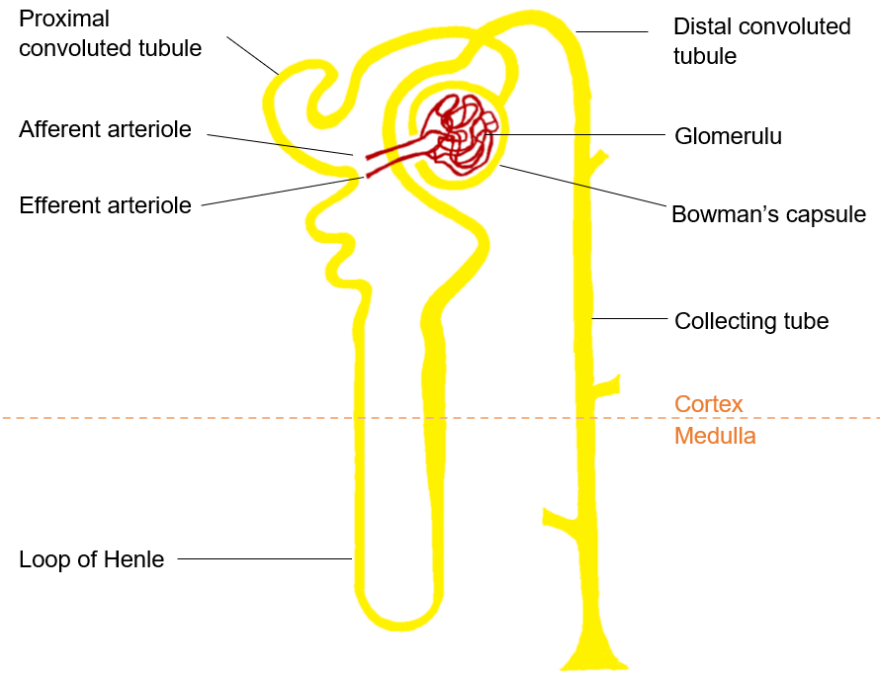

Figure 2: Typical structure of a nephron

(modification of figure from course 'Biology' at OpenStax [8])

The renal corpuscle is a combination of a glomerulus, a collection of capillaries, and a Bowman's capsule, a cup-shaped structure that encases the glomerulus. The glomerulus filters the blood and forms the primary urine, which is then captured by the Bowman's capsule. This is where the glomerular filtration process starts.

Glomerular Filtration Rate:

The glomerular filtration is a process by which fluid and solutes are filtered from the bloodstream and then passed into the urinary system. It is arguably the primary function that determines the overall health of a kidney [13, 14]. The glomerular filtration process begins with the glomerulus, which is a network of capillaries in the kidneys. Blood is pumped into the glomerulus and then filtered. The filtration process involves a semi permeable membrane which allows small molecules and fluids to be passed through while larger molecules and cells are retained. This is a passive process where the fluids and solutes are passed through by the hydrostatic pressure without requirement of any energy [15]. The filtered fluid is then passed into the renal tubes where it is further processed and then finally passed into the urinary system. Glomerular filtration is an important process that helps to maintain a balance of fluids in the body. It also helps to remove toxins and waste products from the blood stream and prevent them from damaging other organs. Additionally, the glomerular filtration process plays an important role in maintaining the correct levels of electrolytes and other important substances in the body.

The parameter to assess kidney functionality is to determine/estimate the glomerular filtration rate. The GFR is considered as a primary indicator of kidney health and is used to grade the progression of chronic kidney disease (CKD) as well as for dosing strategies in treatment procedures [16, 17].

Reabsorption:

Reabsorption is the process in which substances such as water, glucose, amino acids, and ions are removed from the filtrate in the renal tubules and returned to the blood. This process is vital for maintaining the body's homeostasis or a state of balance. During reabsorption water and small molecules are moved from the filtrate into the surrounding cells of the tubules. This is done by active transport which requires energy from the cells. Reabsorption is important for maintaining the body's fluid an electrolyte balance by regulating the amount of water and ions that are lost in the urine. The proximal convoluted tubule has the most absorptive capability, and it absorbs the glucose, amino acids, vitamins, water, and urea [18, 19].

Tubular Secretion:

Secretion may be seen as the reverse process of reabsorption where substances are secreted from the capillaries into the renal tubules. Clearing of drugs from the body is one of the major processes in tubular secretion. Along with medications, many other toxins and waste substances are secreted from the capillaries. This secretary clearance is crucial for excreting substances that cannot be filtered, such as uremic toxins which cause muscular and cardiac problems [20, 21].

In summary, the nephron is responsible for filtering the blood, collecting the primary urine, reabsorbing essential substances, and concentrating the urine. The nephron is essential for maintaining homeostasis in the body.

1.2 Kidney function estimation techniques

Early detection of functional abnormalities in kidneys is crucial for the treatment of acute kidney injury (AKI). The most common methodologies to assess the kidney health are through blood sampling. Here, urea and creatinine levels are quantified, however as indirect estimations of renal function [22]. Most used indicator of GFR is the serum creatinine which has a drawback that it takes significant influence from biological parameters like race, age, body composition and mass [23]. The direct measurement of GFR requires an exogenous biomarker which is filtered by the kidney without undergoing tubular secretion or reabsorption [24]. In rodents, infusion-based measurement of elimination of inulin is the gold standard for GFR estimation [25, 26]. However, the measurement of renal functions based on blood and urine analyses are known to be time consuming and causes strain to the subject [27, 28].

Non-invasive techniques have been researched upon extensively over the past including various imaging techniques like X-ray, MRI, and optical imaging based on dynamic and continuous methodologies [29-34]. While the dynamic method involves intermittent collection of samples, the continuous method measures the specific function in real-time over a defined duration [35]. For continuous monitoring, a biomarkers clearance is estimated over time with the help of sensors [25].

Following the administration of an optimal glomerular filtration rate (GFR) marker, its concentration in the plasma peaks and subsequently undergoes exponential decay as

it diffuses from the plasma into the extracellular space. As the marker diffuses into the extracellular space, equilibrium is established between the extra- and intravascular fluid, while the kidneys are already filtering the marker. Subsequently, as the GFR marker is filtered and excreted by the kidneys, there is a net diffusion from the extravascular space to the intravascular space [36, 37]. The clearance of the ideal GFR marker can be determined by evaluating its rate of disappearance from the plasma through compartmental pharmacokinetic analysis [38]. The distribution of the marker in various physiological compartments impacts its disappearance curve, and only the selection of an appropriate pharmacokinetic model can offer an accurate mathematical representation of the data for estimating the GFR based on the plasma clearance of the tracer. Administration of marker is primarily based on bolus injection in most GFR estimation procedures. Another popular approach involves infusion until a steady state of marker concentration is attained in the distribution volume. Intermittent dosage infusion is performed to reach such a steady state with the use of a feedback mechanism[39]. This setup requires a connection to a PC and repeated infusions. There are devices with varied degrees of ease-of-use based on their size and electronic modules.

The transcutaneous use of electronic sensors has been gaining popularity in being able to estimate in real-time the rate at which marker molecules are removed from the body [40]. Many of these devices use a photodiode or photomultiplier as the sensing component, which detects the emission from the marker when excited by light sources such as LEDs or lasers. Other types of detectors, such as radioactive and current detectors, have also been documented to measure marker concentration [37]. All such devices may differ in the type of dye used and the signal processing involved. Some are designed with a flexible sensor that can be placed on the skin, while others have been miniaturized for improved usability. The primary advantage of transcutaneous measurement of GFR is that it avoids cumbersome blood/urine analysis, thus, many such transcutaneous devices have been developed over the years [39, 41-44].

Among the various devices designed for detecting marker concentration, the small-size transcutaneous devices for measuring GFR have been gaining popularity in research set ups due to their ease of use and measurement methodologies. These devices do not have long probes or parts that are attached to a larger hardware hindering the overall experience of GFR measurement. Inulin, the standard for measuring GFR, is costly to extract. To address this, FITC-inulin was developed, but it poses solubility

issues. Sinistrin, a water-soluble alternative, offers similar activity to inulin. Fluorescein Isothiocyanate Sinistrin (FITC-S) is a widely used GFR marker, cleared by renal filtration without tubular cell involvement. Despite its efficacy, Sinistrin's high cost and limited availability persist as challenges. One of the transcutaneous devices developed, uses FITC-S dye as a marker [41]. This device consists of two LEDs and a single photodiode in between them. The LED sources have an emission peak of 470nm which is in accordance with the absorption spectrum of the marker. In the recent times, near infrared dyes have gained prominence as they bring the benefit of not being susceptible to absorption by many biological molecules [37]. A miniature device which is used with a dye 'ABZWCY-HPβCD' which lies in the near infrared region providing deeper penetration depth as compared to FITC-S has also been used in research groups [45, 46]. One such device developed by MediBeacon GmbH (later called MediBeacon device) is a small transcutaneous device, also made of two LEDs and one photodiode.[41].

It is known that the signal generated by the device after illumination and detection of the fluorescent marker takes influence from several physiological and electronic parameters. Based on existing GFR device data in our research group, it is seen from a large dataset of raw signals from the MediBeacon device that the signal magnitude is often compromised (too low or too high). This makes the detection of the GFR unreliable. The main reason for this is when the dye injected into the body is not optimally titrated in terms of the quantity or concentration. Even though the dye injection is in accordance with a standardized dosage (BW dependent), this still cannot guarantee a good resultant signal due to several physiological factors, for instance, the functioning of the kidneys. These issues and the frequency of their occurrence are explained further in sections 3.2 and 4.1.

1.3 New transcutaneous device

The new device is aimed at measuring GFR, reabsorption and tubular secretion with one device. To do so, three different biomarkers (dyes) that will be injected will need to be detected, quantified, and extrapolated to examine kidney function. This calls for the need of three light sources of different wavelengths for exciting the biomarkers based on their respective absorption spectrum. Thus, we chose three LEDs – red, infrared, and green as the three sources of illumination. The red LED corresponds to

the detection of the reabsorption marker, while the infrared and green correspond to the GFR and tubular secretion, respectively. The specific markers are developed and described by a fellow researcher from the same project.

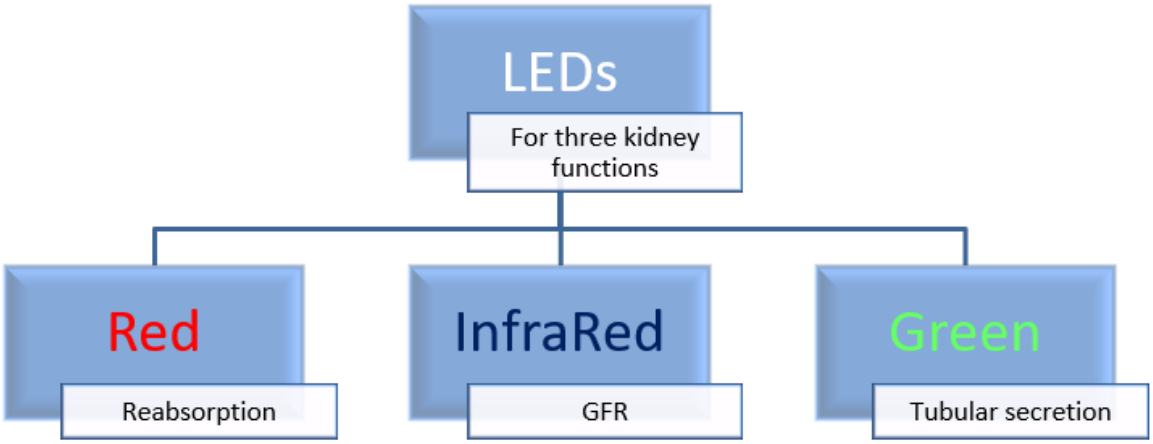

The need for a device which is capable of targeting deeper compartments along with considering the issues related to the photodiode signal strength will be considered while designing the new device.

1.3.1 Source-detector distance

The primary design consideration in this thesis will be to have multiple rows of LEDs that serve to facilitate different distances with the sensor (photodiode). We will discuss the effect of such a setup on the signal strength of the device which will eventually provide a method of solving issues encountered in the use of previously available devices. Such a setup where distance between photodiode and light source is larger, comes with the advantage of deeper penetration depth [47].

Though the absolute penetration depth of any light source would be the same irrespective of where it is kept on the skin if we neglect the differences in scattering and absorption irregularities, however, keeping the detector close to the source would mean that only the penetrated light, which is shallow is picked up. To be able to catch the light, which has travelled into the deeper regions of the skin tissue, the detector must be placed a little further from the light source. The larger the distance between the source and the detector, the deeper is the region from which the light is detected [47, 48]. When we increase the distance, it can be said that only the light, which has penetrated

deeper is being picked up by the photodiode. Since our aim is to target the deeper compartments like muscles, tissues, and organs, it seems more favorable to not keep the two optical components very close to each other. The strength of the signal reduces as the distance increases, but the point of interest is targeting deeper into the tissue. Hence, there will be a trade-off when one intends to decide the optimum distance between the source and the detector. Near infrared spectroscopy and its applications have also described the effect of distance between source and detector. Over-the-skin oxygenation measurements, which also contain LEDs and photodiodes are designed based on the specific application; for peripheral tissues, it is performed by placing the detector closer to the source, while deeper tissues are targeted by increasing the distance [49]. Based on these considerations, we aim to develop a new device with light sources and sensor placed at various distances from each other.

1.3.2 Device fixation, ambient light separation, and optical insulation

The fixation of the device on the skin is crucial for any sensor based transcutaneous measurement. In addition to the primary function of stable fixation and ambient light separation, such a patch also serves the function towards insulating the optical components from each other [50]. This is especially important as the photodiode is meant to receive the light from the LED that has penetrated the skin surface and not the direct light, which may incident on the photodiode without entering the skin. Such direct light hitting the photodiode will result in a signal which may be too high and potentially saturate. This will in turn cause a burden on the electronic capability of the device to manipulate the gain and the current driving the light intensity. Figure 3 shows how the presence of a proper fixation patch reduces the ambient light separation and insulates the optical components from each other.

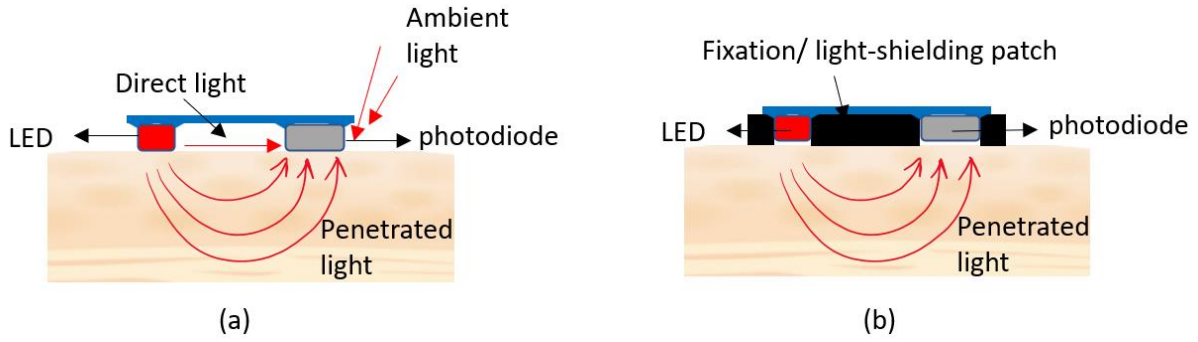

Figure 3: Device on skin with and without patch. *(a) device without patch where the LED and PD are directly touching the skin. Ambient light and direct light from LED hits the PD in*

addition to the penetrated light. (b) device with patch where only the penetrated light is allowed to incident on the PD. All other ambient lights are blocked. Such an insulation also creates a safe gap between the optical components and the skin surface.

In Figure 3a, we see that the optical components are directly sitting on the surface of the skin. Such a design could cause harm to the skin at the point where the LED is, due to heat generated at the time of illumination. Further, the photodiode has a high tendency to catch both the ambient light of the surrounding as well as the direct light from the LED. Upon adding a fixation patch with optimum thickness, the ambient light will get blocked, and this will also provide insulation between adjacent optical components (shown in Figure 3b). The thickness of the patch highly impacts the strength of the signal (see section 4.3.4).

1.3.3 Kinetic modeling

Pharmacokinetic modeling describes how markers are distributed and excreted within the body with the help of the concept of compartments like plasma, interstitial space, tissues etc. The clearance is calculated by taking a ratio of the dosage and area under the plasma concentration vs time curve [38, 51]. Various compartment models have been described for the estimation of GFR markers. According to the single compartment-model, it is modelled such that the GFR marker is eliminated directly from the plasma. Such a model can be expressed using a single exponential equation. For two compartment modeling, where the vascular and extravascular spaces are considered, the equation is depicted as a combination of two exponential functions [37].

The terminal exponential function in a two-compartment model is generally considered to be closely associated to the amount of extra-cellular fluid (ECV) filtered by the glomeruli over a given period of time.

A one compartment model is widely used in clinical setups as they are less cumbersome in terms of the number of blood samples required. However, a one compartment model leads to an overestimation of GFR due to the fact the elimination of the entire decay curve is not considered. The area under the curve for a one compartment model will eventually be smaller than the actual curve [37, 38]. Transcutaneous measurement of GFR have also been developed incorporating various compartment models in the past. In most cases, however, a semi-empirical formula is used to convert the half-life of the

marker into GFR values. Such a formula is animal specific and based on assumptions with respect to the ECV based on bodyweight. Hence, it is arguable that the evaluation of GFR based on the half-life only is a safe approach as it becomes free from body-weight dependent assumptions [52].

Such estimations of GFR have been widely studied based on various markers and kinetic models, while not much work has been done in terms of assessing secretion and reabsorption. Due to various drawbacks and absence of a gold standard measurement technique for assessing tubular clearance, this area seems to be a relevant topic which needs extensive research to eventually be able to individually assess the three components of renal clearance [53]. The development of specific tracers to mark the secretion and reabsorption is the primary step to address this concern. The calculation of clearance based on the elimination of the tracer for GFR has its own limitations and assumptions regarding the ECV and bodyweight, but much work has been done to assess various models and equations to closely estimate the clearance. Similarly, the equations described for theoretically estimating secretory clearance are based on assumptions of an equilibrium state of concentration in the plasma over time [1]. The scope in optimizing the models to distinctively measure secretary clearance after extensive in-vitro and in-vivo studies is vast. The transcutaneous evaluation of these additional clearances (secretion and reabsorption) needs to be determined in the future with the use of specific biomarkers. This aspect of studying the kinetic models for all the three renal clearances was not possible to be completed in this work, however, a device with the potential to be used for this purpose has been developed and its functionality is validated by oxygenation experiments.

2 AIM OF THE STUDY

The eventual goal of this research is to develop a transcutaneous device that has the potential to measure different renal functions in an experimental animal model. The device is aimed to have the functionality to detect the change in a biomarker concentration to estimate the desired kidney function. The extension of the developed novel device may find its applications as a diagnostic device in humans. However, this requires extensive trials on animal models before being tested on humans while considering the regulatory framework for medical devices.

This thesis describes the development of a device which is aimed to find its applications in two areas- 1. kidney function measurement and 2. oxygenation measurement over the skin. This thesis primarily seeks to address the limitations in the existing transcutaneous devices for GFR measurement while extending the functionality of the device thereby contributing towards developing a reliable sensor which aims to measure kidney functions more accurately.

However, due to the onset of COVID pandemic, we faced limitations in terms of work flexibility and availability of resources along with delays in animal permissions, hence, the developed device versions could not be tested for kidney function measurements. To overcome this problem, it was decided to test and validate the device by performing oxygenation measurements in human volunteers along with some animal experiments.

The aims of this work can be broadly classified into the following aspects:

2.1 Aim 1: Re-evaluate raw data from an existing GFR-measurement device.

There are devices that have been developed previously which aim at measuring the glomerular filtration rate. The results from one of these devices were studied and one major drawback related to the dosage (concentration) of the biomarker was detected and analyzed. The already available transcutaneous device for GFR estimation is re-evaluated and the results are analyzed based on the usability of the raw data obtained. To give us an idea on the frequency of instances where the signal obtained is not reliable for GFR estimation, we count the events where the signal from the device

(Medibeacon's transcutaneous device) is either too high or too low. This analysis will give us an idea on the frequency of instances where the signal obtained is not reliable for GFR estimation.

2.2 Aim 2: Develop a transcutaneous device capable of measuring GFR, reabsorption and secretion.

The new device will implement dynamic signal processing techniques along with layout changes to minimize the drawbacks found in previous devices while extending the functionality to three kidney functions. The overall aims of this work are:

2.2.1 Construction of the device

Based on the results from aim 1, we will optimize the device such that the user will have a flexibility in choosing different combination of LEDs and photodiode to be able to fetch a resultant signal which is suitable for estimating different kidney functions.
The outline of the device construction is as follows:

- Study the effect of the source-detector separation on the signal magnitude which is the output of the photodiode.
- Incorporate a triple LED setup in a single housing which will be placed in rows having different separation from the photodiode.
- Test the layout on a rigid and flexible base (frontends – part of the device with LEDs and photodiode) in combination with a hardware board (Part of the device which has the drivers, microcontroller, amplifier, etc.). (**Version 1** of the device).
- Update the layout of the device to reduce the size of the overall device by combining the frontend along with the different hardware parts in a single body. (**Version 2** of the device).

2.2.2 To test the device by oxygenation measurements as proof-of-principle

Oxygenation measurements serve the basis for establishing the functioning of the developed device. The measurements of oxygenation were performed on human forearms and animal models (pigs under the influence of ongoing surgery).

For transcutaneous GFR measurements, as the marker concentration in the body is measured over time for estimation of GFR, similarly the amount of oxygenated and deoxygenated blood in the body can act as markers to study the oxygen saturation in the body. The oxygenated blood (oxyhemoglobin) and the deoxygenated blood (deoxyhemoglobin) have different absorption spectra. As a result of this, lights of different wavelengths get absorbed differently based on the concentration of oxy/deoxy hemoglobin.

The two wavelengths for the LEDs which are commonly used for oxygen saturation measurements lie in the red and infrared region [54, 55]. The absorption spectra for both wavelength regions are shown in Figure 4.

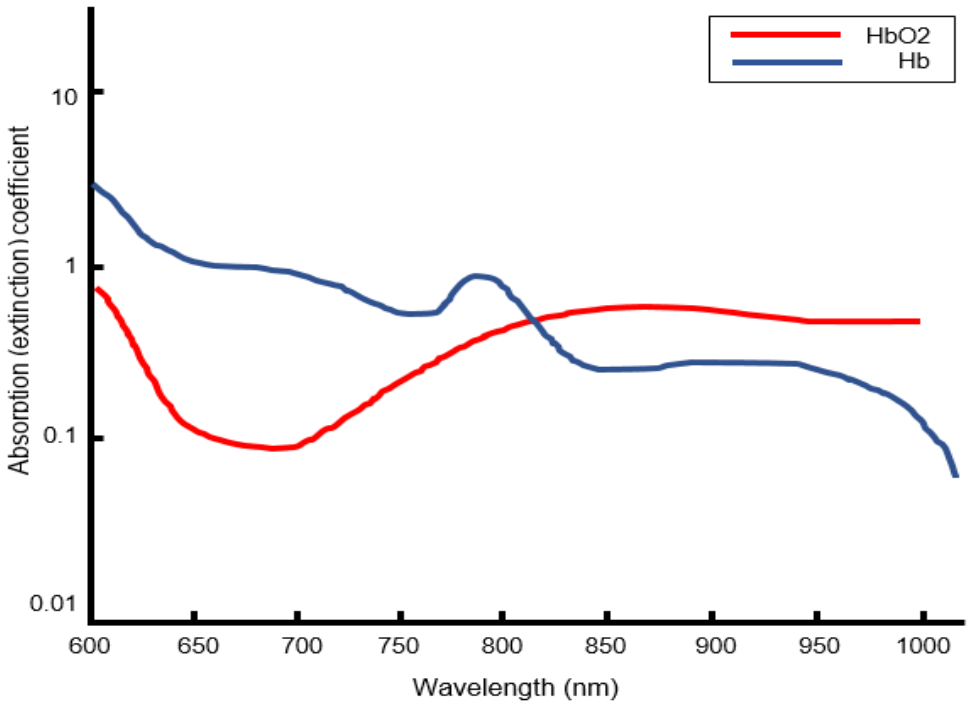

Figure 4: Absorption spectra of Hb and HbO2 [56]

2.2.3 To test and refine/optimize the device to evaluate kidney function

Prerequisites for evaluating the novel device are:

1. the development of respective dyes capable of reflecting the respective kidney function, GFR, reabsorption and secretion and
2. animal experiments to evaluate the device on healthy and diseased mice.

For both, intense collaboration with the two other PhD students within the RenalToolBox network working on these parts was essential. Unfortunately, progress in these aspects was hampered by the corona pandemic and the serious illness of the first supervisor, Professor Dr. Norbert Gretz. Subsequently the device development was validated with oxygenation measurements only serving the proof of concept.

3 MATERIALS AND METHODS

3.1 Components and Software

Table 1: Components and Software used.

Components and Software	Manufacturer
Arduino IDE	Arduino
Benchtop Multimeter	Keithley
Double sided patches	Lohmann
Hterm	Der-hammer (Tobias Hammer)
LED infrared	Kingbright – APT2012SF4C-PRV
LED red	Lite ON – LTST-C190CKT
MATLAB	Mathworks
NIR kidney device	Medibeacon
Photodiode 1	Vishay – VEMD8080
Photodiode 2	Vishay – VBP104S
Power source	BaseTech BT-153
Power supply device	BaseTech BT-153
Skin imitation polymer	URGO
Spyder (Python software)	Anaconda
Thermal sensor	Pico TC-08
Triple LED	OSRAM chip SFH 7016

3.2 Medibeacon devices used for re-evaluation of data

The experimental data for this analysis (Aim 1) was taken from previous researchers in the group. The devices were designed to be used with two dyes: FITC-Sinistrin [52, 57] and ABZWCY-HPβCD, respectively [46]. The device and the dyes that were used by the researchers are presented below in Figure 5 and Table 2.

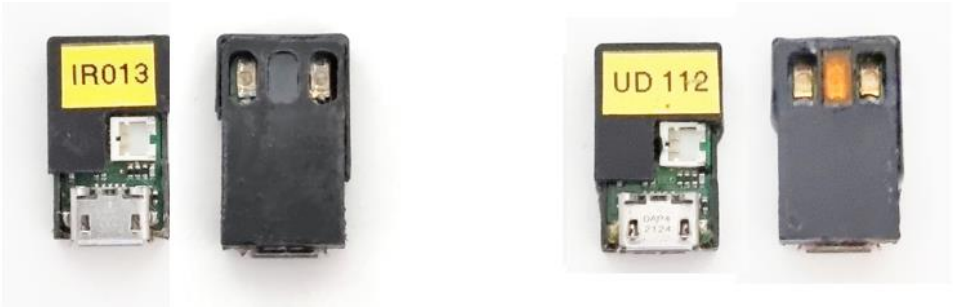

Figure 5: Miniaturized devices for GFR measurement. *The device 'IR013' on the left-hand side has two infrared LEDs with one photodiode in the center. This device will be used in combination with the ABZWCY-HβCD dye. On the right-hand side is the UD112 device which has two green LEDs. This device is used in combination with the FITC-S dye [41].*

Table 2: Dyes used with the Medibeacon Device

Dye	Developer	Dosage
FITC-S λ-excitation= 475nm λ-emission= 530nm	Fresenius Kabi AG	5mg/100mg of bodyweight (Stock: 40mg/ml)
ABZWCY-HβCD λ-excitation= 700nm λ-emission= 780nm	Cyanagen, Italy	15mg/100mg of body weight (Stock solution: 160mg/ml)

The raw data sets taken from the devices were plotted using MATLAB software on a graph with x-axis corresponding to the time and y-axis showing arbitrary signal magnitude. Ideally, the magnitude shoots up. Initially to get a peak which depicts the injection of the marker. The dye then starts to distribute into the body while the elimination process also starts simultaneously (depicted by the signal decay phase after the peak). The peak of the signal is noted and analyzed to check if it is high or low causing signal magnitude issues. The issues can thus be classified into two events: Over-dosing (high concentration) and Under-dosing (low concentration). The high concentration signals

tend to go into a saturation phase and the signal peaks are lost (Figure 6 and Figure 7). The curves represent the decay of the biomarker concentration over time. The sudden rise of the signal soon after timepoint 0 depicts the event of injection administration. The two figures show examples where the shoot in the signal magnitude either is ‘cutoff’ due to “overshoot” or diminished due to weak signal strength.

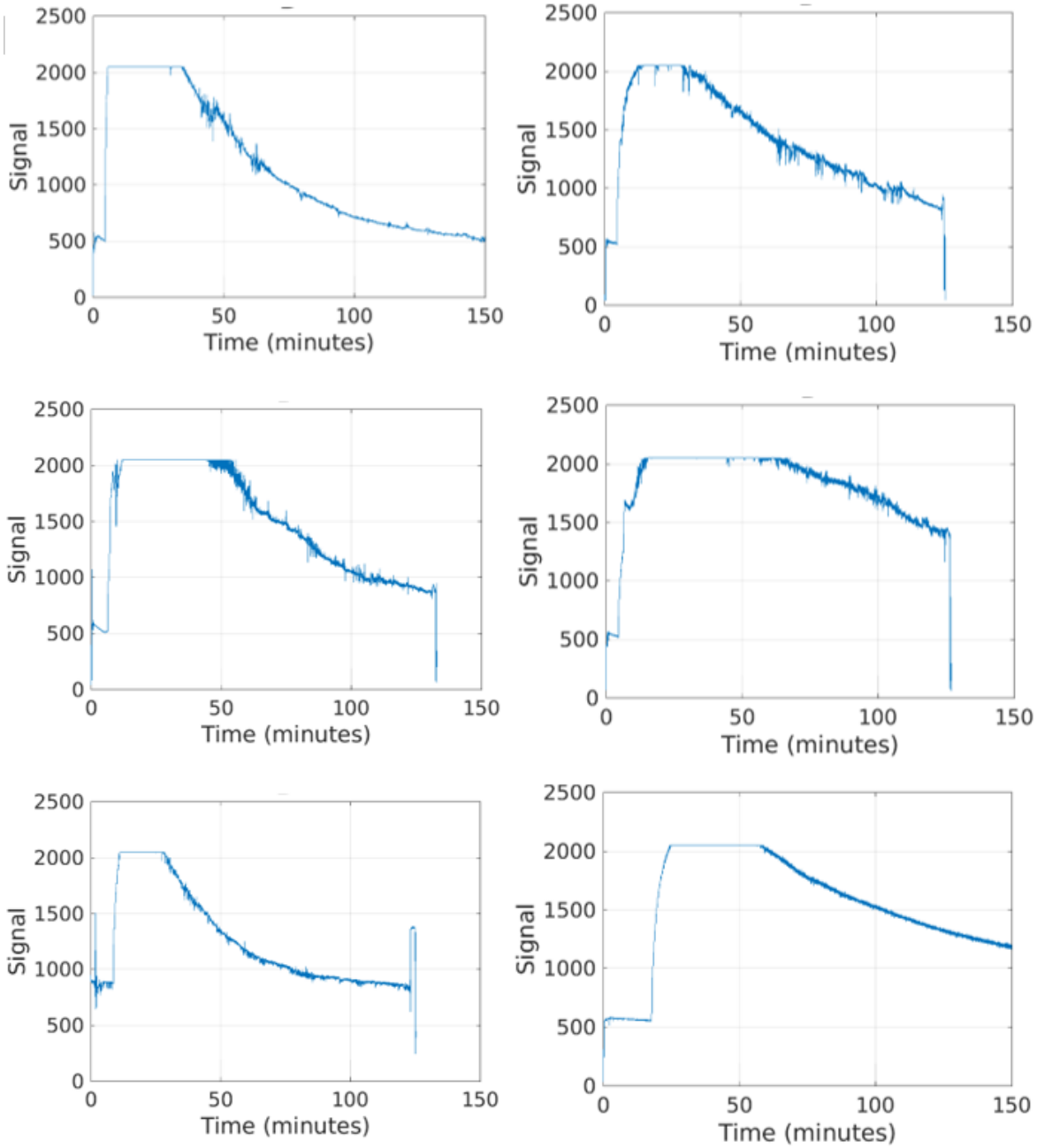

Figure 6: Examples showing events of high signal peaks

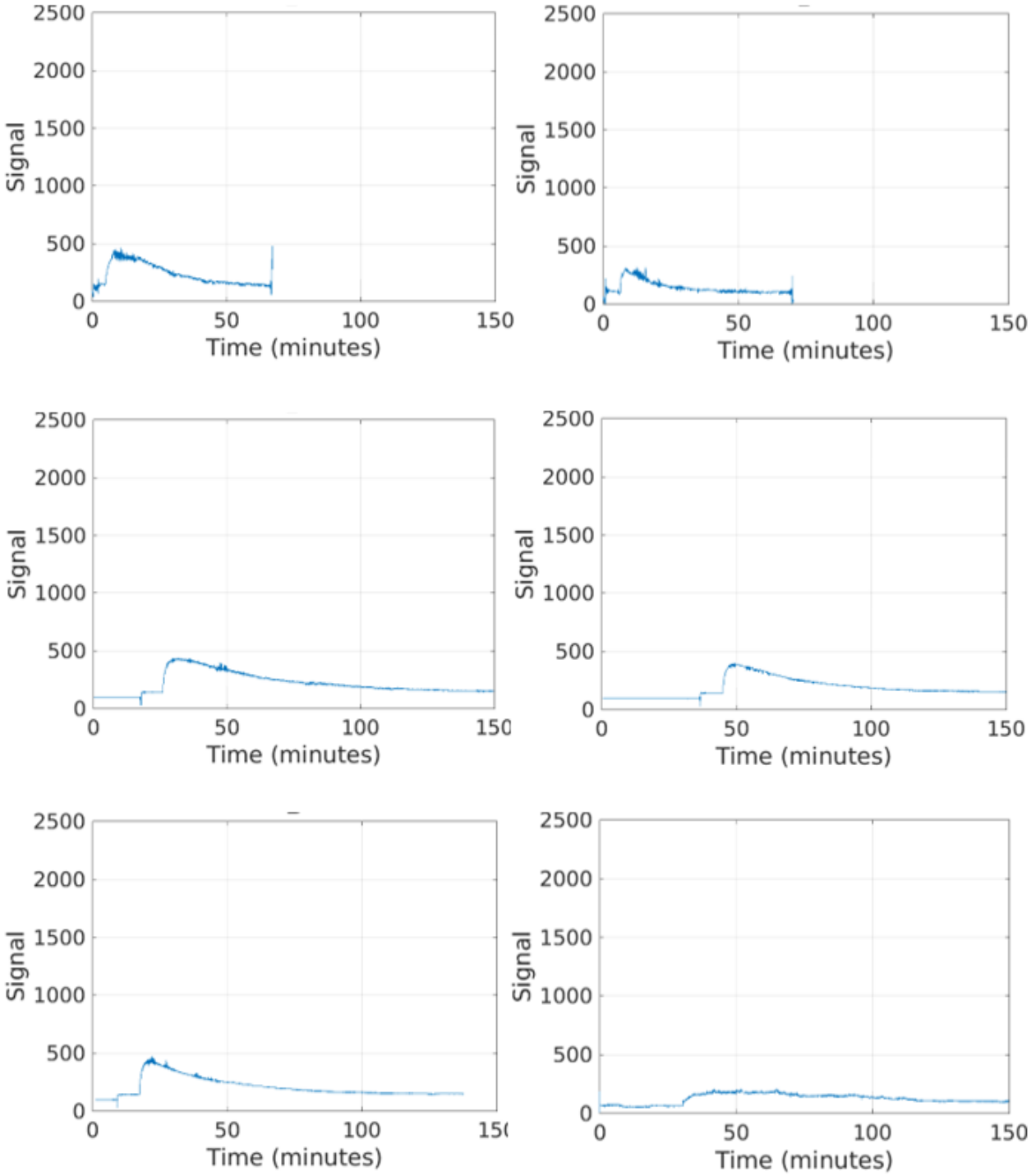

Figure 7: Examples showing events of low signal peaks.

Based on the examples shown, we clearly recognize two issues based on the concentration of dye injected. The issues and their effect have been divided as follows:

High dosage (concentration)	Low dosage (concentration)
▪ Either the concentration or the amount of dye is high with respect to the BW of the animal	▪ Either the concentration or the amount of dye is low with respect to the BW of the animal
▪ High signal causing signal peak losses	▪ Low signal causing weak peaks

Such events need to be addressed if their frequency is high which may lead to experiments being unreliable creating the need for rework. In the results section, further analysis of how frequent these events arise is documented.

3.3 Software used for device data transfer and signal processing

These two software applications are used along with the developed device versions 1 and 2 (described in results sections). The H-term is used to communicate with the computer while the Arduino is used to alter the device parameters via a computer.

3.3.1 H-term

This is a terminal software available for windows which we use to read and save the data coming from the USB of the device. First, we load a configuration file made in accordance with our device after we connect the data and power USB cable of the device, respectively. The data cable must be connected first into a USB slot of the computer. Once this is done the correct COM port has to be selected in the top menu bar of the h-term window. Once the COM port is selected, we press the connect button and then insert the power cable into another USB port of the computer. The Baud rate in the top menu of the software must be set to 1152000 to set the rate of transfer of data from device to PC. Once we finish the device measurements, we can disconnect and save the data in the computer hard drive. This data is further used for analysis. A screenshot of the software is shown below in figure 8.

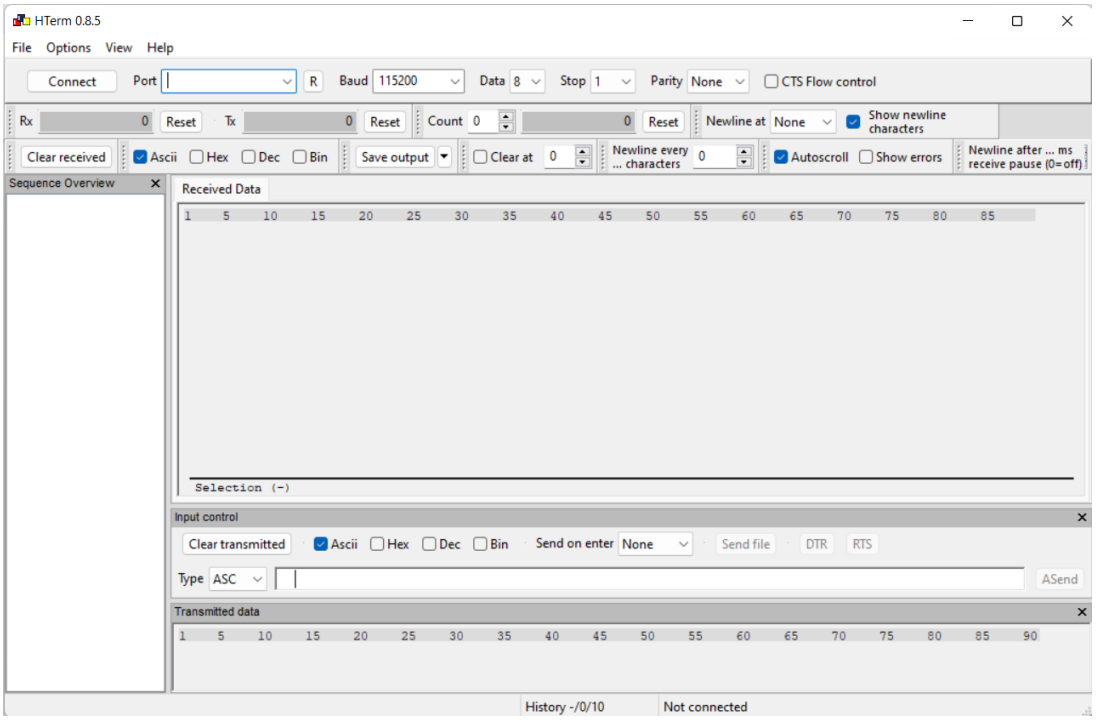

Figure 8: Terminal software which provides transfer of raw data from device to PC.

3.3.2 Arduino

This is the software that we use for changing device parameters like LED intensity, gain etc. Figure 9 shows a screenshot of the Arduino window.

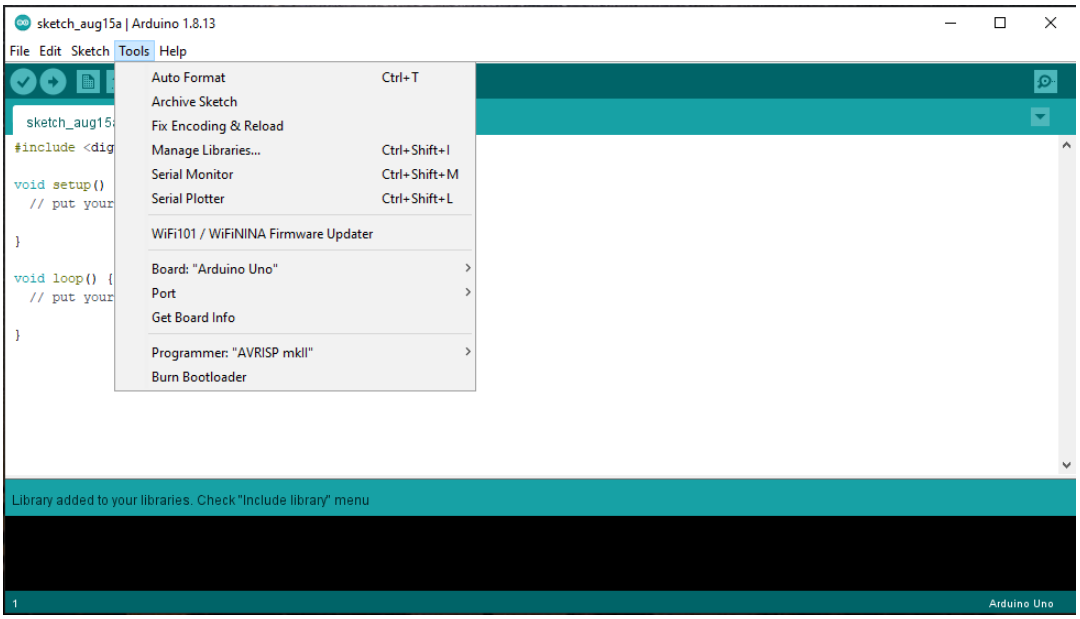

Figure 9: Arduino software window. Software used for optimization of parameters into the device.

Here we select Tools from the top menu and select “Serial Monitor.” This opens another window where we can input our commands to change the various parameters of

the device. The commands along with the specific changes that can be made are discussed in section 4.3.4.

3.4 Preliminary LED-PD experiments

We postulated that the problems with signal strength from the previously available device could be managed using a new design where the distance of LED to photodiode is variable to increase/decrease measurement sensitivity. We considered placing multiple LEDs in rows which could be driven according to the respective need.

3.4.1 Test strip with slider mechanism

Accordingly, we created first a measurement set-up with one detector – the photodiode - and one source –LED of which the distance could be adjusted. The specific aim was to study the changes in the photodiode current based on the varying distances between the source and the detector. The setup consisted of a rectangular plate with saw-teeth on both sides to fix an LED and a photodiode at different places across the length of the plate (Figure 10). This facilitates the provision of having different distances between the LED and photodiode, which can be measured. The rationale behind such a set-up was to make use of the change in signal magnitude at different distances to solve the issues encountered in the previous devices. In an event where the signal magnitude is high, an LED-PD pair which is placed at a farther distance can be used for measurements.

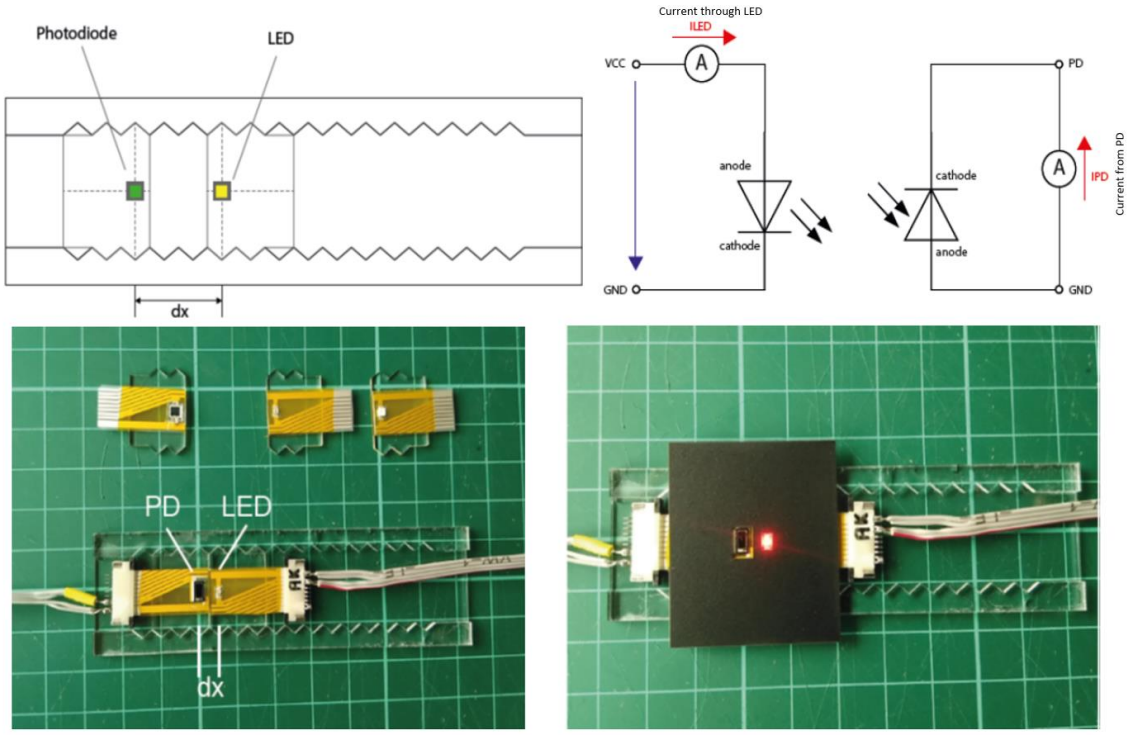

Figure 10: Preliminary set up using one LED and photodiode with interchangeable distances. *Shows the mechanism which facilitates change in distance between LED and PD. The distance is depicted by 'dx'.*

3.4.2 Test strips on flexible base

The slider mechanism discussed in the previous section was updated by mounting the LEDs and photodiodes onto a flexible base with printed circuit lines (Figure 12). Two of such strips were made, one with an IR LED and the second one with a red LED. Each strip has seven photodiodes placed at incremental distances of 5mm. This provides a range of 5 to 35 mm separation between the source and the LED.
In these experiments, we used a skin imitation polymer (developed by URGO GmbH), upon which the test strip was placed during current measurements (Figure 11).

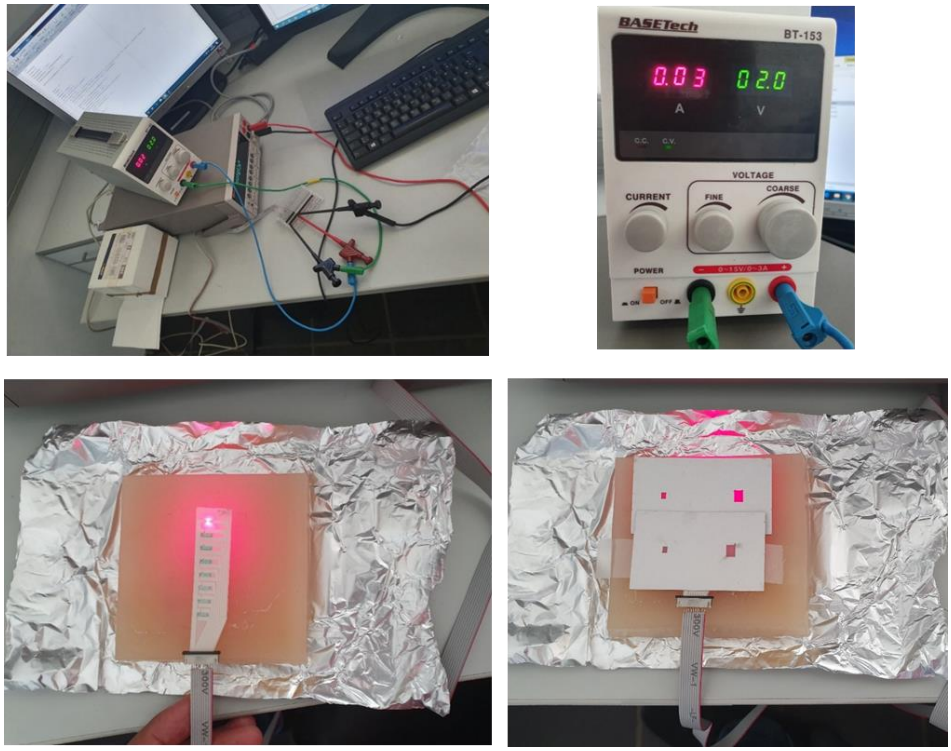

Figure 11: Measurement set-up with flexible base LED strip. *The strip containing PDs and LED is kept on the skin imitation polymer. Probes are connected to give power to the LED and record current generated by the PD by using a circuit breadboard.*

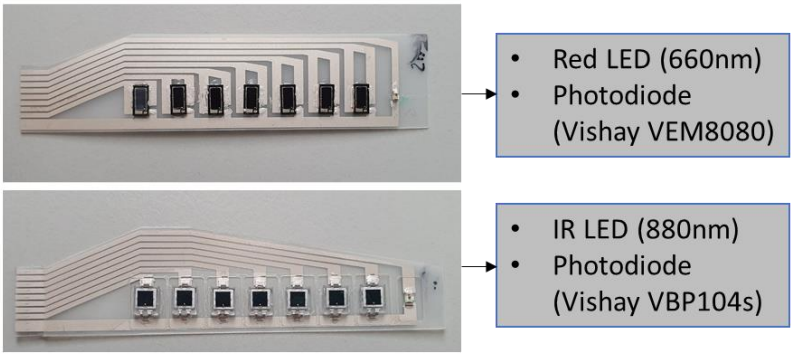

Figure 12: LED strip with one LED and seven photodiodes on flexible base. *Two test strips are shown which consist of seven PDs and one LED each. The distance between LED and each of the PD is in multiples of 5mm.*

3.4.3 Effect of single versus dual LED

We speculated that multiple rows of LEDs may solve the problem of dosing. Accordingly, we performed an experiment to measure the intensity of light through a skin imitation tissue with single or dual LED illumination. This setup shows the significant effect of single versus dual LED on the signal received.

Measurement components- (Figure 13 and Figure 14):

1. ‘Newport’ power meter to measure the light intensity
2. NIR LEDs
3. Skin imitation polymer

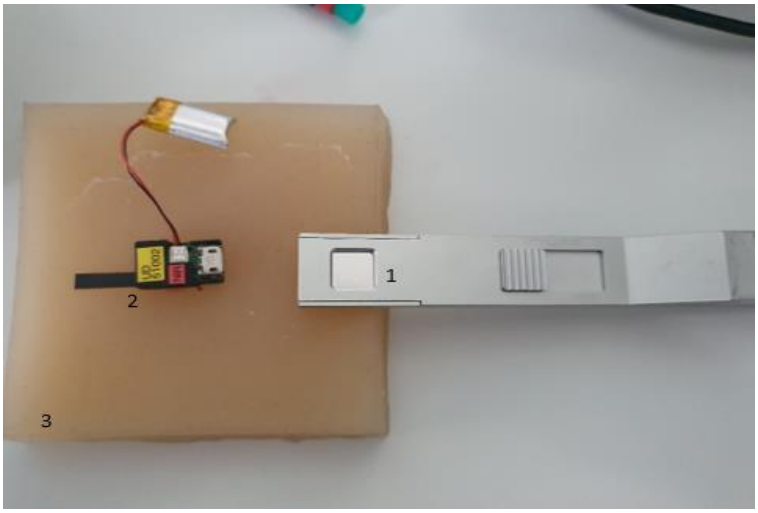

Figure 13: Skin imitation polymer with NIR device and power meter

.

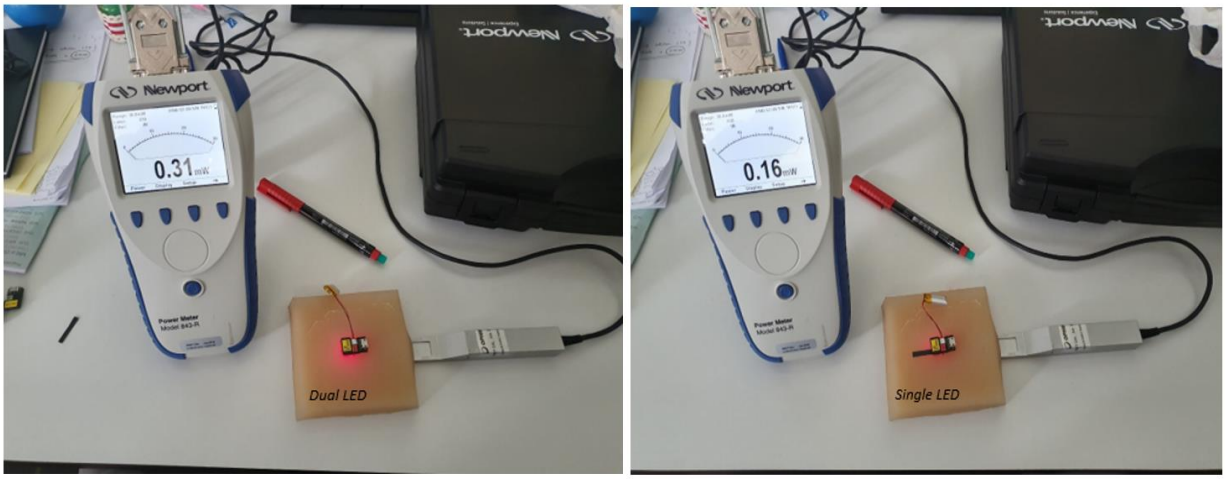

Figure 14: Signal power using single vs dual LED. *The device containing LEDs is placed above the skin polymer while the power meter sensor is placed underneath*

3.5 Design of the new device

With the idea of having different width of separation between the sensor and the light source, we came up with a layout with one large spectrum photodiode and multiple rows of LEDs. Initially we decided to have a triple LED combo to be used to measure the three different kidney functions that we aim to analyze.

3.5.1 Layout development

The first layout consisted of two rows of LEDs (Figure 15). Each row consists of the three LEDs to measure three different kidney functions. In addition, it has three photo-diodes along the length of the device.

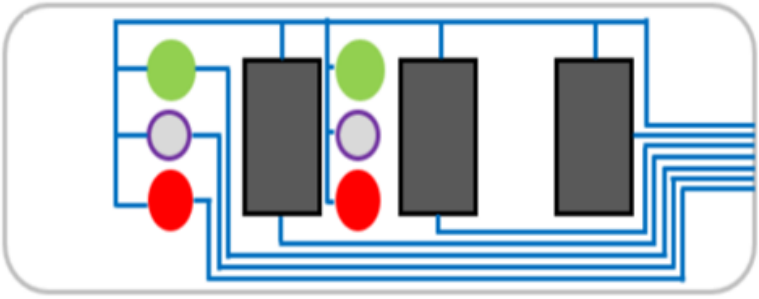

Figure 15: Layout of the components on the new device. *Three photodiodes shown as 'grey rectangles' and two rows of triple LED-combo (red, IR and green) on each side of one photodiode.*

For simplification in terms of electronic processing and design, we change the design to have multiple rows of LEDs and one single photodiode as shown in Figure 16.

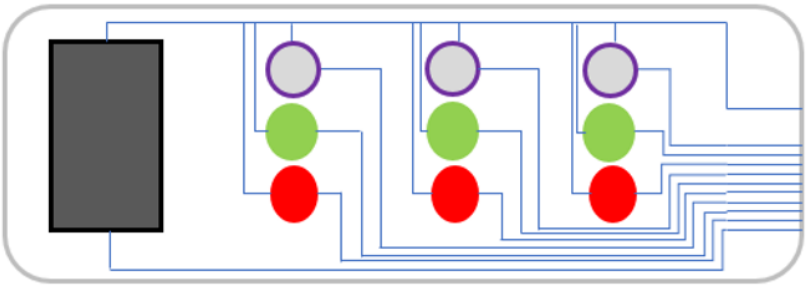

Figure 16: Modified layout of the components on the new device. *Three rows of triple LED-combo and one single photodiode.*

Figure 17 shows the evolution of the device versions. Each of these versions have been discussed in detail in the following sections. The first version of the device along

with its subsequent flexible version were used in combination with an external hardware board which consists of electronic components like drivers, microcontroller, amplifier etc. The second version of the device was stand alone with all the hardware components attached to it in a reduced overall size.

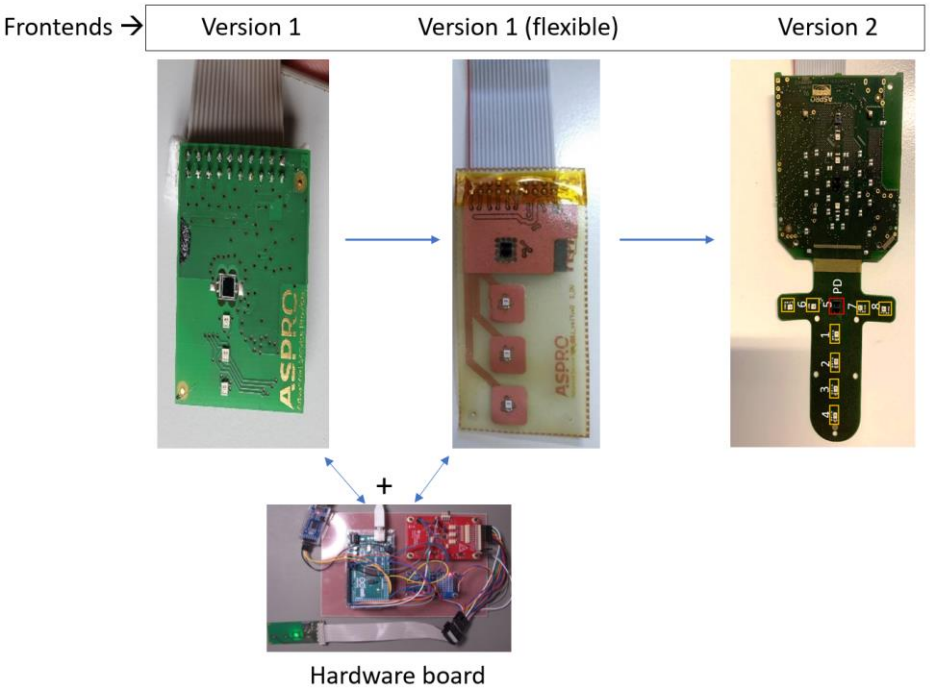

Figure 17: Device versions evolution

3.5.2 First version of the new device

The first version of the developed device is as shown in Figure 18. The novel design consists of a single large photodiode along with three rows of LEDs. Each row of LED consists of a combination of three LEDs – red, infrared, and green. The distance between each of the LED combos is 0.5 cm which is the same as the distance between the photodiode and the first LED combo. Another version of the front end was also made which had a larger distance between LED and photodiode- where the closest LED is 1.5 cm away, followed by 3 cm and the last LED at 4.5 cm. Figure 19 shows the layout of the LED combo which is manufactured by OSRAM.

Figure 18: "Frontend" containing LEDs and photodiode. *LED-Combo placed in three rows after a single photodiode. The distance between any two adjacent components is 0.5 cm.*

Figure 19: Triple LED combo from OSRAM. *A single housing containing three LEDs- red, infrared, and green (picture taken from amd-osram web portal).*

Further, the frontend of the device was developed on a flexible base to enable a better fixation on the skin surface as opposed to the rigid base frontend. The figure below shows the new version of the frontend.

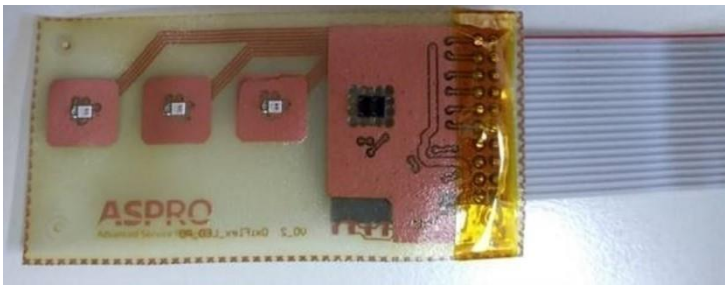

Figure 20: Flexible version of the frontend. *LEDs and PD mounted on a flexible base.*

3.5.2.1 Hardware Set-up

The complete hardware currently consists of a “frontend” (which consists of the LEDs and photodiode) and a separate circuit board comprising of microcontroller, LED-drivers, analog-digital converters, and the data interface. The frontend is the only part of the set-up which is attached to the surface of the skin from which the signal goes to the circuit board for further processing before it is transferred on to a PC via the data interface (Figure 21).

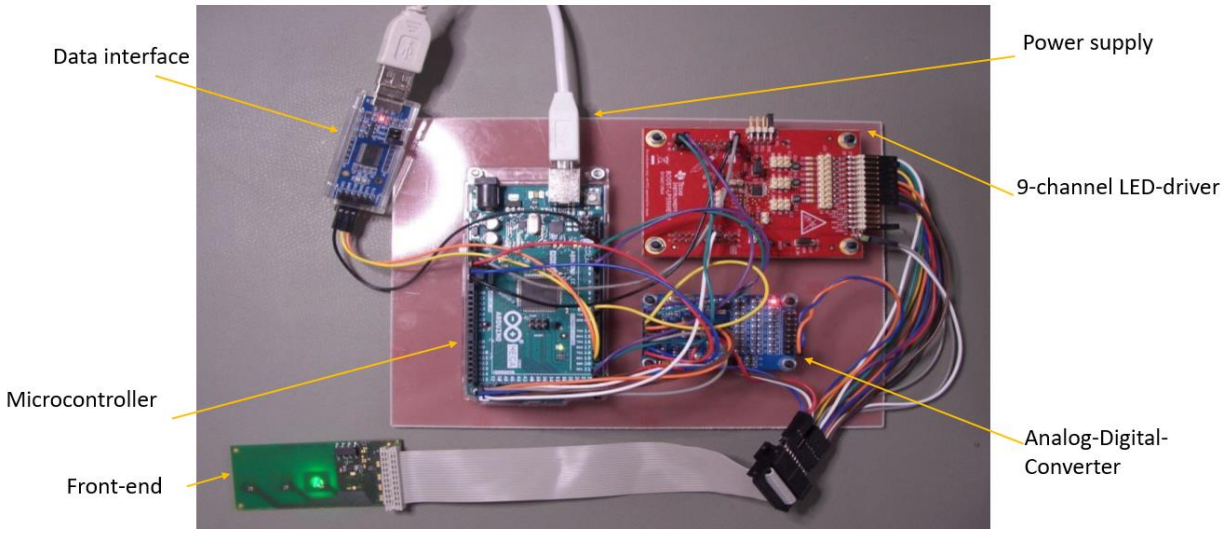

Figure 21: Frontend along with the hardware board used as first version of the new device. *Complete hardware along with a connected frontend part. The board is placed on a table while the front end (connected to a long cable) is placed on the skin.*

3.5.3 Device workflow and electronic parameters

The electronics workflow of the developed device versions will be able to process the signal with suitable gain at various stages. The LED drivers illuminate the LED combos sequentially by applying current in amperes as specified by the user using software as described in section 3.5.1. The workflow of the device is depicted in Figure 22. Upon illumination, the photodiode also detects the light at the same interval of time as the LED illumination. This happens for each of the LEDs that are present inside the triple combo structure. The current produced by the photodiode as result of light is then amplified and converted into voltage by a transimpedance amplifier which also has the

capability to give an appropriate gain to the signal. Analog to digital conversion (ADC is performed before the data is logged and transferred to the PC via software.

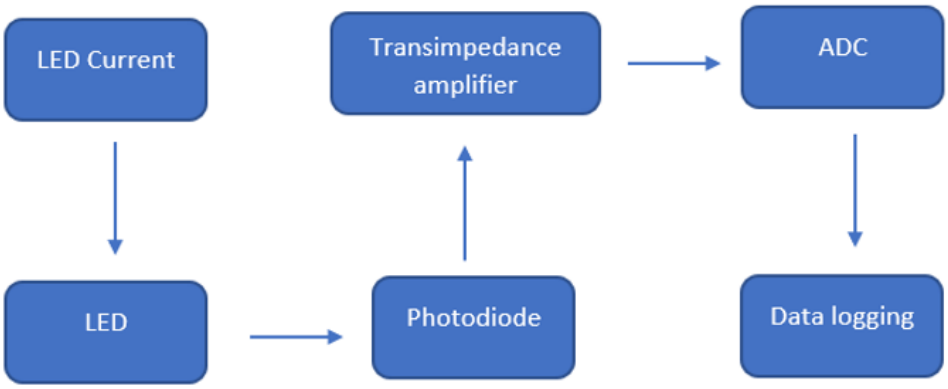

Figure 22: Workflow of the device

For the experiments with device version 1 shown in section 4.4.3, manipulation of the signal data can be performed based on several parameters within the device- LED intensities, transimpedance amplifier gain, ADC gain and light shielding. Figure 23 shows the different parameters that can be changed. The LED intensity can be changed by changing the current in the range of 0 to 25 mA. The transimpedance amplifier's resistor values can be changed to give three different effective resistances which result in three different possibilities of gains. The ADC converter also has a programmable gain which can further increase the strength of the signal if required. Lastly the thickness of the light shielding used between the skin and the frontend also affects the signal strength significantly.

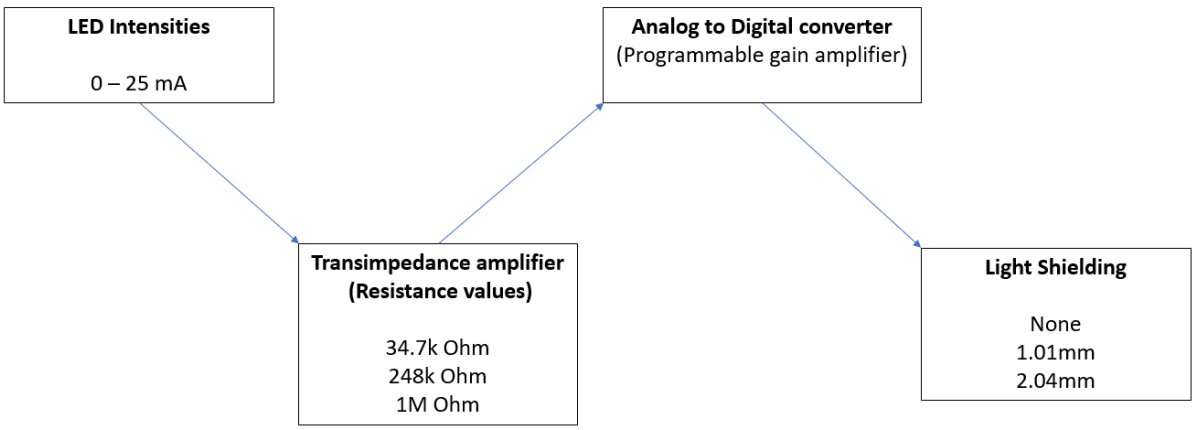

Figure 23: Different parameters that can be changed in the device. *Four stages of modifiable parameters to manipulate the photodiode signal.*

3.5.3.1 LED Current

The intensity of the LED can be manipulated by changing the current given through the LED drivers. The value can be set for each LED individually. The values that are to be set for different LED intensities (current) are shown in the table below. These values are set before the measurement using the Arduino software to communicate with microcontroller.

Table 3: LED parameter settings. *The current given to the LED can be fluctuated between 0 mA to 25 mA. The higher the current value, the higher the intensity of the LED light.*

LED Current	Control parameter
0 mA	0
25 mA	255
N mA	N/25*255 (rounded off)

3.5.3.2 Analog-to-Digital converter

Here, the analog voltage coming from the transimpedance amplifier is converted into a digital signal. In the converter, a programmable gain amplifier (PGA) is built-in which gives the scope of further increasing the PGA factor and increase the range of the measurable input signal (Table 4).

3.5.3.3 Transimpedance amplifier

A transimpedance amplifier is a current to voltage converter implemented using an operational amplifier and a combination of feedback resistors for a suitable overall gain in the output voltage (amplification). Such amplifiers are suitable drivers for the signal being fed into an analog to digital converters. The effective resistance of the circuit gives us the amount of gain which is applied. Each LED chip can be given a different gain. In the Arduino software, it is possible to select 4 different values of resistances which correspond to four levels of gain (Table 5).

Table 4: ADC parameter settings

Amplification	Control parameter	Input voltage range (min/max)
1	32	+/-5V
2	33	+/-2.5V
4	34	+/-1.25V
8	35	+/-625mV
16	36	+/-312.5mV
32	37	+/-156.25mV
64	38	+/-78.125mV

Table 5: Gain parameter settings (transimpedance amplifier)

Resistance	Control parameter	Amplification
3.00 M Ohm	0	1V = 0.333 µA
2.02 M Ohm	1	1V = 0.495 µA
1.01 M Ohm	2	1V = 1.000 µA
0.86 M Ohm	3	1V = 1.161 µA

3.5.4 Second version (smaller hardware)

This version has been fairly reduced in size in terms of the hardware attached to the frontend. There are 8 LEDs in total and one photodiode. The distance between any two components is 1 cm. The arrangement of LEDs and photodiode is as shown in Figure 24.

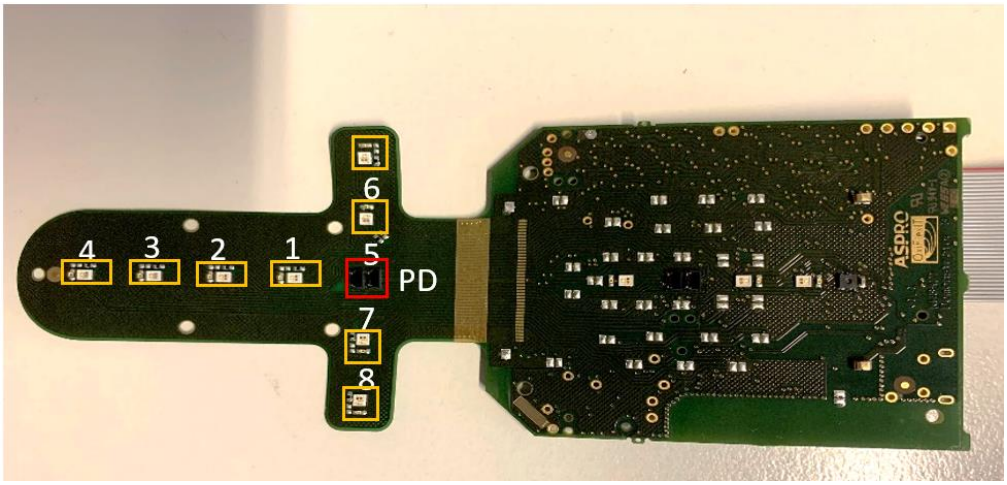

Figure 24: New device – version 2

This device is also fixated on the skin using a light shielding patch developed by Lohmann GmbH (Figure 25). We use such fixation patches to facilitate device fixation on to the skin. The purpose of such a patch is two-fold; first is to provide an even fixation on the surface of the skin ensuring a homogenous attachment along the device dimensions, second is to provide insulation from ambient light as well as keeping the LEDs and PD insulated from each other. Different patches were used for different versions of the device during the development process which are shown in the results section.

This device is incorporated with automatic gain settings along with sample averaging which is performed at about 9.5 seconds. There is a periodic sampling of ambient light after each LED pair sampling, which is further subtracted from the final signal for ambient compensation. The device is connected via two USB-ports; one for data communication and the other one for power supply. The data is extracted via the h-term software in the laptop.

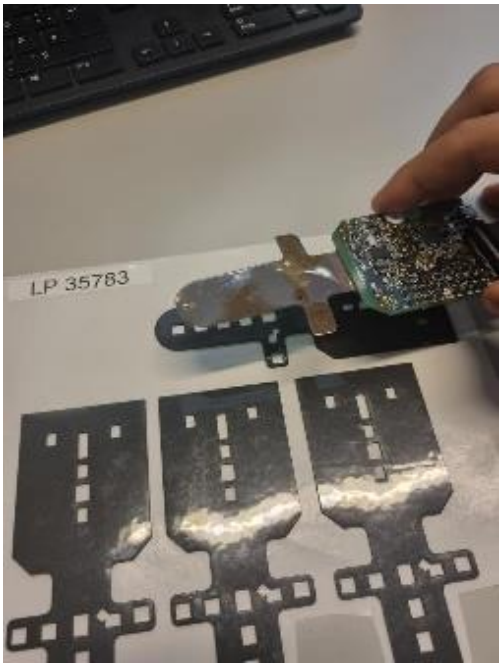

Figure 25: Lohmann patches for version two device

3.6 Validation experiments

Since the main idea is to track the changes of a marker inside the body, we performed analogical experiments to measure oxygenation using a human arm of a voluntary healthy person, in place of kidney function measurements. We used a blood pressure cuff on the arm to restrict the circulation blood, thus reducing the oxygenation in the forearm.

The oxygenated hemoglobin (HbO_2) in the blood absorbs more infrared light while the deoxygenated hemoglobin (Hb) absorbs more red light. Thus, we used the red and infrared LED sources present on the device and recorded the signals coming from the device. The blood-pressure cuff was used to stop the blood flow by applying pressure on the arm for about two minutes and then the pressure is released. This cycle is repeated to record the change in the signal coming from the device as result of red and infrared illumination. A ratio of these signals was also calculated to estimate the oxygen saturation. Finally, the results were compared with two other commercially available devices.

The first step was the fixation of the frontend on the surface of the skin. For this purpose, we used double-sided adhesive patches developed by Lohmann. This patch has cut-outs for exposing the LEDs and photodiode and helps in fixation while blocking the

ambient light. This patch also provides insulation between the LED and photodiode so that the light does not directly go to the photodiode before skin penetration.

In the next step, we connected the data and power cable from the hardware board to a computer. Once the device was connected, we use the H-term software for reading and saving the data. In order to change the device parameters (see 3.5.3), we used the Arduino IDE to change the parameters in the microcontroller.

3.7 Light Shielding

It is crucial to ensure that the frontend of the device is well fixated on the surface of the skin to avoid ambient light affecting the measurements. During our initial measurements we used an adhesive to wrap the frontend on the skin surface. We observed that a minor change in the pressure with which the adhesive was wrapped around affected the signal amplitude as well as its behaviour to a great extent. Hence it is necessary to have a proper adhesive patch that sits between the frontend and the skin which ensures a proper fixation. This also helps in reducing the ambient light from the room to hit the surface of the photodiode.

Figure 26 shows the front end on the forearm without a fixation patch. We have shown the results of signal from different LEDS positions without and with use of an adhesive patch in 4.3.4.

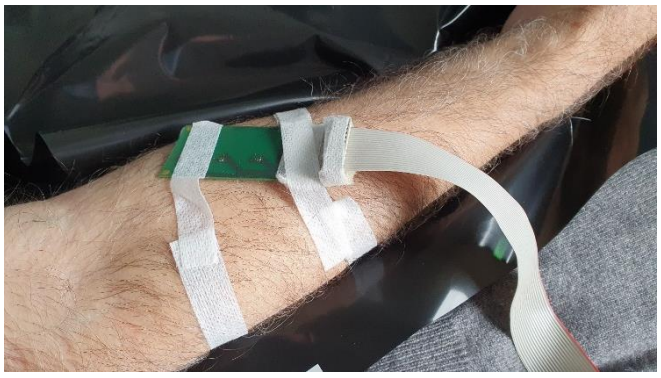

Figure 26: Fixation of device without a light shielding patch. *Unstable device fixation on skin due to the size and rigidness of the device.*

3.7.1 Temperature measurement

Temperature increase due to LED illumination may potentially be a hazard to the skin depending on the maximum temperature the device reaches during its application time. According to the international standard IEC 60601-1, the maximum permissible temperature limit for active medical devices which are in contact with the skin is 41^{o} Celsius [58]. We used a probe attached to a thermal data logger (Pico TC-08) and placed it between the skin and the sensor and measured for over 25 minutes continuously. Signals were read over time to study the maximum temperature with and without the active device on the skin surface.

3.8 Protocol for device validation experiments

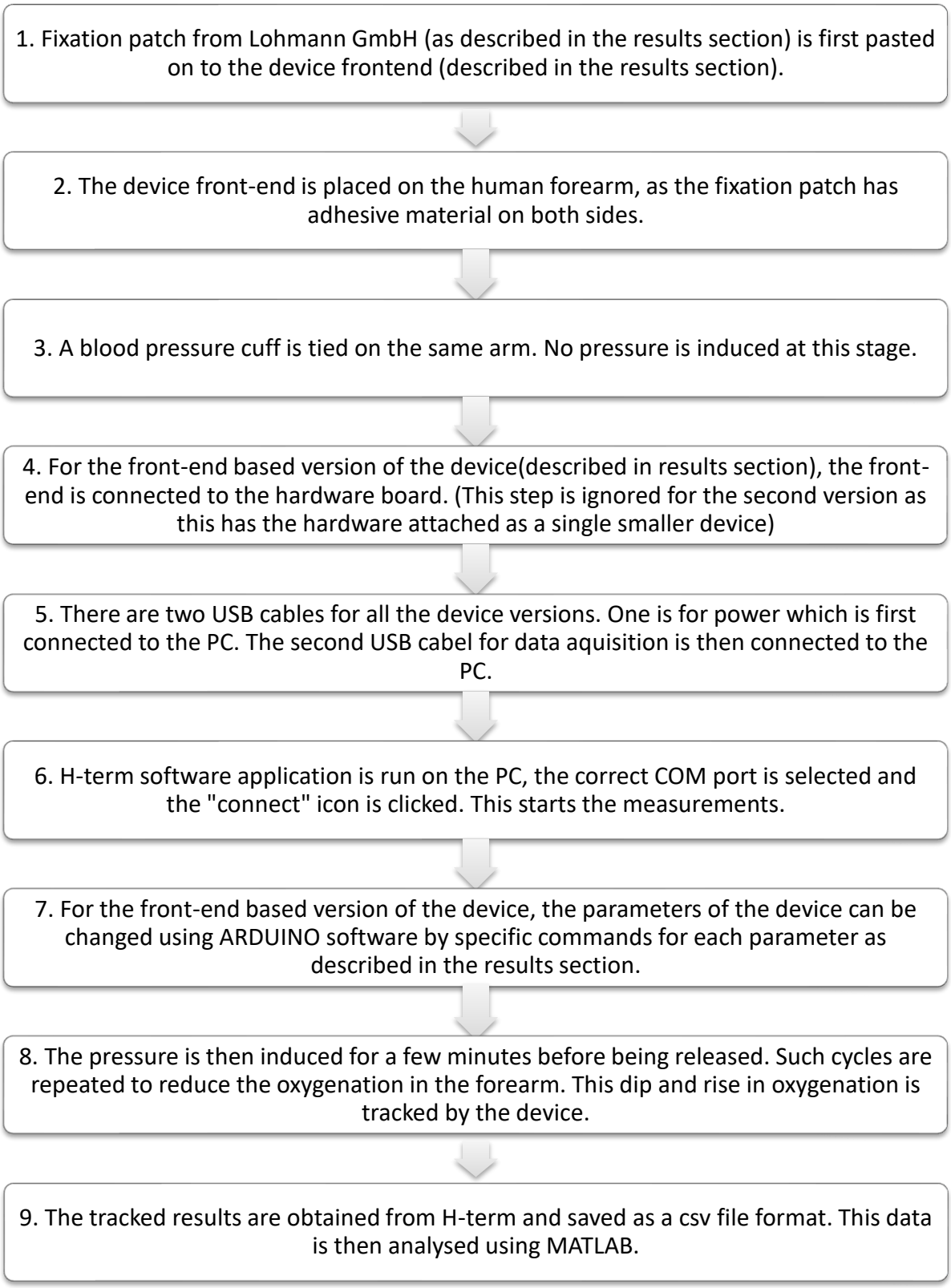

Figure 27: Protocol for oxygenation measurements: *This describes the procedure followed for the experiments for device validation which have been explained in the results section.*

3.9 Oximeters for comparison of the prototype devices

O2C device: This is a diagnostic device used for non-invasive measurement of oxygenation of perfused tissues. This device uses white light spectroscopy to measure the oxygen saturation of the hemoglobin. It has a small sensor which is placed on the skin. This sensor is attached to a display system via cable where the oxygenation values are displayed and recorded as raw data. This file containing the data can be extracted via a memory stick.

MOXY: This is a small wearable monitoring device used in the sports industry to measure the tissue oxygenation in athletes. It uses infrared light to monitor oxygen saturation continuously in a non-invasive fashion. This patch is placed on the skin with the help of an adhesive tape. The MOXY device is connected to the computer wirelessly using the company provided software application. The data is fed into the system and can be extracted via the software as needed.

Both the devices mentioned above are commercially available. We used these two devices in combination with our newly developed device to compare the oxygenation changes and trends. The Moxy device was also used in animal experiments that we performed on pigs. The pigs were scheduled for surgery to test an external circulation machine by the surgeon at the University Hospital, Heidelberg. Since the change in circulation in the body would cause drastic changes in the oxygenation, we tapped these changes using the developed new devices along with MOXY device.

4 RESULTS

4.1 Re-Analysis of data from existing GFR device

The currently available device to measure GFR has issues with over- and underdosing of the fluorescent tracers. We addressed these drawbacks by analyzing more than 1300 datasets to quantify the frequency of occurrences of the two events described in section 3.2. The data were fed into MATLAB, plotted, and then sorted into different ranges of <500 to >2000 of signal magnitude. The signal magnitude is in arbitrary units which depicts the strength of the light detected by the photodiode upon presence of fluorescent marker. This signal which we receive from the photodiode is directly proportional to the amount of light which hits the diode. It is seen that the number of times the signal is higher than the desired value comes close to 16% when the FITC-S dye is injected, while it is 13% when the signal is lower than desired. In the case of AB-ZWCY-HβCD dye, the events of high signal strength are low ~1%.

Table 6: Percentage occurrences in different ranges with FITC-S. *Eight users were recorded to have used FITC-S dye for GFR measurements using the transcutaneous device. The peak value of the signal curve from the device was recorded and counted for the range in which the value falls.*

Range	User 1	User 2	User 3	User 4	User 5	User 6	User 7
<500	16.3 %	21.3 %	2.9 %	4.5 %	0.3 %	1.0 %	44.4 %
500-750	14.0 %	13.8 %	4.1 %	22.3 %	0.3 %	6.0 %	44.4 %
750-1750	50.3 %	50.0 %	80.2 %	69.0 %	64.1 %	55.5 %	11.1 %
1750-2000	8.8 %	11.3 %	7.1 %	2.1 %	16.3 %	9.0 %	0 %
>2000	10.3 %	3.8 %	5.3 %	1.9 %	18.8 %	28.2 %	0 %

Table 7: Percentage occurrences in different ranges with ABZWCY-HβCD. *Two users were recorded to have used ABZWCY-HβCD dye for GFR measurements using the transcutaneous device. The peak value of the signal curve from the device was recorded and counted for the range in which the value falls.*

Range	User 8	User 6
<500	9.72 %	4.4 %
500-750	43.33 %	19.2 %
750-1750	46.94 %	74.7 %
1750-2000	0.00 %	1.2 %
>2000	0.00 %	0.4 %

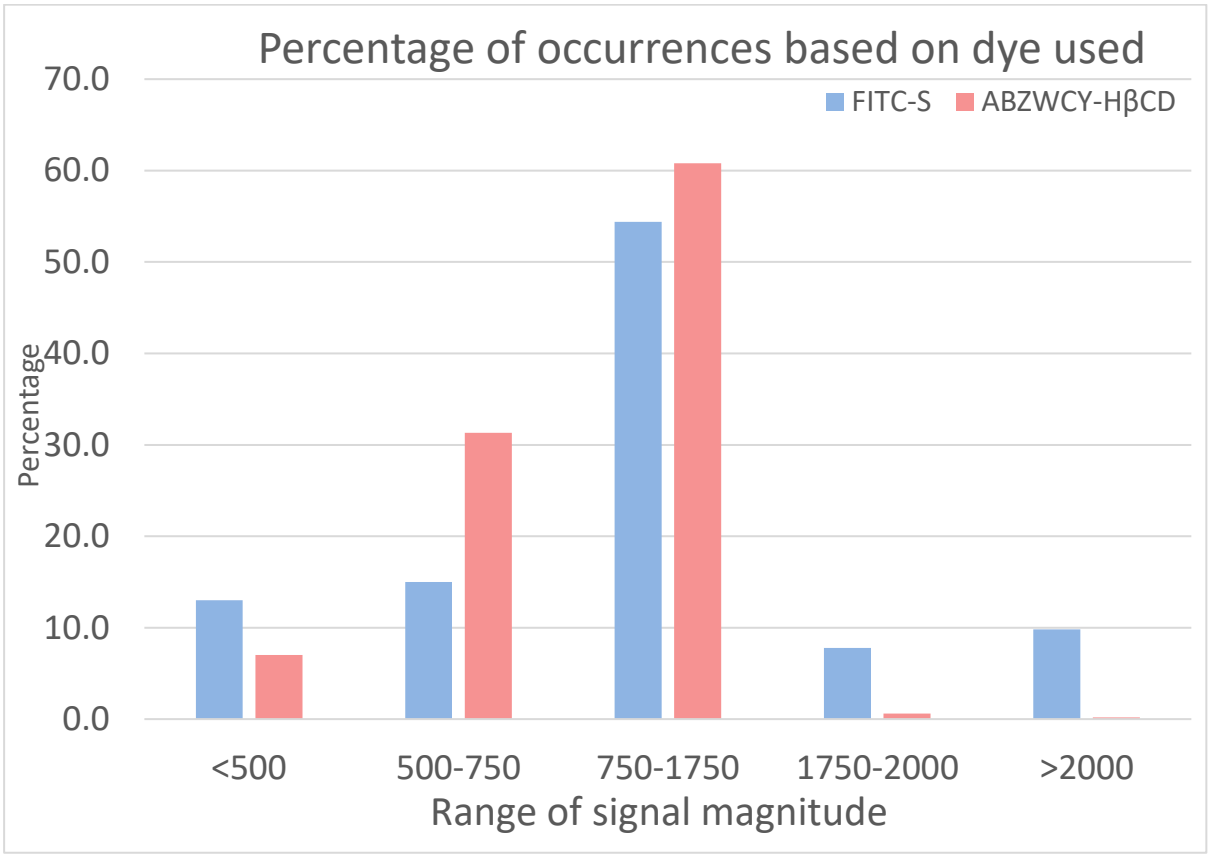

Figure 28: Percentage of occurrences based on the dye. *Bar graph representation to depict the frequency at which the signal falls into the respective magnitude ranges.*

4.1.1 Data with rats and mice

The experiments performed by all the users were conducted on either a rat or a mouse. Based on the animal used, the counts of different events are shown in the next sections. Table 9 and Figure 29 depict the results of when the experiments were performed on rats. Table 10 and Figure 30 depict the results of when the experiments were performed on mice. In both the cases, the results are further classified based on the dye that was injected into the animal.

We note that in the case of higher signals with FITC-S, the percentage is quite high in rat experiments (25%) while in mice it stands at 9%. Values that are close to 2000 units of signal strength (>1750) loose the signal strength due to quenching -where high concentration of dye attenuates the signal peaks- and hence the overall occurrence rate of the event of high signal further increases [59, 60].

Table 8: Percentage occurrences with FITC-S in rats. *Four users were recorded to have used FITC-S dye for GFR measurements using the transcutaneous device on rats. The peak value of the signal curve from the device was recorded and counted for the range in which the value falls.*

Range	User 1	User 4	User 5	User 6
<500	16.3 %	4.5 %	0.3 %	1.0 %
500-750	14.1 %	22.3 %	0.3 %	6.1 %
750-1750	50.4 %	69.1 %	64.2 %	55.6 %
1750-2000	8.9 %	2.2 %	16.4 %	9.1 %
>2000	10.4 %	2.0 %	18.9 %	28.3 %

Table 9: Percentage occurrences with ABZWCY-HβCD in rats. *Two users were recorded to have used ABZWCY-HβCD dye for GFR measurements using the transcutaneous device on rats. The peak value was counted for the range in which the value comes.*

Range	User 8	User 6
<500	9.7 %	4.4 %
500-750	43.3 %	19.3 %
750-1750	46.9 %	74.7 %
1750-2000	0.0 %	1.2 %
>2000	0.0 %	0.4 %

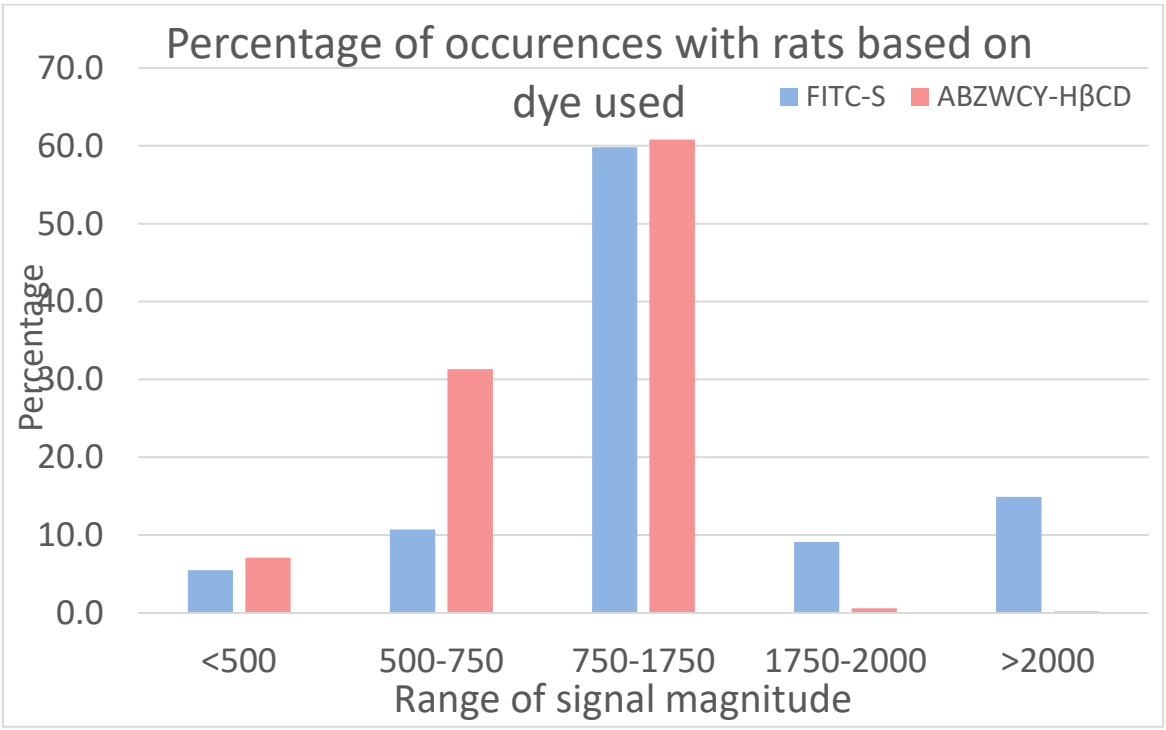

Figure 29: Percentage of occurrences in rats based on dye. *Bar graph representation to depict the frequency at which the signal falls into the respective magnitude ranges for experiments performed on rats.*

Table 10: Percentage occurrences with FITC-S in mice. *Three users were recorded to have used FITC-S dye for GFR measurements using the transcutaneous device on mice. The peak value of the signal curve from the device was recorded and counted for the range in which the value falls.*

Range	User2	User3	User7
<500	21.3 %	3.0 %	44.4 %
500-750	13.8 %	4.2 %	44.4 %
750-1750	50.0 %	80.2 %	11.1 %
1750-2000	11.3 %	7.2 %	0.0 %
>2000	3.8 %	5.4 %	0.0 %

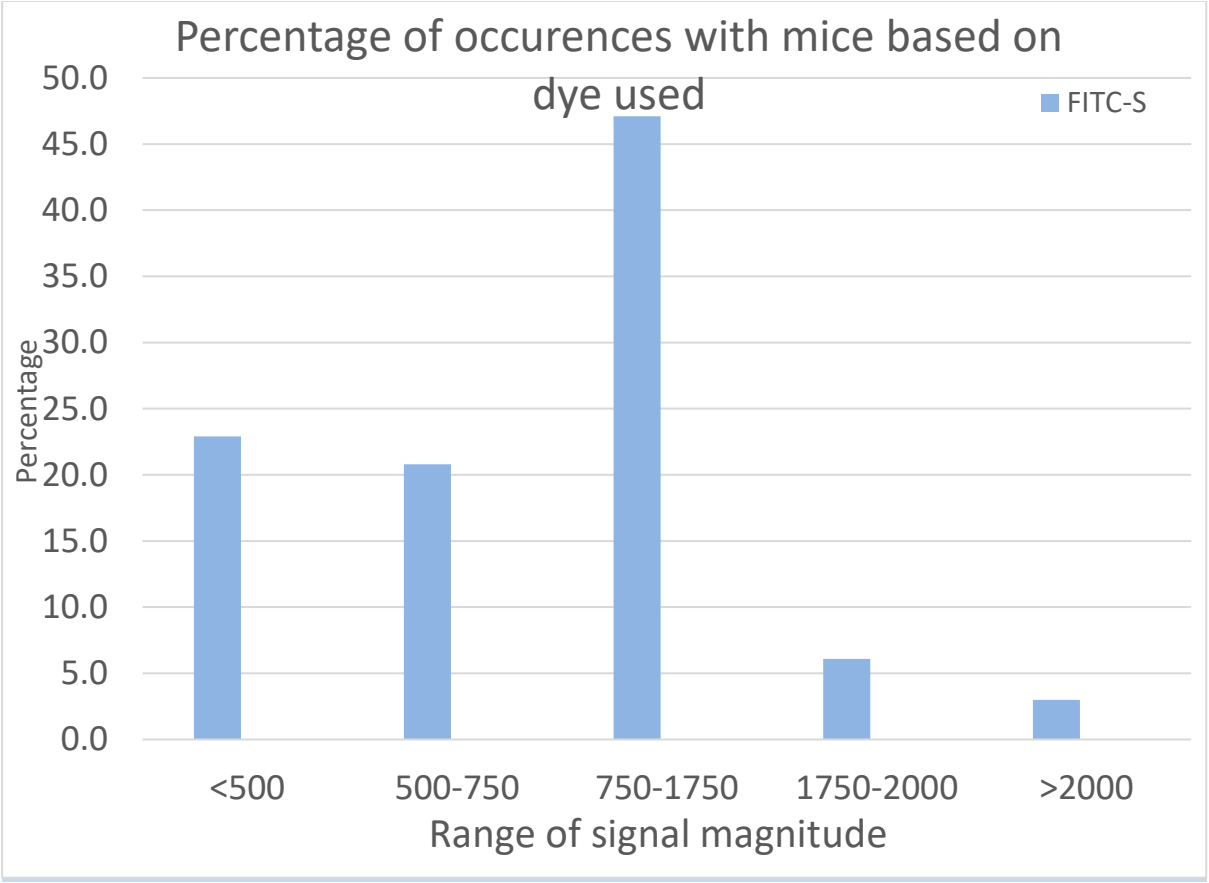

Figure 30: Percentage of occurrences with mice using FITC-S. *Bar graph representation to depict the frequency at which the signal falls into the respective magnitude ranges for experiments performed on mice.*

From the above graphs we can conclude that there is a pressing need to solve the issues that arise as a result of dosage errors. More than one in five experiments that are performed result in a situation where the signal strength does not fall into the desired window.

Our goal is to take these issues into consideration while designing the new device which will be capable of dynamically processing the signal to be more readable facilitating the eventual estimation of the kidney function. In addition to the electronic processing, the design and layout of the new device will be such that the user will have a flexibility in choosing different combination of LEDs and photodiode to be able to fetch a resultant signal which is suitable for estimating different kidney functions.

4.2 LED-photodiode strip results

4.2.1 Test strip with slider mechanism

With the setup described in section 3.5, we started with a distance of 5mm between LED and photodiode, which can be incremented in multiples of 5. The current from the photodiode was recorded and plotted to analyze the decay rate of the signal with increasing distances. Red and IR LEDs were used in two separate measurements at increasing distances (Table 11).

Table 11: Current measurements with Red LED and IR LED. *The value of the current in milli-amperes is shown for increasing distance between red LED and PD**.***

Distance	PD Current (Red)	PD Current (IR)
5	6.2	5.1
10	0.9	2.2
15	0.51	0.66
20	0.28	0.28
25	0.22	0.18
30	0.16	0.16
35	0.1	0.07

4.2.2 Test strips on flexible base

The results from the setup with flexible LED-PD strip described in section 3.5.2 are shown below. The curve fitting to show the exponential decay of current magnitude with increasing distances is shown in Figure 31 and Figure 32 for red and IR respectively.

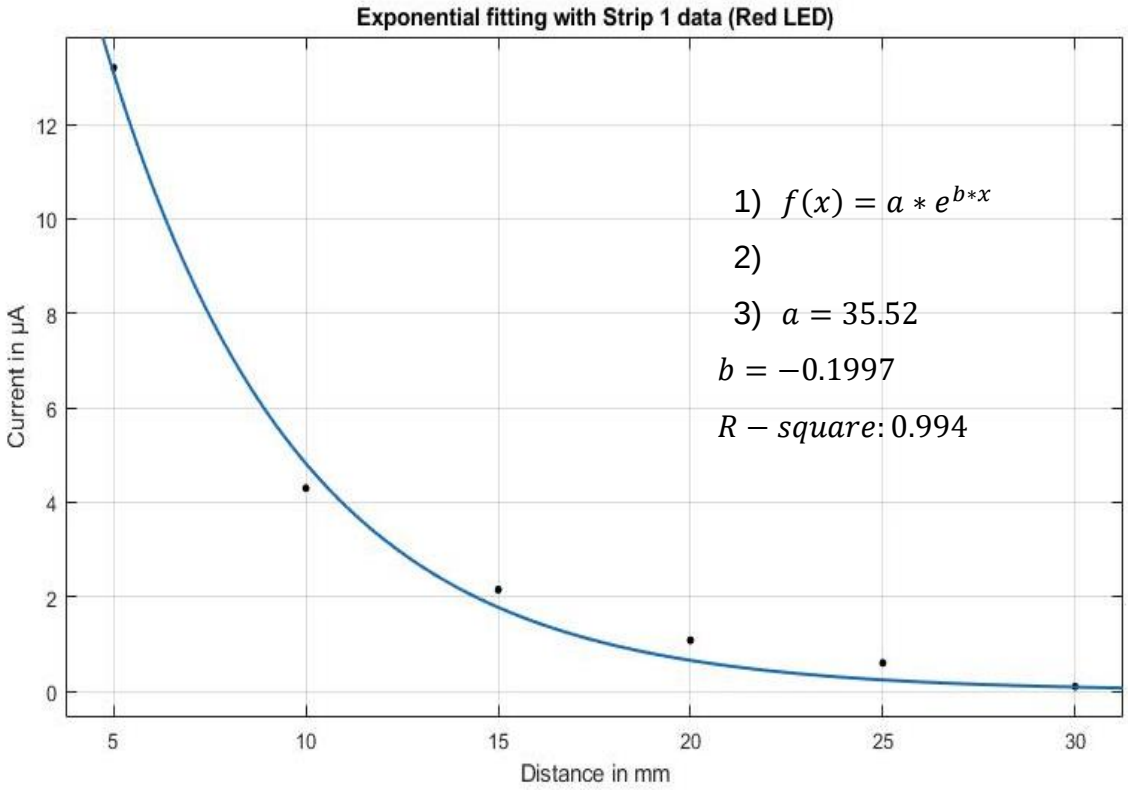

Figure 31: Curve-fitting of signal data from each photodiode with red LED switched on.

Curve fitting performed on the data points plotted on current versus distance graph in MATLAB software. The result is an exponential decay.

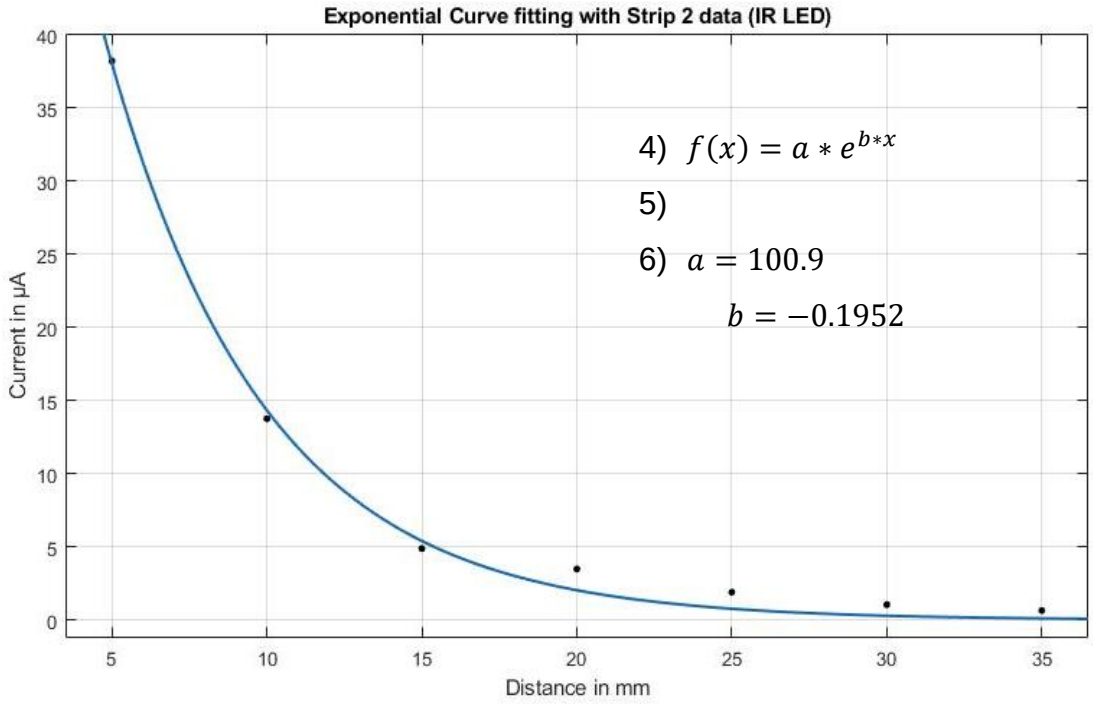

Figure 32: Curve-fitting of signal data from each photodiode with IR LED switched on.

Curve fitting performed on the data points plotted on current versus distance graph in MATLAB software. The result is an exponential decay.

From the above experiments, it is evident that the signal strength is greatly influenced by the distance between the photodiode and the LED. This effect can be utilized to find a solution for the over-dosing and under-dosing issues that were encountered previously. When the device signal overshoots, an LED-PD pair which is more distant from each other can be considered for further evaluation as the resultant signal will have a lesser magnitude eventually avoiding peak loss.

4.2.3 Effect of single versus dual LED

Comparison of power measurements with single and dual LED illumination in ten repetitions is tabulated in Table 12. A significant difference in the light intensity was observed by performing a t-test on the data measured.

Table 12: Current at single VS dual LED illumination. *Power values in milli-watts using the device with two LEDs. Experiments were performed two times- first with both LEDs switched on and then with just one of the LED switched on*

Dual LED power (mW)	Single LED power (mW)
0.27	0.15
0.26	0.15
0.27	0.14
0.29	0.14
0.24	0.15
0.28	0.15
0.31	0.16
0.27	0.15
0.28	0.15
0.28	0.15

The Student's t-test was performed to check if there was a significant difference between the two cases.

Table 13: Mean value of power with single and dual LED

LED	Dual	Single
Mean	0.273	0.148
p-value	1.44E-15	

From the p-value (1.44*10-15), we see a significant difference of intensity through the tissue with single and dual LEDs. Thus, having multiple rows of LEDs may solve the problem of dosing. The concept behind such a solution is that, since overdosing results in a very high signal from the photodiode (saturated signal), we can utilize the signal resulting from the combination of LED-PD which are placed at larger distances, hence giving a signal which has acceptable magnitude range.

4.3 Experimental validation of device functionality

4.3.1 Results from device with frontend

Several different experimental trials were performed by changing the values of the device parameters as described in the previous sections. The optimum values were then obtained (Figure 33) and measured (Figure 34). These were obtained after repeated measurements with different parameters.

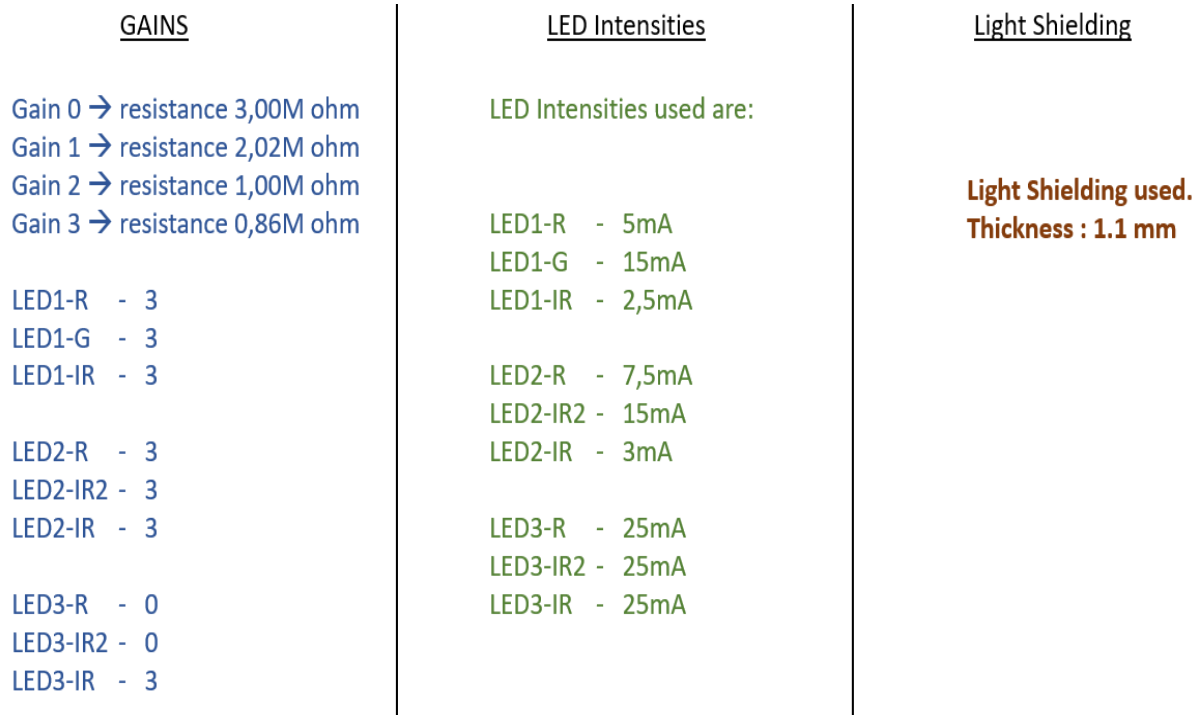

Figure 33: Device parameters during validation

We saw that the signal strengths (from both red and infrared) reduced as the distance between the photodiode and the LED pair increased. Position 1 is closest to the photodiode followed by position 2 and position 3 and thus gives the strongest raw signal intensity, followed by Red 3. Upon pressure cuff changes, indicated by arrows in the graph, the raw signal intensity drops to become high again – at the same level in Red 1 with a mild decrease over time. The signal intensity from Red 3 shows steeper/pronounced responses. Raw values after cuff pressure use exceed the initial resting value. The amplitude of signal change is most pronounced in Red 3, followed by red 1 and then red 2.

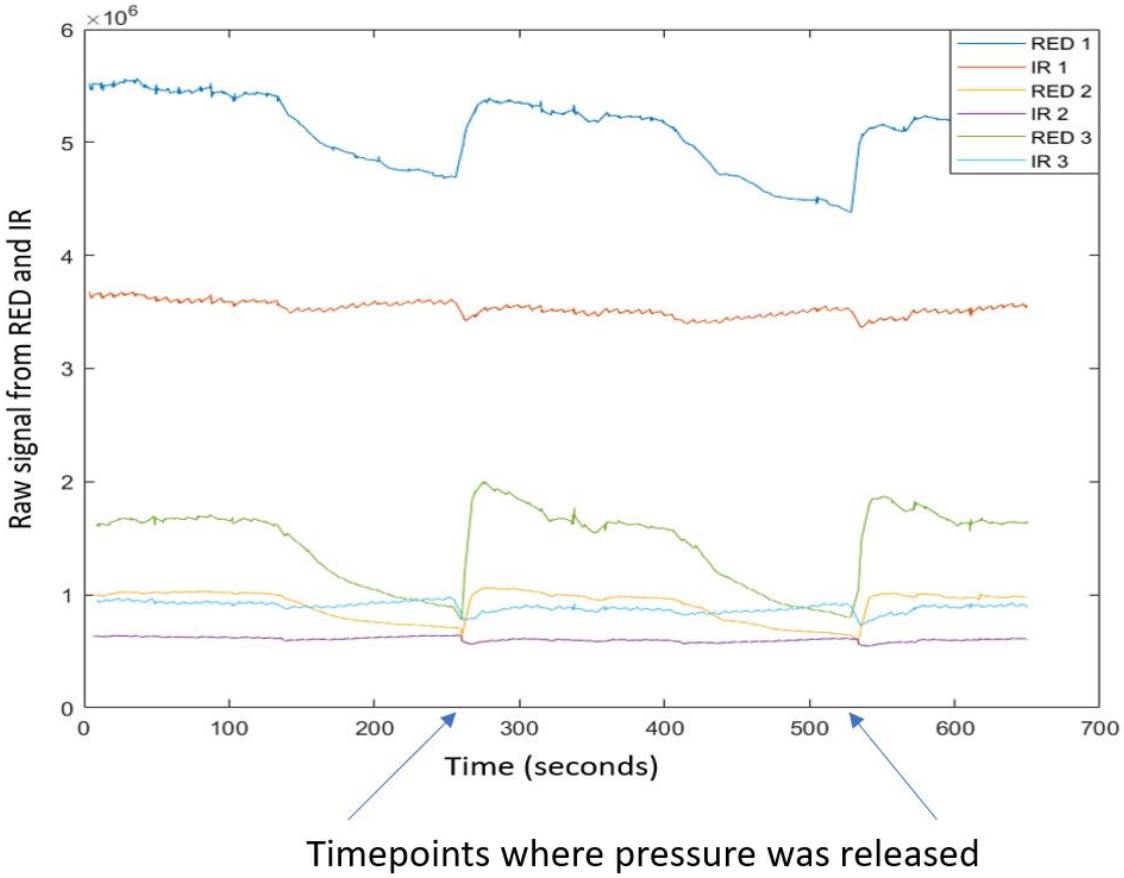

Figure 34: Results of three LED positions after optimizing parameters.

4.3.2 Penetration depth of the signal

It can be seen from the previous section that as the pressure cuff is released the instant where the red signal shoots up perfectly coincide with the sharp dip in the infrared signal. This is better observed in positions 2 and 3. This means that there must be some distance between the source and the detector for the light to travel through the tissue to penetrate deep enough and catch a meaningful signal (Figure 35).

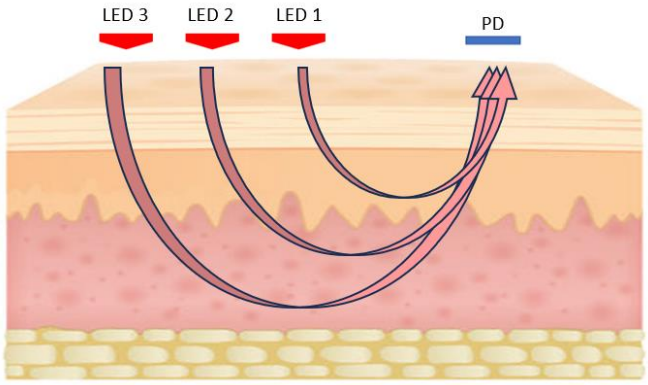

Figure 35: Light propagation at different source-detector separation

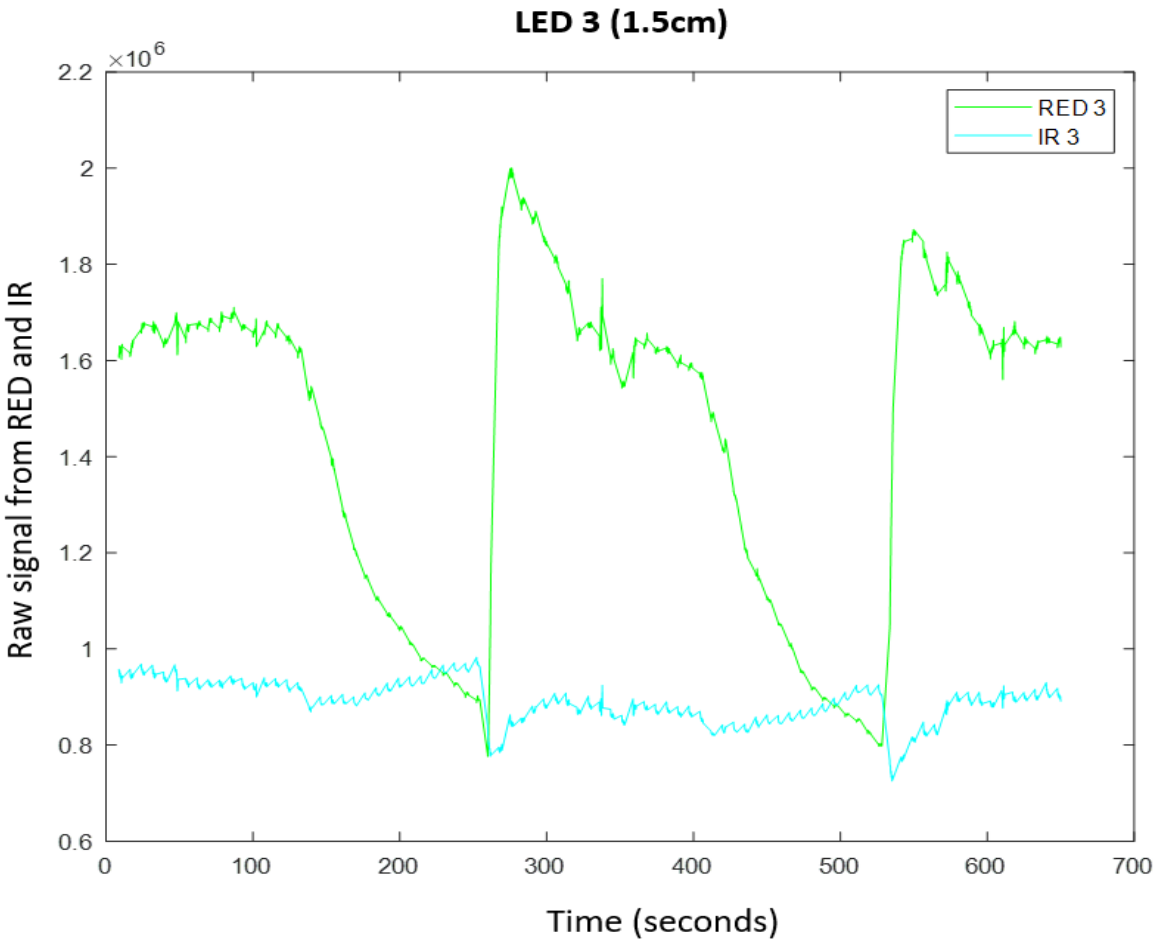

Figure 36: Closer look at position 3. *The signals from position three are shown. At around 270 seconds of time, the point at which the pressure is released, the red signal shoots up while the infrared signal dips at the exact instant of time.*

The results from position 3 are magnified and shown in Figure 36 to observe the described signal changes.

The ratio of the signals (Figure 37) has been shown to further explain how the signal peaks tend be more defined at position 3 upon comparison. At position 1 the signal peak is diminished due to the diminished red signal at this distance. Thus, an optimum distance between the LED and PD is crucial to get a meaningful signal.

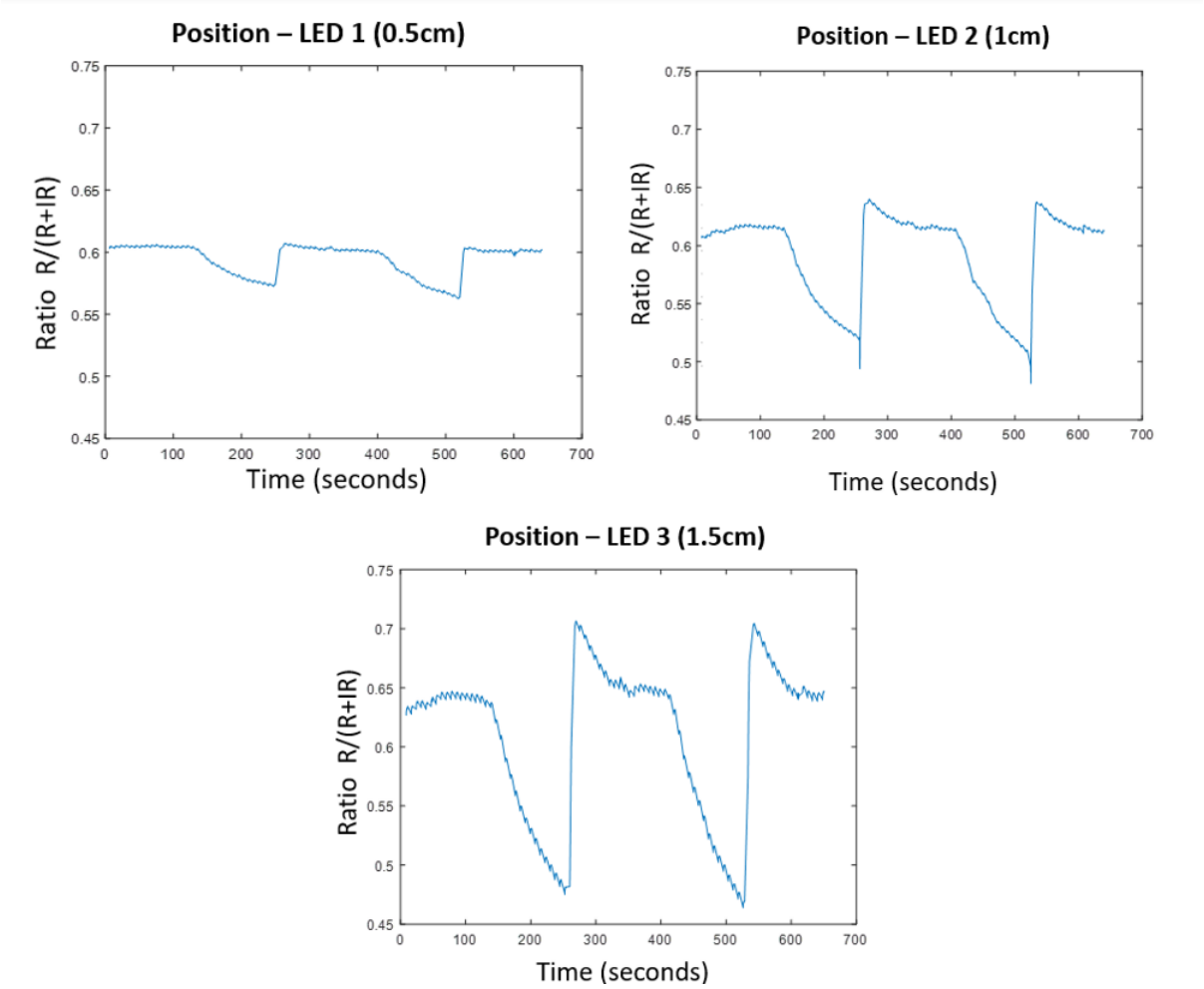

Figure 37: Ratio of signals at three positions

4.3.3 Comparison with other devices

To compare the results with other available oximetry devices, we use a ratio of the signals from red and infrared (which basically is the ratio of the concentration of oxygenated hemoglobin over deoxygenated hemoglobin) to depict oxygenation value [61]. Since we find the best results at position 2 and 3, for comparing, we use the ratio signal from position 3 and the signals from two other commercially available devices (O2C and MOXY). We normalize all the signals from each device in a range of zero to hundred to study the change of signal curves at different time points. Such a comparison is shown in Figure 39. The arm with all three devices is shown in Figure 38. It can be seen from the comparison that the rise and fall of oxygenation aligns over time with all the three signals. The purpose of this comparison is to provide a similarity in the signal response from the new device to other device caused due to the blood flow restriction (pressure cuff).

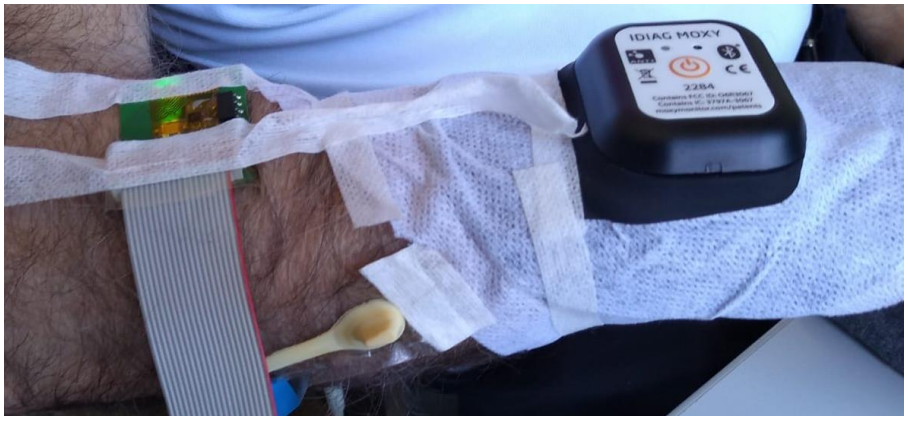

Figure 38: New device along with MOXY and O2C. *The green front end on the left side of the figure is the new device. The black rectangular device seen on the right side is the MOXY device used for comparison. Another small sensor placed on the bottom between the two devices is the O2C device which is also a commercially available system.*

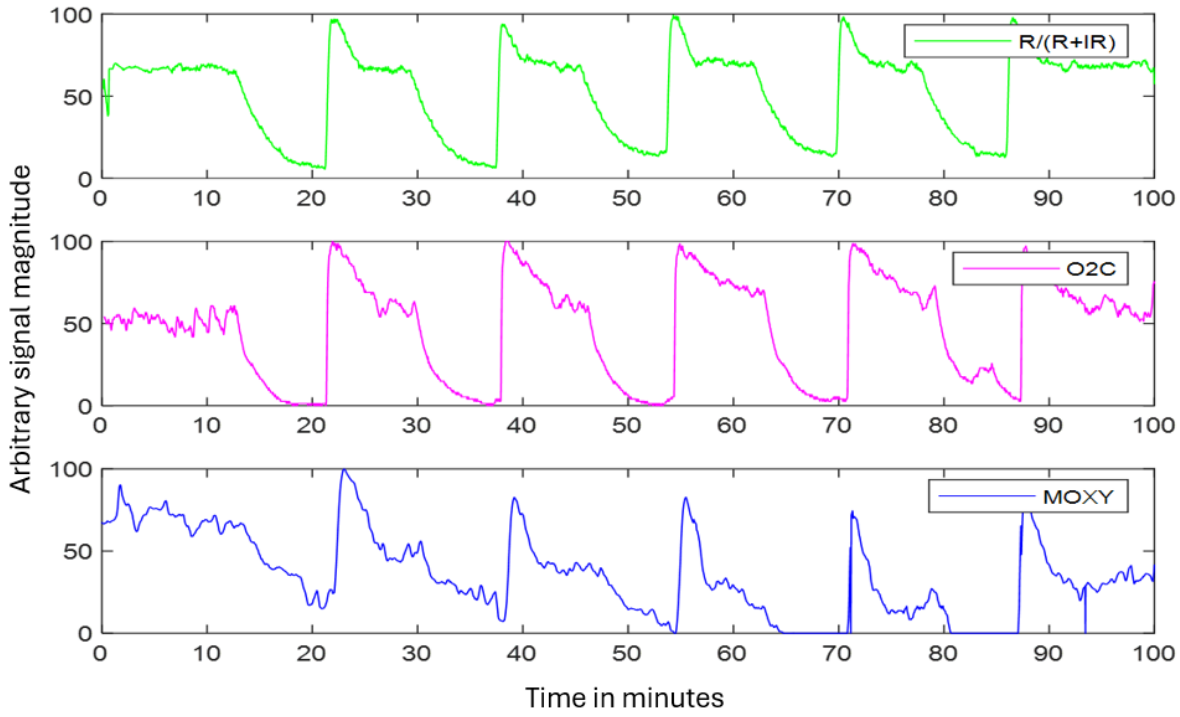

Figure 39: Comparison of device validation results with other oximeters

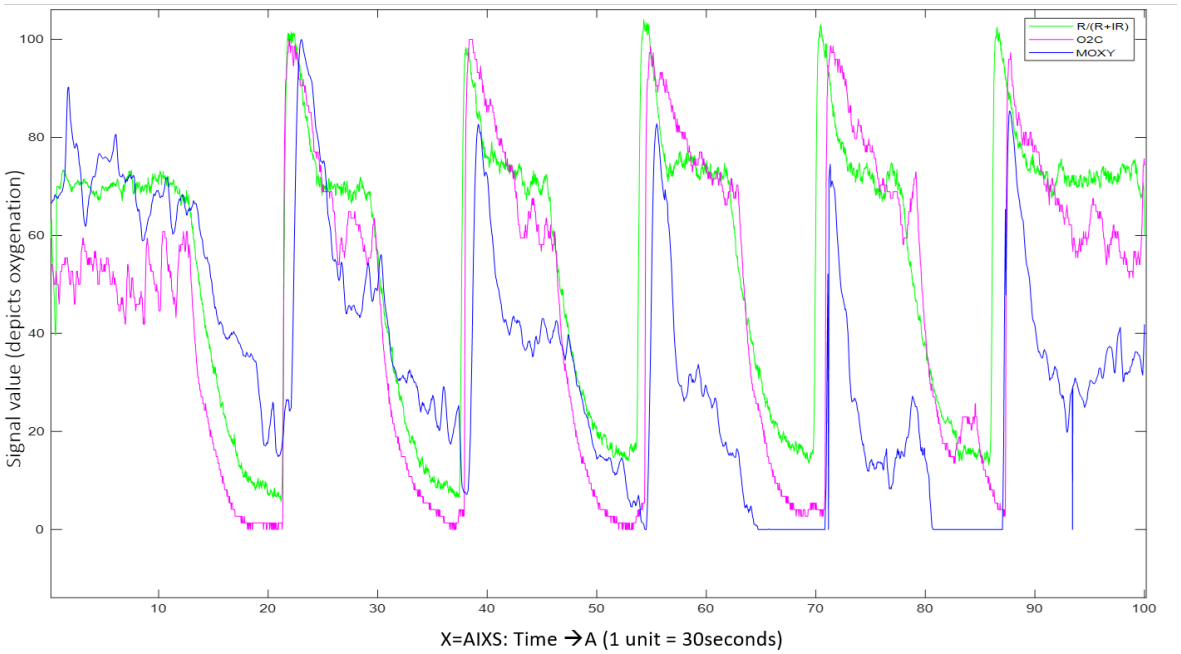

Figure 40: Overlay of signal from the three devices

4.3.4 Light Shielding

Without the use of a proper fixation patch, the results were found to be very prone to serious errors, especially at longer distances. Figure 41 shows the front end on the forearm without a fixation patch.

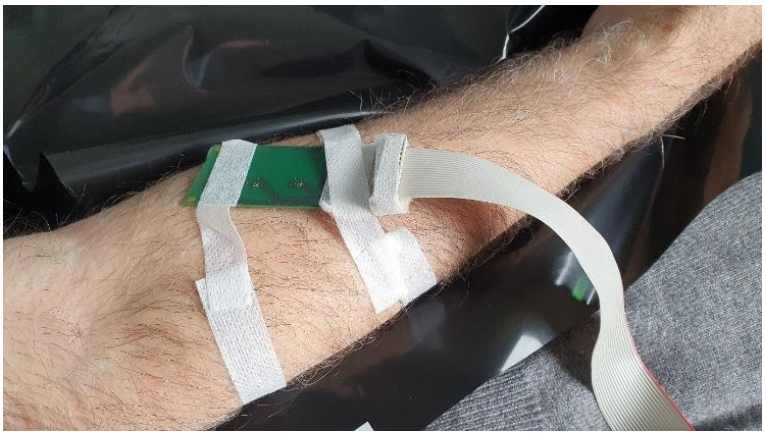

Figure 41: Fixation of device without a light shielding patch. *Unstable device fixation on skin due to the size and rigidness of the device.*

The results at three positions from this experiment are shown below in Figure 42. It can be seen that the signal is noisy at position 1 and 2 (ambient light and fixation error). The signal at position 3 is almost flat with random noise (definite fixation error).

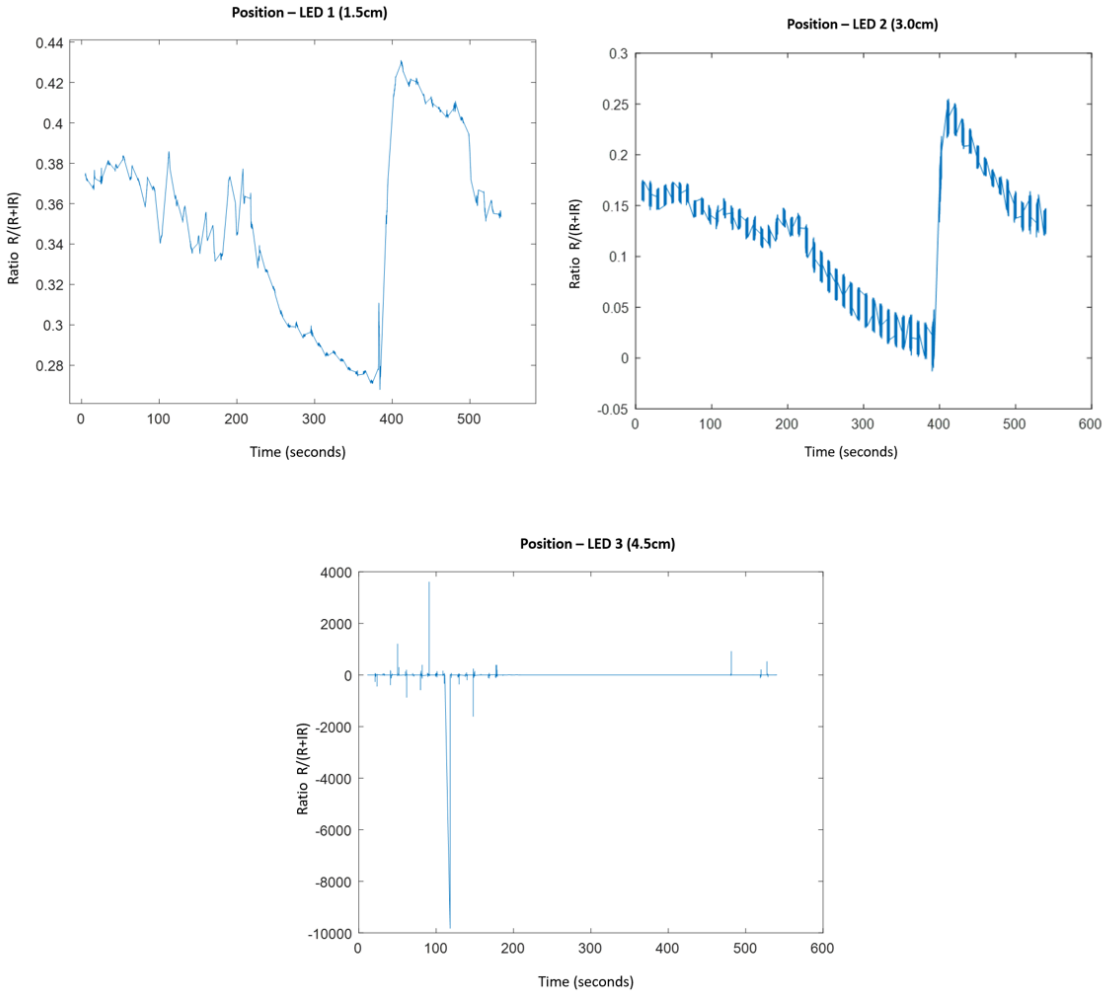

Figure 42: Signal from three positions without light shielding patch. *Ratio(R/(R+IR)) at three positions is shown. Since the device is not fixated firmly, the result gets more noise and distorted as the distance increases resulting in just noise at 4.5cm.*

The addition of a light shielding patch which provides better fixation, provides a much more meaningful signal with less ambient light and better peaks as shown in Figure 44. Without the use of a proper fixation patch, the results are found to be very prone to increased noise making the signal unreadable, especially at longer distances. The fixation patches are shown in Figure 43. The signal from LED3 without a fixation patch has just noise and does not follow the expected pattern showing peaks. However, upon addition of the fixation patch, the signal follows the expected trend over time. Thus, it is crucial to incorporate a patch between the skin and the device surface which prevents the LED light directly hitting the surface of the photodiode in addition to providing ambient light insulation. This also ensures a standardized pressure with which the device sits on the skin unlike using an elastic band or adhesive tape. A double-sided

adhesive patch with cut-outs for LED and PD were developed for each device version and successfully tested.

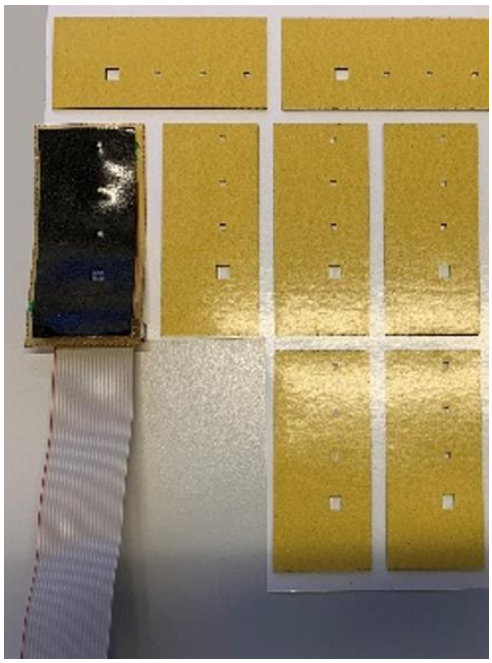

Figure 43: Light shielding patches. *Fixation patches used for the front end for proper fixation on the skin surface.*

We also performed experiments with two different thicknesses of the light shielding patch (1.1 mm and 2.04 mm). It was found that the thickness also had a significant effect on the amplitude of the signals (Figure 45).

The absolute value of the signal peak and its change in response to the light shielding thickness was also analyzed. We see a significant decrease in the peak value of the signal as shown in Table 14.

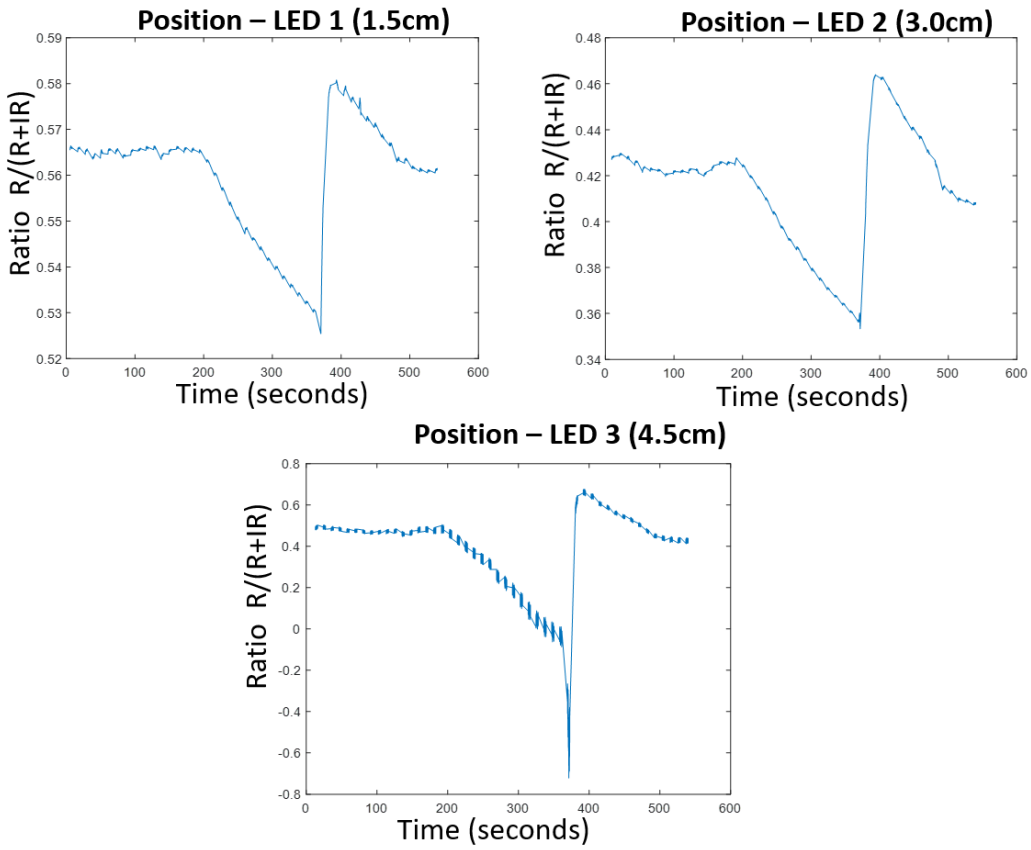

Figure 44: signal from three positions with light shielding patch. *Ratio signal at larger distances shows better results with clear peaks and troughs upon the addition of the fixation patch. The signal is now responsive to application and release of pressure as compared to flat noisy signal seen in figure 40.*

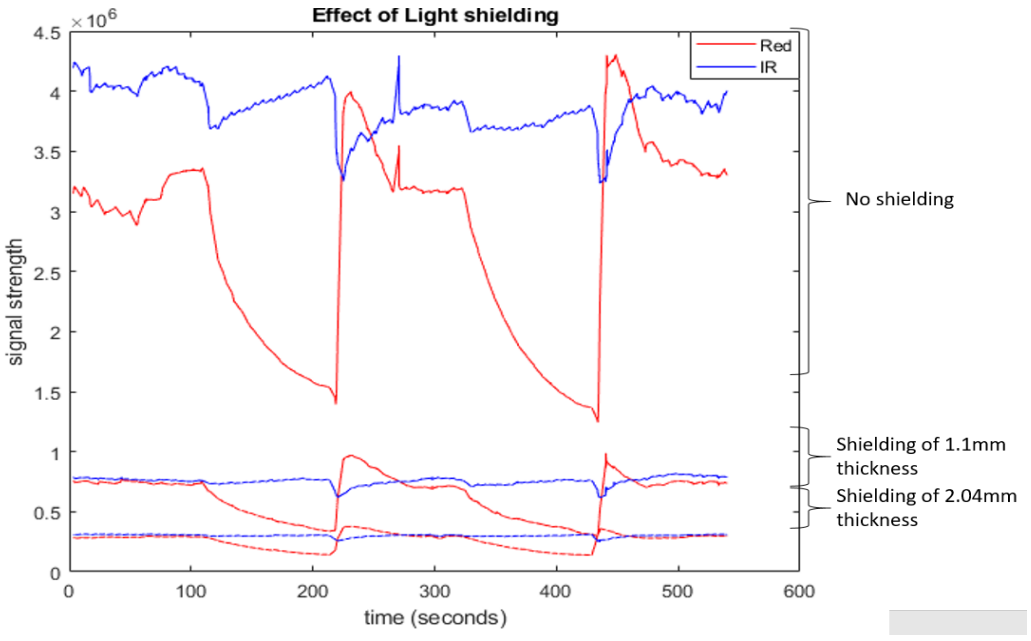

Figure 45: Effect of light shielding patch thickness.

Table 14: Effect of light shielding thickness on absolute value of the signal. *Reduction in the absolute value of the signal is seen upon addition of a fixation patch. As the thickness of the patch increases, the value further decreases. Peaks are not significant at IR illumination, hence the peak values for IR are not given. The trend of signal decay can be observed in peaks as well as the troughs.*

	No light shield		1.1mm		2.04mm	
	Red	IR	Red	IR	Red	IR
Initial signal value	3,191,123	4,198,735	750,996	781,823	282,461	309,757
Peak value	3,951,716		969,269		378,981	
Trough value	1,396,770	3,251,149	342,755	620,085	140,461	257,464

4.3.5 Temperature measurement

To study the temperature changes upon application of the new device on the skin surface, measurements were performed for over 25 minutes. The maximum temperature that was recorded was ~35.2^{o} Celsius (Figure 46) which is well below the standardized limit. Hence, prolonged usage of such a device will not result in any temperature related hazard to the skin.

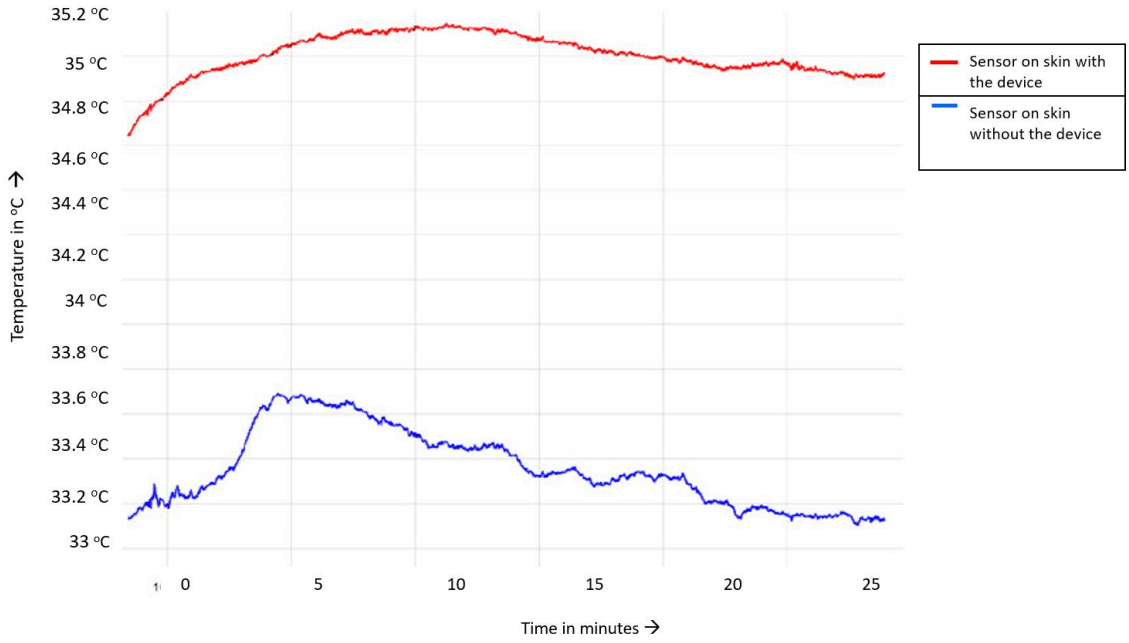

Figure 46: Temperature measurements with and without device

4.3.6 Results from second version

Experiments were performed in an analogous way to the previous version of the device wherein the device was placed on the forearm and measurements were performed based on the oxygenation changes caused by application of pressure cuff. After a few minutes of baseline measurement, we induced pressure for about two minutes after which the pressure is released. Three such cycles were performed with a cooling time of four minutes between every pressure release and subsequent pressure induction.

Results from two volunteer arms are shown in Figure 47 and Figure 48.

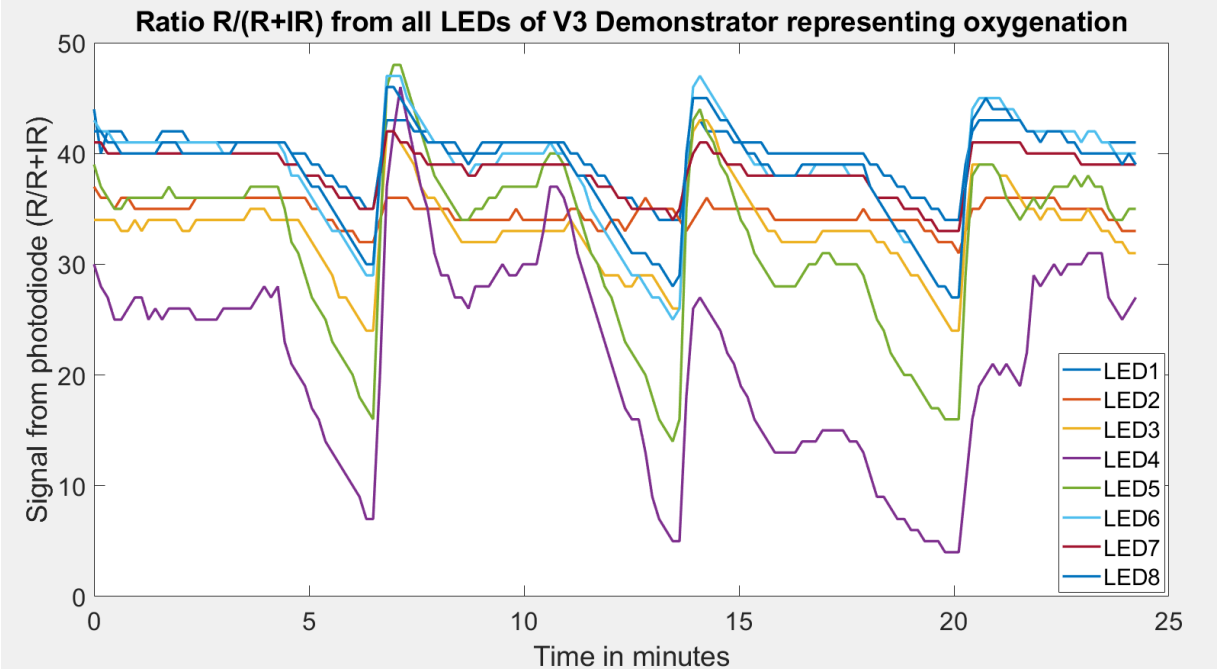

Figure 47: Results from all LED positions in Volunteer 1. *Signals from all the eight positions are shown. All signals are represented as the ratio - R/(R+IR). It is clearly seen that the signals at all positions follow the expected change with respect to pressure cuff application.*

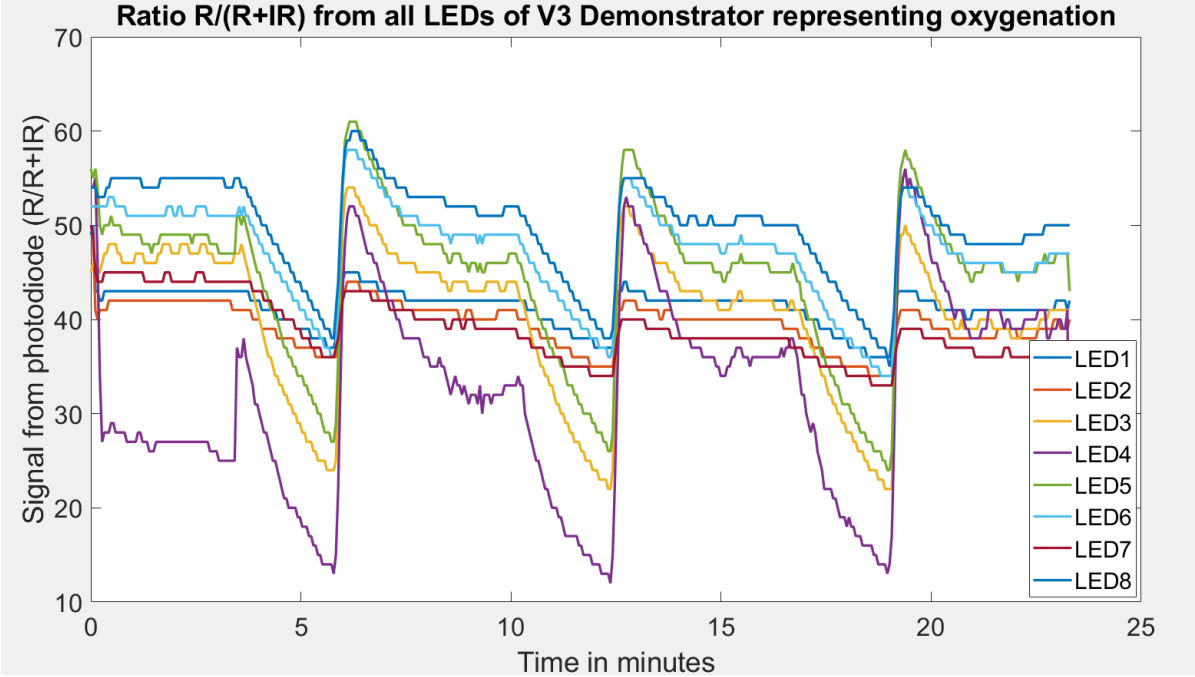

Figure 48: Results from all LED positions in Volunteer 2.

Figure 49 shows a closer look at the signal from one of the LED positions to clearly see the changes in the signal as a response to the pressure cuff.

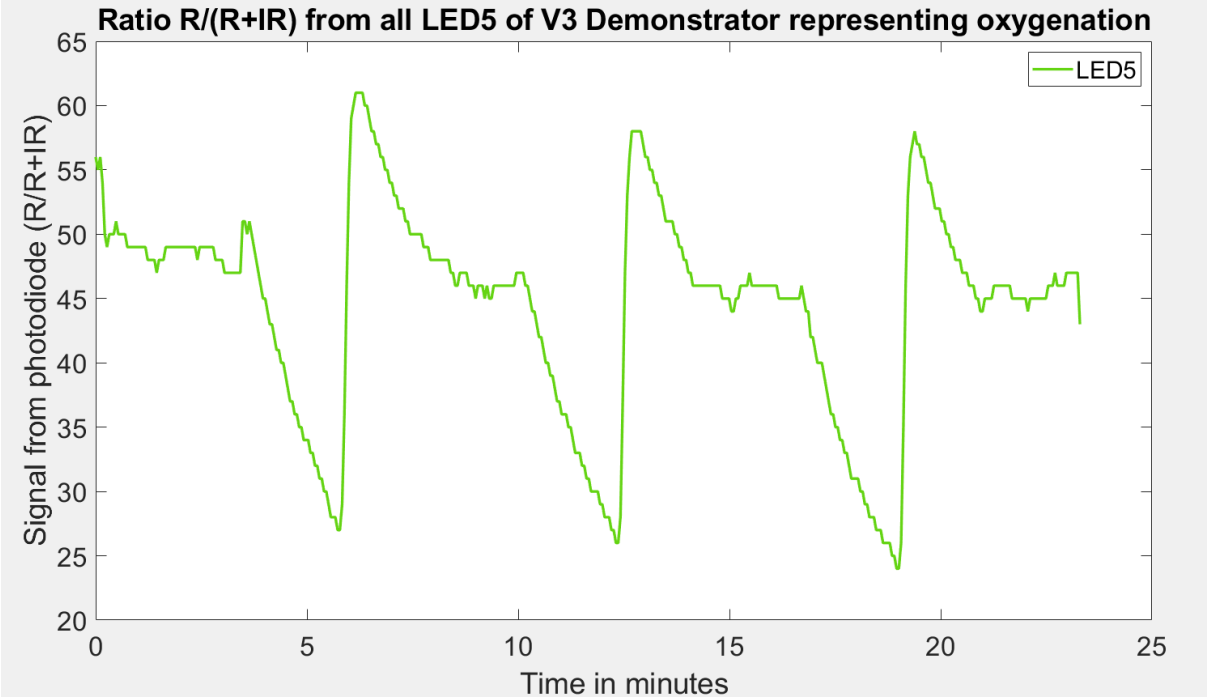

Figure 49: Results from position 5

From the above results, we can conclude that the new device is designed to penetrate deeper into the tissue and the signals obtained are sensitive to the physiological changes. The signal magnitudes shown in the figure have not been calibrated to depict the actual oxygen saturation of the device. The calibration needs to be performed, however the goal here was to verify the fluctuation of the device signal successfully tracks the oxygenation changes in the body.

4.4 Animal Experiments

The device functionality of oxygen measurements was evaluated in comparison with other known devices on animals, in our case pigs, under surgery. In collaboration with the Department of Anesthesia and Intensive Care Medicine of the University of Heidelberg, the devices were used to measure oxygen during the surgery performed by surgeons of the respective department. The goal of the surgery was to assess an external blood volume exchanger based on the phenomenon known as extracorporeal membrane oxygenation (ECMO). Animal experiments were performed under license 35-9185.81/G-9/22 issued by the Regierungspraesidum Karlsruhe.

As part of the surgery, after few minutes of anesthesia, endotoxin was administered to the body to induce a septic shock with subsequent intervention with ECMO to exchange the blood volume using the ECMO device. Two of our devices were simultaneously placed on the skin of the pig and comparison between the measurements was performed. At the start of these experiments, we also tested the devices on the “picnic region” (area near the limbs which are closer to the neck). However, as the surgeons used surgical saw-cutter during the surgery, there were a lot of artifacts due to movements and vibrations. Hence, the leg ham region of the pig was preferred for our experiments. The flow of the experiments is depicted in Figure 51a.

The devices were placed on both sides of the body as seen in Figure 50.

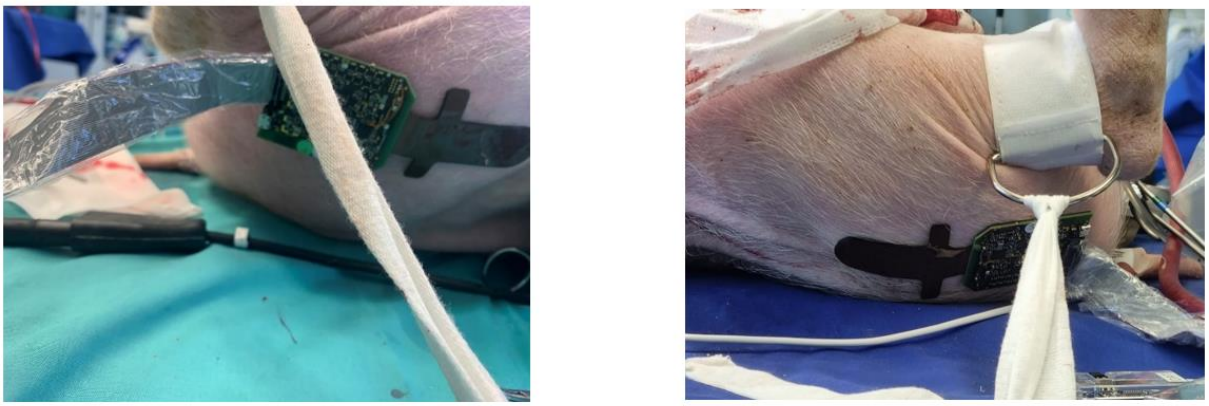

a b

Figure 50: Device version 2 application on the leg ham regions of the pig. *a) right side; b) left side*

The results from both sides were comparable and a similarity of the signal trends from all LED positions was observed (figure 56b and 56c).

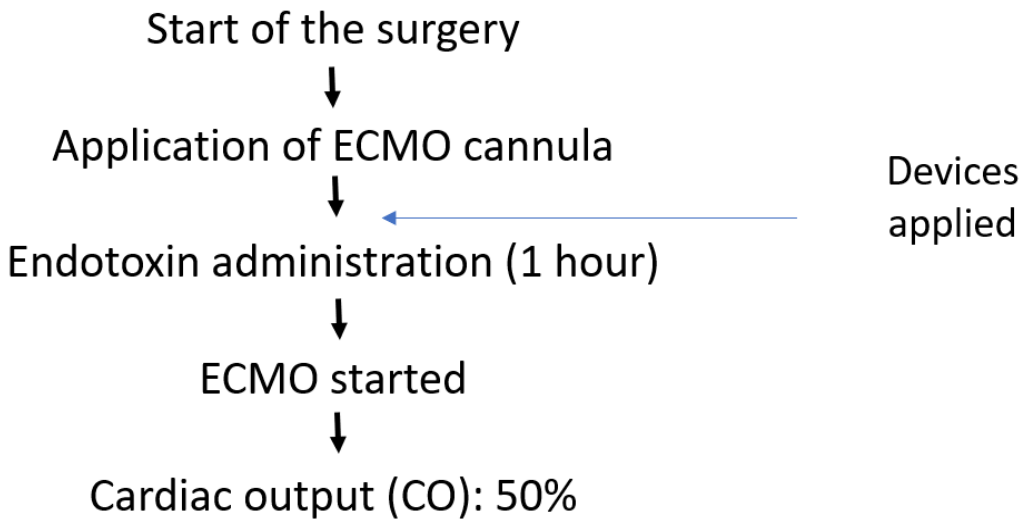

a

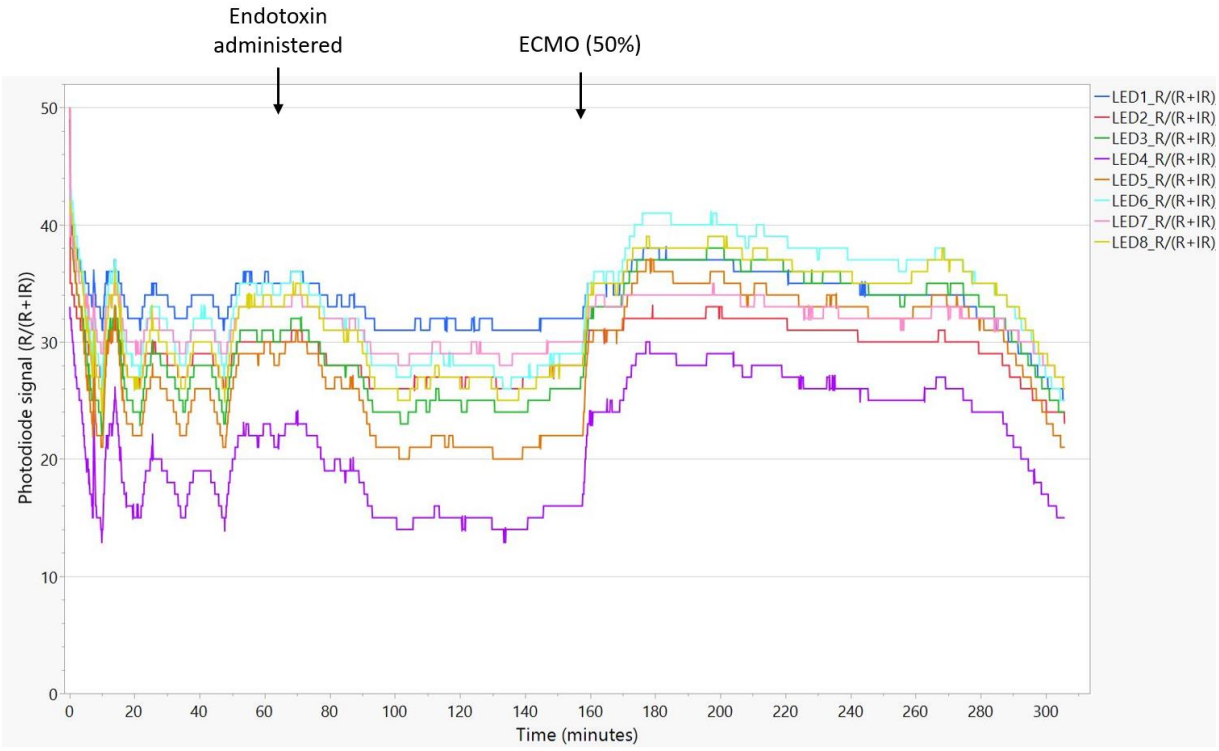

b

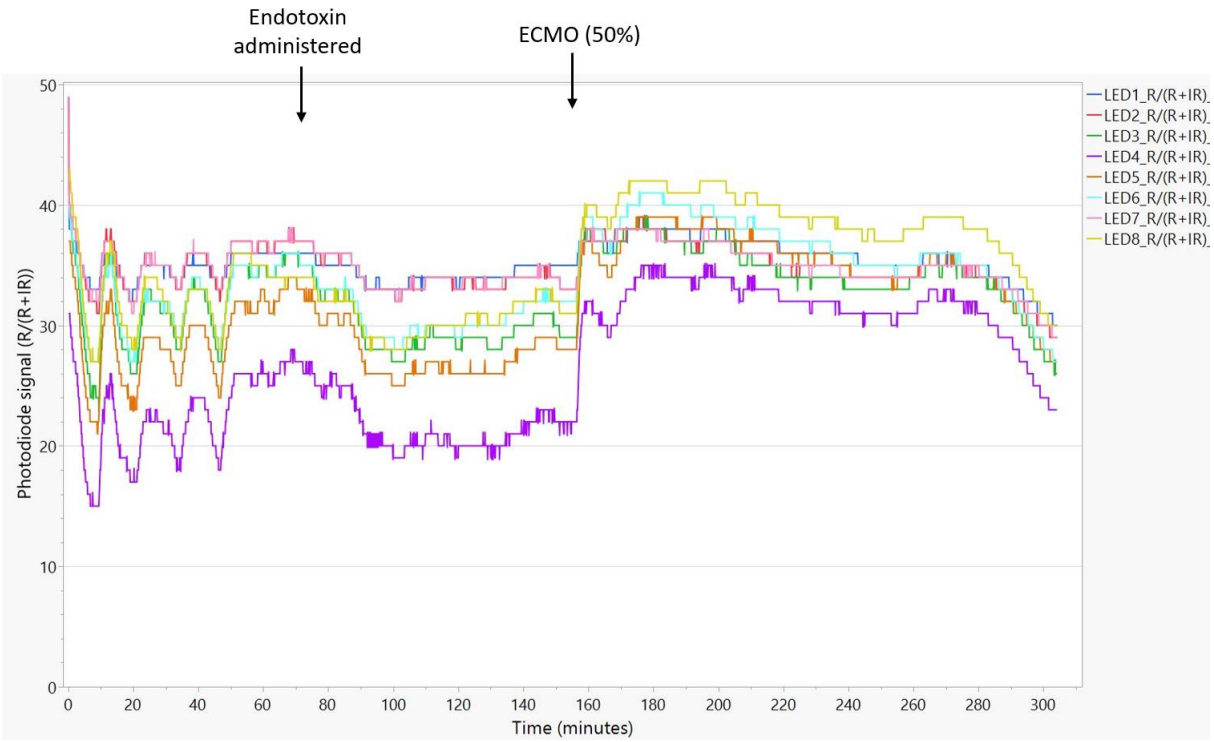

C

Figure 51: Results from two devices during animal experiments. *a) Signals originating from the device placed on the right side. b) Signals from the device placed on the left side.*

4.5 Software for kidney function estimation

Any physiological entity can be described by several different systems or sub-systems put together working in complex collaboration with each other. To study the distribution of a biomarker or a tracer in a body, the most convenient method is to divide the system into one or more parts which are commonly called compartments. The analysis of estimating marker concentration in the various compartments and the diffusion of the marker between them is called compartment modeling.
Several types of compartment models have been described by various researchers. In this project we use a three-compartment model to depict the elimination kinetics of the marker used for glomerular filtration rate estimation. The dye which is used for GFR estimation is ABZWCY-HPβCD [46] , we use the model that has been previously described [45, 62].

To utilize the time during the limitations of Corona period, it was decided to implement a software in advance which can later be modified based on new kinetic models and functionalities of the final version of the device. Development of a software application was not a part of the project initially, but this was rather taken as an opportunity to learn programming in python as there was ample time due to the lockdown period and to compensate the lack of progress in other areas of the project. Hence, based on the three-compartment model, an open-source python application for windows- “Kidney-Func” has been developed which has the functionality of adding up to three models (one, two and three compartments). It also has the framework to add models for the secretion and reabsorption along with the GFR estimation.

The workflow of the python application “KidneyFunc” is shown below:

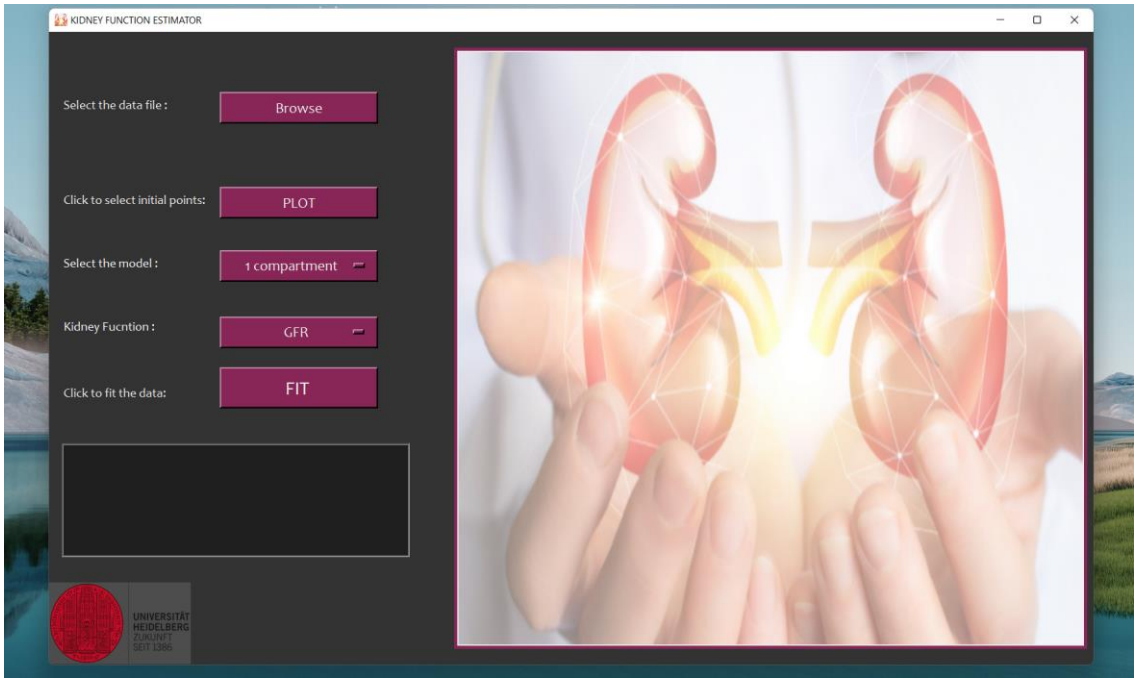

Figure 52: Screenshot of the app's main window. *Here the user has the first option to browse a file saved in the PC. This file contains the raw data of signal values derived from the device's output.*

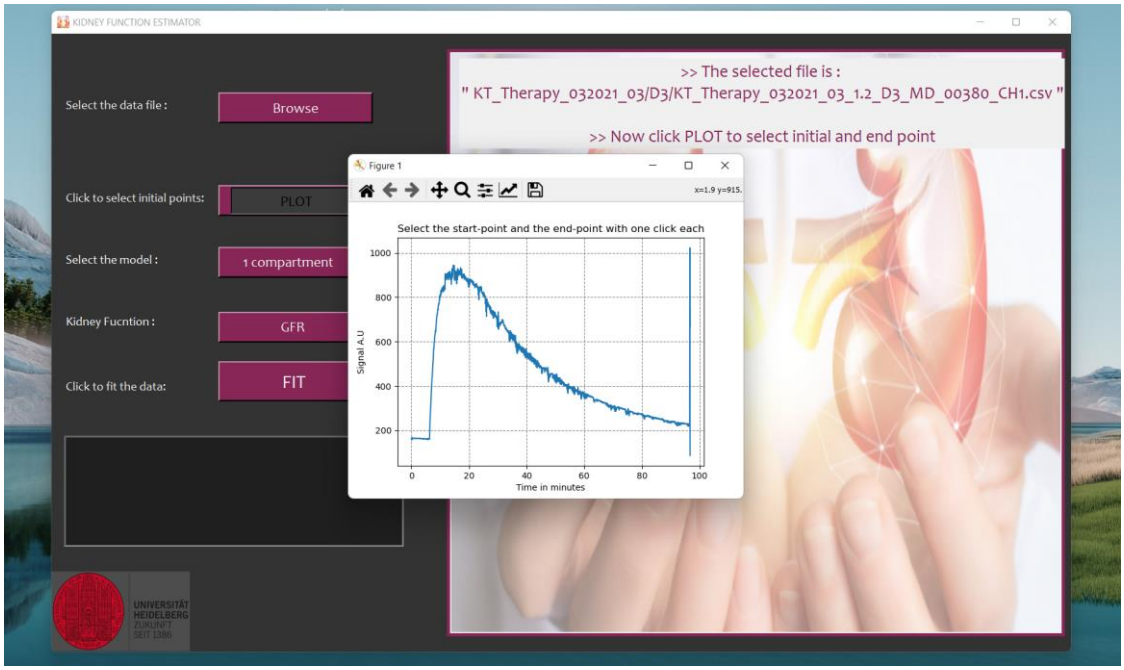

Figure 53: Application showing window pop-up for points selection. *Once the file is selected, the 'PLOT' icon plots the raw data and allows the user to use the mouse to click and select the start-point and endpoint.*

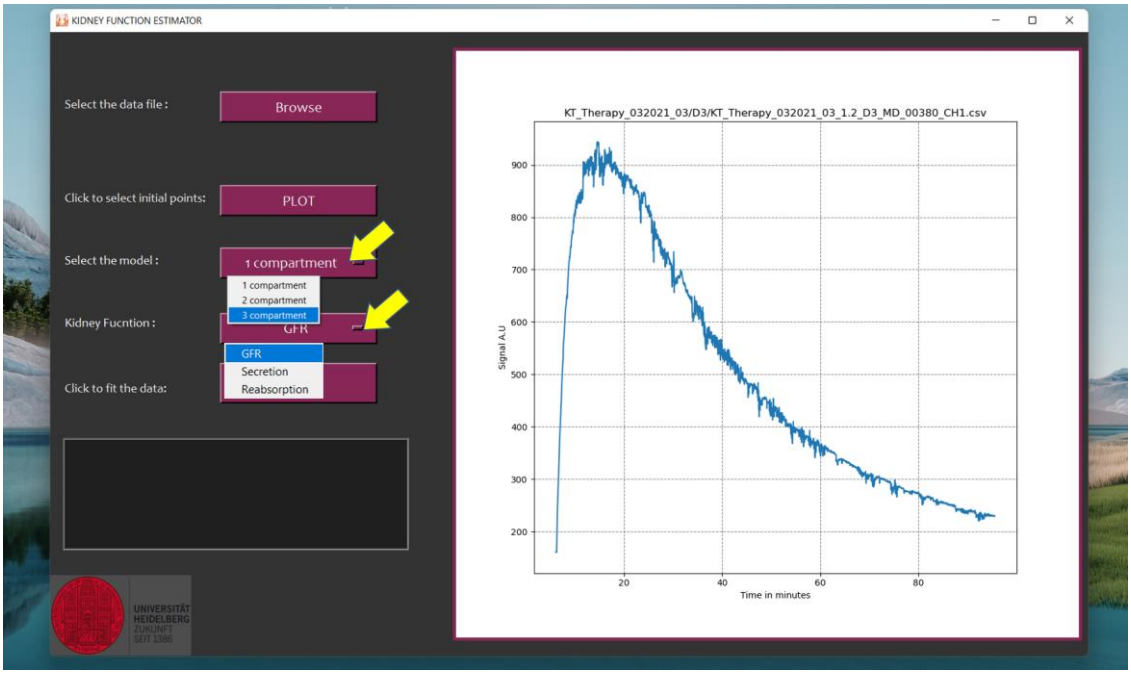

Figure 54: Application showing compartment model and function options. *Here the app snips the data as per the points given by the user and plots the curve. The user then selects the compartment model and the function which is being estimated.*

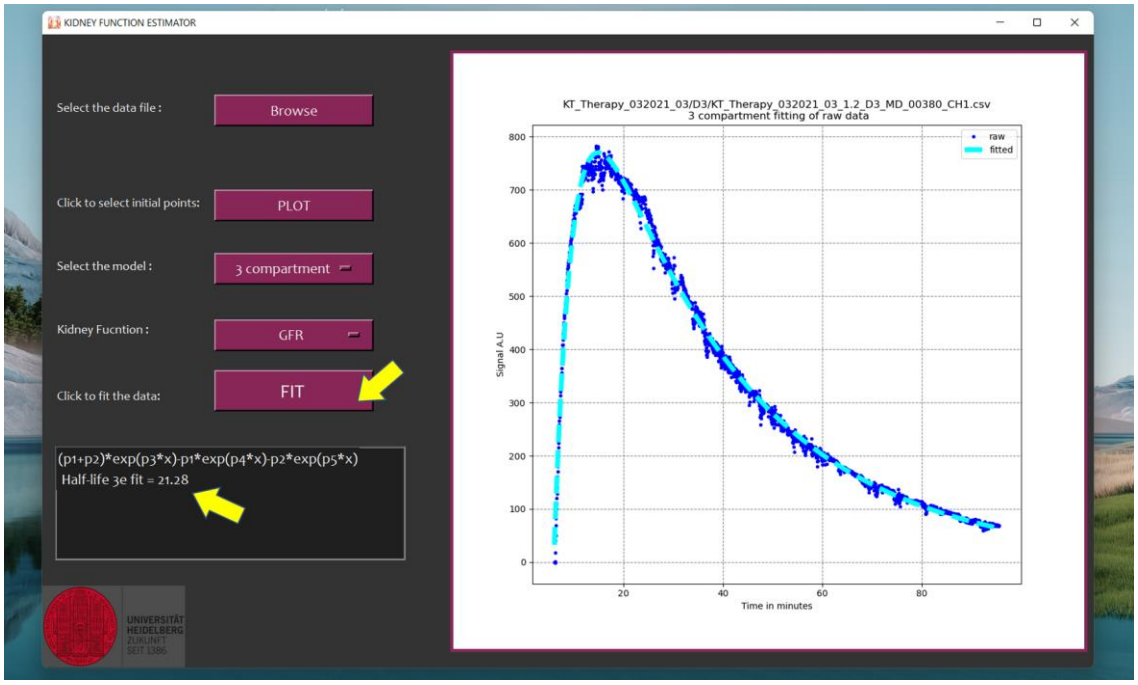

Figure 55: Application window showing equation and curve fitted curve. *The icon "FIT" is clocked to give the final output in the display window shown on the bottom left.*

As seen in Figure 55, once the user clicks on the “FIT” icon, the data points are fitted based on the compartment model chosen (three compartment in this case). The display window in the bottom left also displays the equation of the curve and half-life.
The GFR is generally calculated using an empirically derived conversion formula which is calculated using enzymatic concentration measurements of the dye (marker) [41]. However, the conversion formula is based on assumptions and does not take into consideration the change in vital parameters of the subject- age, bodyweight, sex. [63]. Thus, we only use the half-life value obtained after the data analysis, to give an estimate of the desired kidney function.

Using identical datasets, a comparison of the results was performed with this application along with two other software - Medibeacon’s MBstudio2.0 (Figure 56) and another MATLAB based software (Figure 57) developed previously at ZMF, Medical Faculty Mannheim, UHEI. Figure 58 shows the results from the new KidneyFunc. The results document that the new software results are comparable to the existing software. Thus, the new software has the potential to be used in the future.

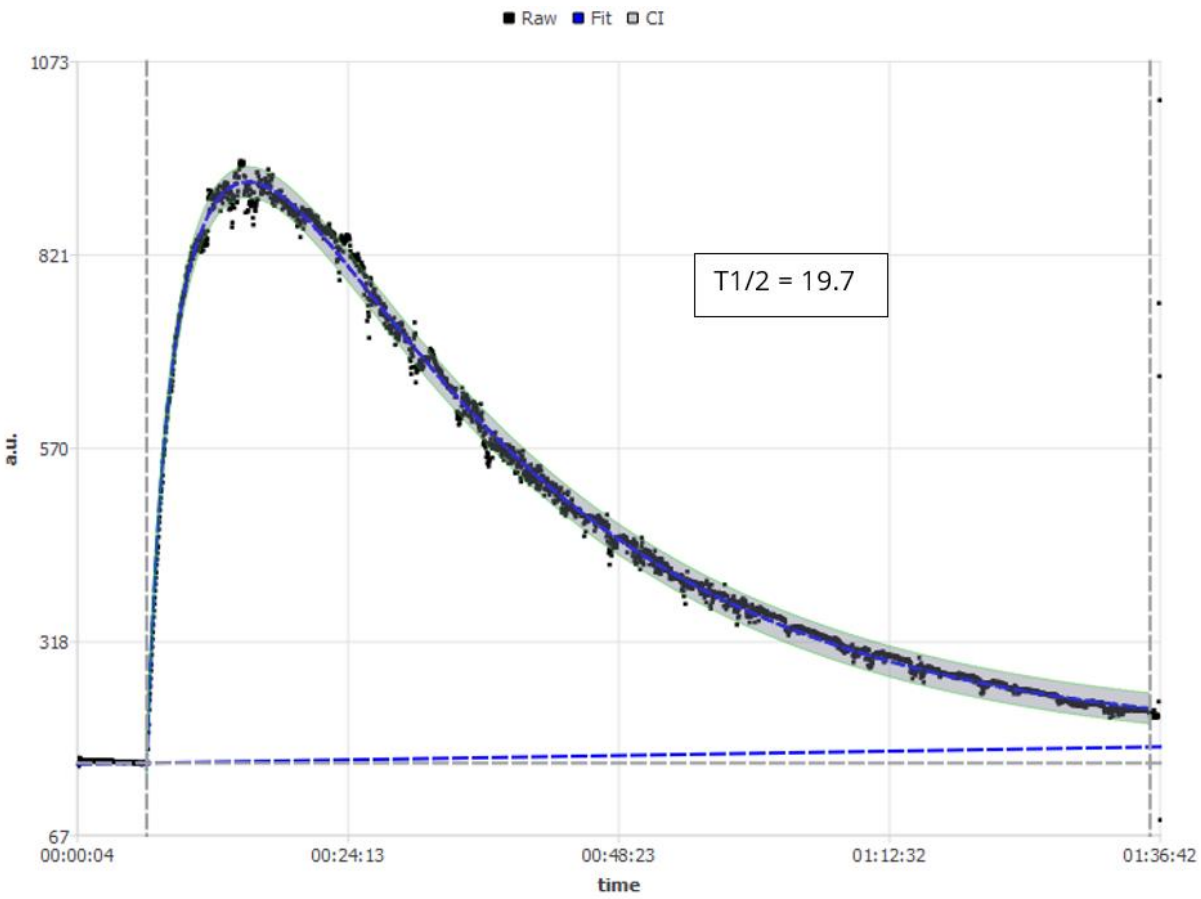

Figure 56: Result using MBstudio2.0.

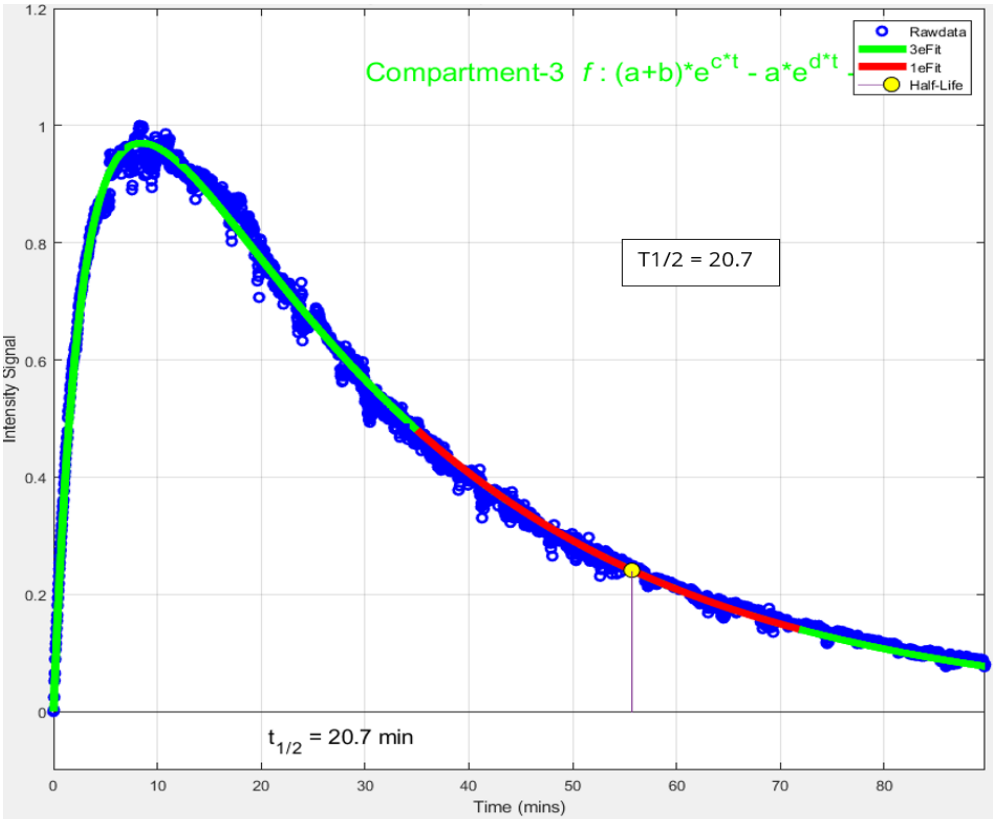

Figure 57: Results using MATLAB software.

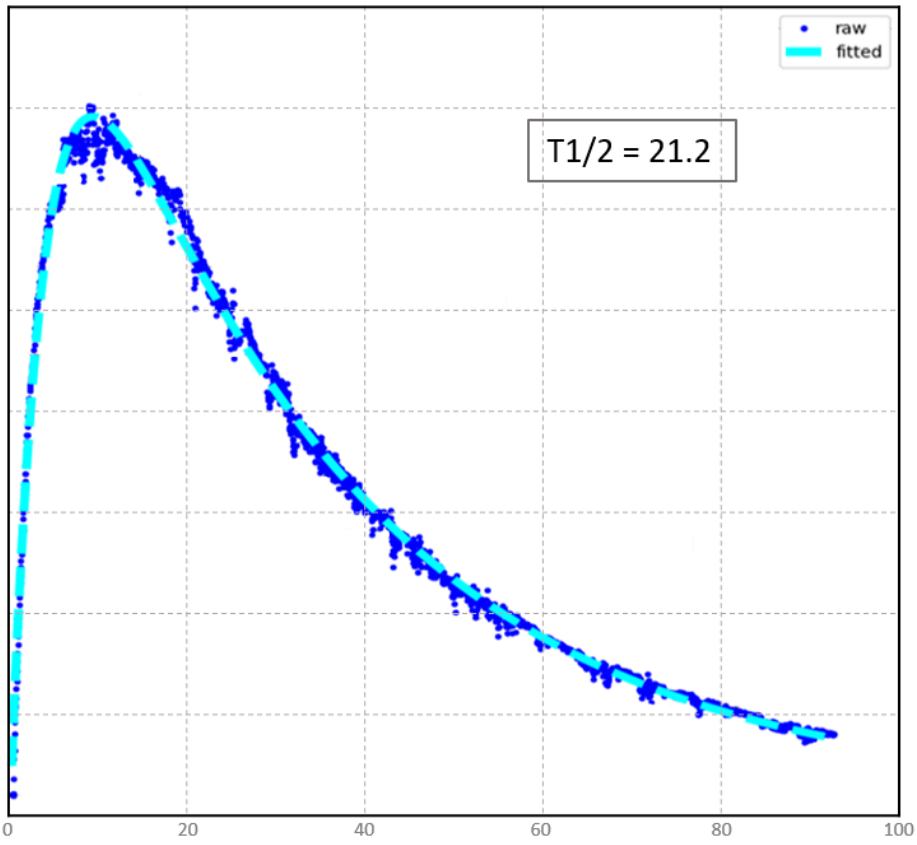

Figure 58: Results using KidneyFunc application.

5 DISCUSSION

The switch from the routine methods to transcutaneous assessment of a GFR marker to monitor kidney function comes with advantages of faster, non-invasive, and more patient friendly procedures. While the most common work in this field has been in combination with light of the visible spectrum, NIR has been gaining focus in the recent times. This thesis provides a foundation for its primary aim which is to potentially measure more than one kidney function using a single device. In addition to the GFR, secretion and reabsorption estimation were also the initial aims. However, these could not be materialized due to a chain of obstacles.

This project was part of the International Training Network “RenalToolBox”. The project was planned to come together with the work and results from other early-stage researchers (ESRs). While this thesis focused on development, optimization, and validation of the device, a second PhD student worked on developing dyes corresponding to the chosen wavelength and capable of mirroring GFR, reabsorption and secretion. It was planned that a third ESR, experienced in animal work in the kidney, applied the dyes plus the device to test it. Based on these data a second optimization step of dyes and device, re-evaluation, and further optimization was planned. Unfortunately, due to the Corona pandemic, this close-cooperation and interlocked work was not possible. Dye development took longer than expected, animal experimentation plans were delayed due to delayed permission of the animal experimentation license. As a fallback strategy we focused on oxygenation and postponed those analyses which required input from the collaborating ESRs. In addition, the software was developed, initially not planned as part of the thesis.

Accordingly, at the present stage, we have proven feasibility and function of the newly developed device to be able to sensitively measure biological processes within the body – in our case oxygen saturation in the skin upon pressure cuff changes in the forearm. The next steps are to validate that the device is truly able to measure kidney function, namely GFR, reabsorption and secretion. To enable this, our device is equipped with 3 LEDs, green, red and IR, which can detect different tracers for exactly these functions. A number of biomarkers have been developed by the partner Cyanagen (Italy) which are specific to the three functions intended to be measured. They

were tested for compatibility with the device LEDs based on their emission spectra. The three LED wavelengths that the device is incorporated with are: red (650nm), infrared (940nm), and green (520nm) (Figure 59). Ms. Srishti Vajpayee from Cyanagen Italy, has worked to develop three biomarkers for the three kidney functions. Based on the previous biological studies, ABZWCY-HβCD dye has been found to be a strong option for GFR estimation [64]. Several secretion and reabsorption markers have also been developed as promising candidates which lie in the wide spectral range of 350 to 900nm. This could be utilized to study the possibility of simultaneous estimation as opposed to sequential assessment of all three functions in the future. Simultaneous infusion and measurement would be time saving but makes the fluorescence detection complex. There are ways to filter and separate signals resulting from multiple emissions, however the detection of multiple colors necessitates a complex setup involving several detectors and precisely aligned filters. Frequency division multiplexing is a well-known method used in microscope imaging to separate fluorescence signals using multiple detectors and filters [65]. In addition to a transimpedance amplifier which we used in our device, a lock-in amplifier is also used in some setups where frequencies of the LEDs are matched with the detection intervals [66]. Nevertheless, our device, due to its compact size and application, has been deployed with a single detector, which currently will be suitable only for sequential measurements.

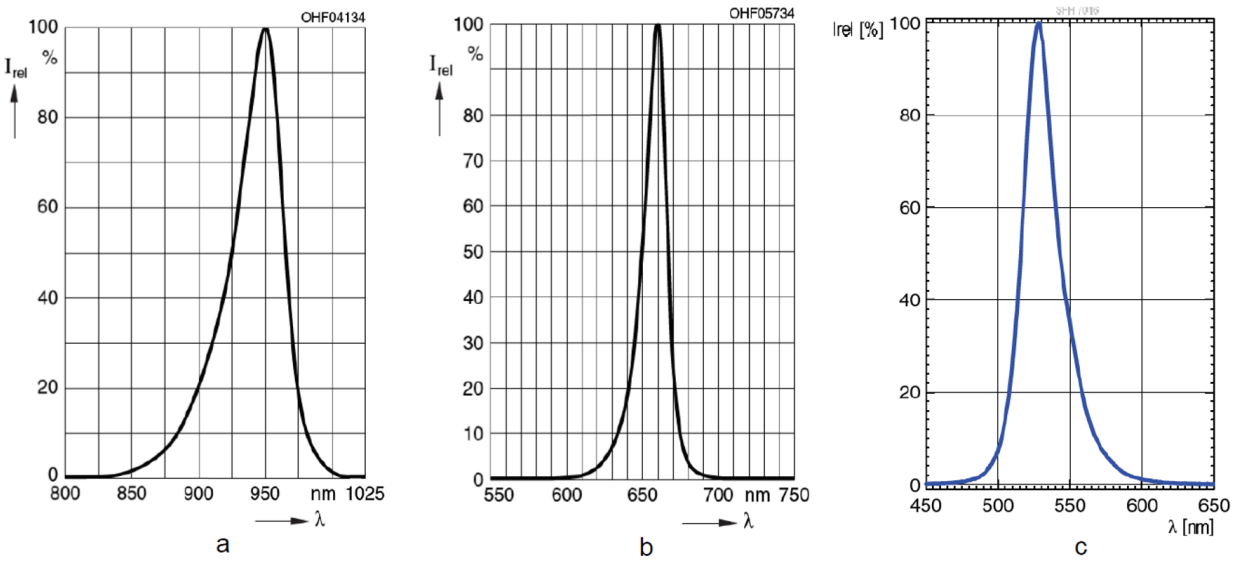

Figure 59: Spectral emission of LEDs. *a) Red, b) Infrared, c) Green*

Further in-vitro and in-vivo studies need to be performed to finalize the three target dyes for GFR, secretion and reabsorption and also to determine which infusion technique is feasible.

5.1 Design considerations

As we have analyzed and found that the frequency of the events, where the resultant signal is either saturated or too low in magnitude, is quite high, the new device was designed to solve this issue by design changes. The results from the analysis in section 4.1 shows that 29% of the experiments using FITC-S dye results in one of the two undesired signal magnitude ranges. In case of ABZWCY-HβCD, the event of high signal is not very frequent while the event of low signal reaches around 7%.

The close placement of LEDs around the sensor of the old devices resulted in many saturated signal events. Small distance between the source and detector causes the signal to saturate due to very high magnitude [3]. Consequently, we developed a design where the distance between the LED and photodiode is adjustable. We first considered a slider mechanism and later to rows of LEDs at increasing distances. This concept was further reinforced with our measurements with test strips where we analyzed the effect on the signal magnitude upon increasing distance of LED from the photodiode (results section 4.2.1). In addition to the distance, the significant increase of signal from the sensor upon adding an adjacent LED to the sensor was documented. The p-value of 1.44*10-15 gives an idea of the significant change on the incident light on the photodiode after passing through a skin imitation polymer.

In the process of the development of our new device, we were able to perform multiple oxygenation measurements with different distances between the LED and photodiode. In our experiments, the separation distances for such oxygenation estimations range from 0.5 cm to 4.5 cm. We found that after multiple trials, when the oxygen measurement was performed using the illumination from the LED which lies at 0.5 cm distance from the photodiode, the resultant signal saturates quickly, and the peaks are lost. This means that the current from the photodiode is too high. However, our device (first version) had the capability of manually tweaking the LED intensity and the gain implemented in the feedback loop of the transimpedance amplifier. Upon changing the driver current for the LED to lower settings and decreasing the resistance values, we could

derive an optimum signal strength, and using the ratio of red and infrared signals, we were able to estimate the oxygenation. Upon further choosing the LEDs placed at longer distances of up to 4.5 cm, the subsequent illumination intensity and gain mechanism were increased step-by-step, which gave us clear results with well-defined peaks and troughs depicting the oxygen changes in the forearm.

Our approach with having larger and importantly adjustable distances, may also reduce another source of variability often observed in transcutaneous sensor-based measurements which arises from the skin type (melanin content). The effect of melanin concentration on the signal has been shown to depend on the separation distance such that, up to a distance of 5mm, the effect on the signal increases, beyond which there is no effect [67]. This may also be due to the fact that longer separation results mainly in the deeper emissions from the marker to reach the sensor.

Further, the advantage of source-detector distance being larger is that it results in lesser light being incident on the photodiode from the direct source. In such cases, the primary light that reaches the detector is from the marker emission. Larger distance eases the necessity to perform complex filtering of source light from the overall light which reaches the photodiode [67].

5.2 Fixation and light shielding

The placement of the device and its proper fixation on the surface of the skin is imperative to obtain reliable measurements. During the course of our experiments, we found several reasons to find a mechanism to stably fix the device on the skin surface. We thus incorporated a patch for our device which fulfils at least dual function: a) the patch provides much stability during little movements of the body and muscles (even breathing), which are very prone to affect the signal shape and magnitude [68, 69], b) the fixation patch also provides ambient light shielding. The presence of bright light in the surroundings can highly influence the signal received from the photodiode. In oximeters the presence of strong light in the treatment rooms has shown to manipulate the signal and, in some cases, falsely diminished oxygenation levels [50, 70].

When a fixation patch is not used, the results are expected to have high variability in different trials and repetitions. In the results section 4.3.4, an experiment to show the difference in output when we use an adhesive tape in comparison to the fixation patch reveals the advantages of the latter. Only after the use of a stable fixation patch, we were able to reach a distance of 4.5 cm to get meaningful oxygenation measurements. In many oximeters which lack proper fixation, the medical personnel needs to use extra tapes and adhesives to fix the sensor on the skin which can cause unreliable measurements [71]. Thus, the use of a patch to fix the device on the skin plays a very crucial role in the entire measurement process, be it for oximetry or transcutaneous measurements of kidney functions.

The fixation patch must not be specific to a patient's body type or the place of application on the body. It should be flexible and be able to firmly stick to the entire surface of the skin in accordance with the size of the device. The fixation patch we decided to use has adhesive films on both sides which firmly stick on the device first and then on the skin surface. The adhesiveness of both the sides has been revised to avoid wear and tear to the device components as well as be comfortable to the user while removing the patch from the skin. Such a band-aid type adhesive approach for wearable health monitoring devices has proven to be a better solution to the fixation problems [72].

The comparison of the ratio of red and infrared signal of the device with other commercial devices has been described in section 4.3.3, where the changes in the signal due to pressure cuff were observed at the same time instance for all the devices. We further reiterated the functionality of the device when used on pigs. From the results of the animal experiments (Section 4.4, Figure 51a and Figure 51b), we can conclude that the device functionality could be validated on the body under the influence of active blood circulation. The signals at the LED positions from both devices follow the same trend as in the event of peaks and troughs against the time axis. The application of endotoxin is consistent with dips in the signal magnitudes while the application of ECMO device causes a temporary increase in the signal depicting the increase in oxygenation. This is expected to happen as the ECMO device is set to circulate 50% of the blood volume through it causing an overall increase in the oxygenated blood circulating in the body. All LED positions were successful in depicting appropriate changes over time.

5.3 Requirements for kidney function testing

Our aim of solving the overdosing and underdosing issue has led to the design with multiple rows of LEDs. This approach has been verified by oxygen measurements to the extent that biological process changes in the body are detectable up to a separation of 4.5 cm (source-detector). However, the reliability of having such distances for real-time kidney function measurements remains to be checked. Even though we have the flexibility of different source-detector distances to accommodate higher and lower tracer concentrations, the capability of accurately estimating tracer decay rate at such distances is to be established with further experiments. The former devices used in research for estimating GFR have rigid capabilities in terms of the source-detector distance. This has been limiting the functionality of the device due to the inability to adapt to the bodyweight variations and dosage errors. The new device, based on its design and testing, is expected to solve these drawbacks by giving flexibility of varied source-detector distances.

In the future, the device will have to be optimized for estimating kidney functions. For testing on rats or mice, the size of the device might also be a point of concern, especially in mice. It could also be that a distance of 4.5 cm may not be needed for estimating kidney function in small rodents. Testing the device with subsequent optimization in size is recommended in the future when the device will be used in combination with the developed tracers for the kidney functions. In addition to the size and the number of LEDs, the idea of simultaneous measurements of three kidney functions is also to be determined. This depends mainly on the degree of spectral overlap of the biomarkers. If such a combination is not possible based on the specific tracers, a sequential analysis would be the safe option.

Our device, as it stands now, has the potential to be used for these experiments with a possible need of optimizations for being used on rodents for kidney function measurements. To summarize, the current state of the device establishes the following capabilities:

1) **Assess the changes in biological processes inside the body:**

This was done by the measurement of oxygenation in human forearm upon application of pressure cuff induced flow changes. Animal experiments were also performed to study the change in oxygenation under a terminal surgery to support this.

2) **Use different source-detector:**

The incremental distance of LEDs from the photodiode and its effect on signal strength has been described. This setup aims to minimize the problems of signal overshoot and weak signals.

3) **Design capability to measure three fluorescent markers:**

The addition of multi-LED chip which has light sources of three different wavelengths provides the functionality of potentially measuring three spectrally distinct biomarkers.

The functional capabilities along with the possibility of tapping signals of higher and lower strengths along with the documented ability of the device to estimate changes in oxygenation in real-time also suggests that the device will be responsive to administration of different dyes (markers) used for detection of kidney functions.

6 SUMMARY

In this study, we analyzed the transcutaneous devices which were used previously for the measurement of GFR in laboratory rodents and identified the common limitations that were encountered by various users. We quantified the occurrences of these adverse events and found significant issues of high and low signals, which were taken into this thesis as the basis and motivation. The new transcutaneous device which has been described in this study aims to solve the described drawbacks. Biomarker dosage errors can make the output signal from the device unfavorable for calculation of half-life of the biomarkers used for function estimation. Thus, the new device has been developed with specific changes in the layout of the optical components along with the electronic capability to tweak the final output signal. This device also has the electronic capability to measure two additional kidney functions (secretion and reabsorption) as opposed to only GFR estimation. The incorporation of three wavelengths of LEDs establishes the functionality of detecting the clearance of three different biomarkers which are specific to the kidney function being measured. The placement of LEDs at different separation distances from the photodiode along with the dynamic signal amplification improves the quality of the signal. This was confirmed in this thesis with the measurement of oxygenation in the forearm. The measurements were taken with the signal being recorded after illuminating with different LED rows as described in the previous sections. We analyzed the oxygen measurements with LED-photodiode separation ranging from 0.5cm to 4.5cm and demonstrated the capability of the device to get meaningful signals.

In addition to the device layout and electronics, the use of a fixation patch was also examined in this study. The addition of fixation patch has a significant effect on the final signal which is highly dependent on the thickness of the patch used. We used patches of three different thicknesses and found that the increasing thickness causes the signal to reduce its magnitude exponentially. However, we also discussed the crucial benefits and need for the use of such a patch. In addition to providing an even and stable fixation of the device to the skin surface, the patch also facilitates insulation from various ambient lights. It also protects the skin surface from direct contact with electronics components.

Successful measurement of oxygenation documented in this study on human forearm and animal experiments establishes the completion of a working device with the possibility of taking into consideration the signal resulting from different depths into the skin based on the chosen LED-Photodiode distance. The three-color (wavelength) LEDs give the basis for the measurement of three kidney functions in the future. In combination with appropriate biomarkers, it should be possible for the device to sequentially (if not simultaneously) measure the secretion and reabsorption in addition to the GFR. The developed windows application can also be modified and used to calculate the half-lives of the biomarkers.

7 BIBLIOGRAPHY

1. Thompson, LE, Joy, MS: Endogenous markers of kidney function and renal drug clearance processes of filtration, secretion, and reabsorption. *Curr Opin Toxicol,* 31, 2022.
2. Stevens, LA, Levey, AS: Measured GFR as a confirmatory test for estimated GFR. *J Am Soc Nephrol,* 20**:** 2305-2313, 2009.
3. Hickey, M, Kyriacou, PA: Optimal spacing between transmitting and receiving optical fibres in reflectance pulse oximetry. *THIRD INTERNATIONAL CONFERENCE ON OPTICAL AND LASER DIAGNOSTICS.* City University, London, IOP Publishing Ltd, 2007.
4. Shimada, Y, Nakashima, K, Fujiwara, Y, Komatsu, T, Kawanishi, M, Takezawa, J, Takatani, S: Evaluation of a new reflectance pulse oximeter for clinical applications. *Med Biol Eng Comput,* 29**:** 557-561, 1991.
5. Soriano, RM, Penfold, D, Leslie, SW: Anatomy, Abdomen and Pelvis, Kidneys. In: *StatPearls.* Treasure Island (FL), 2022.
6. Brenner, BM, Rector, FC: *Brenner & Rector's the kidney,* Philadelphia, Saunders Elsevier, 2008.
7. Stein, JH, Fadem, SZ: The renal circulation. *JAMA,* 239**:** 1308-1312, 1978.
8. Rye, CW, R; Jurukovski, V; DeSaix, J: Choi, J: Avissar, Y;: The kidneys and osmoregulatory organs. In: *Biology.* Houston Texas, OpenStax, 2016.
9. Hoenig, MP, Zeidel, ML: Homeostasis, the milieu interieur, and the wisdom of the nephron. *Clin J Am Soc Nephrol,* 9**:** 1272-1281, 2014.
10. Bertram, JF: Counting in the kidney. *Kidney Int,* 59**:** 792-796, 2001.
11. Dressler, GR: The cellular basis of kidney development. *Annu Rev Cell Dev Biol,* 22**:** 509-529, 2006.
12. Short, KM, Combes, AN, Lefevre, J, Ju, AL, Georgas, KM, Lamberton, T, Cairncross, O, Rumballe, BA, McMahon, AP, Hamilton, NA, Smyth, IM, Little, MH: Global quantification of tissue dynamics in the developing mouse kidney. *Dev Cell,* 29**:** 188-202, 2014.
13. Work, GJSaDF: Measurement and Estimation of GFR in Children and Adolescents. *Clin J Am Soc Nephrol,* 4**:** 1832-1843, 2009.
14. Inker, LA, Titan, S: Measurement and Estimation of GFR for Use in Clinical Practice: Core Curriculum 2021. *Am J Kidney Dis,* 78**:** 736-749, 2021.
15. Ogobuiro, I, Tuma, F: Physiology, Renal. In: *StatPearls.* Treasure Island (FL), 2022.
16. Musso, CG, Alvarez-Gregori, J, Jauregui, J, Macias-Nunez, JF: Glomerular filtration rate equations: a comprehensive review. *Int Urol Nephrol,* 48**:** 1105-1110, 2016.
17. Levey, AS, Tighiouart, H, Titan, SM, Inker, LA: Estimation of Glomerular Filtration Rate With vs Without Including Patient Race. *JAMA Intern Med,* 180**:** 793-795, 2020.
18. Agnoli, GC, Garutti, C: [Renal water-electrolyte excretion and its control mechanisms. Current status of knowledge]. *Minerva Med,* 67**:** 3673-3702, 1976.
19. Chung, S, Kim, GH: Urate Transporters in the Kidney: What Clinicians Need to Know. *Electrolyte Blood Press,* 19**:** 1-9, 2021.
20. Bhatraju, PK, Chai, XY, Sathe, NA, Ruzinski, J, Siew, ED, Himmelfarb, J, Hoofnagle, AN, Wurfel, MM, Kestenbaum, BR: Assessment of kidney proximal tubular secretion in critical illness. *JCI Insight,* 6, 2021.

21. Wu, W, Bush, KT, Nigam, SK: Key Role for the Organic Anion Transporters, OAT1 and OAT3, in the in vivo Handling of Uremic Toxins and Solutes. *Sci Rep,* 7**:** 4939, 2017.
22. Moggio, A, Geraci, S, Boido, A, Sticht, C, Gretz, N, Bussolati, B: Assessment of acute kidney injury in rhabdomyolytic mice by transcutaneous measurement of sinistrin excretion. *Nephrol Dial Transplant,* 32**:** 1167-1175, 2017.
23. Ebert, N, Bevc, S, Bokenkamp, A, Gaillard, F, Hornum, M, Jager, KJ, Mariat, C, Eriksen, BO, Palsson, R, Rule, AD, van Londen, M, White, C, Schaeffner, E: Assessment of kidney function: clinical indications for measured GFR. *Clin Kidney J,* 14**:** 1861-1870, 2021.
24. Gaspari, F, Perico, N, Remuzzi, G: Measurement of glomerular filtration rate. *Kidney Int Suppl,* 63**:** S151-154, 1997.
25. Ellery, SJ, Cai, X, Walker, DD, Dickinson, H, Kett, MM: Transcutaneous measurement of glomerular filtration rate in small rodents: through the skin for the win? *Nephrology (Carlton),* 20**:** 117-123, 2015.
26. Forster, RP: Kidney, Water, and Electrolytes. *Annu Rev Physiol,* 27**:** 183-232, 1965.
27. Schock-Kusch, D, Geraci, S, Ermeling, E, Shulhevich, Y, Sticht, C, Hesser, J, Stsepankou, D, Neudecker, S, Pill, J, Schmitt, R, Melk, A: Reliability of transcutaneous measurement of renal function in various strains of conscious mice. *PLoS One,* 8**:** e71519, 2013.
28. Levey, AS, Stevens, LA, Schmid, CH, Zhang, YL, Castro, AF, 3rd, Feldman, HI, Kusek, JW, Eggers, P, Van Lente, F, Greene, T, Coresh, J, Ckd, EPI: A new equation to estimate glomerular filtration rate. *Ann Intern Med,* 150**:** 604-612, 2009.
29. Goiffon, RJ, Akers, WJ, Berezin, MY, Lee, H, Achilefu, S: Dynamic noninvasive monitoring of renal function in vivo by fluorescence lifetime imaging. *J Biomed Opt,* 14**:** 020501, 2009.
30. Grattan-Smith, JD, Chow, J, Kurugol, S, Jones, RA: Quantitative renal magnetic resonance imaging: magnetic resonance urography. *Pediatr Radiol,* 52**:** 228-248, 2022.
31. Sadick, M, Attenberger, U, Kraenzlin, B, Kayed, H, Schoenberg, SO, Gretz, N, Schock-Kusch, D: Two non-invasive GFR-estimation methods in rat models of polycystic kidney disease: 3.0 Tesla dynamic contrast-enhanced MRI and optical imaging. *Nephrol Dial Transplant,* 26**:** 3101-3108, 2011.
32. You, S, Ma, X, Zhang, C, Li, Q, Shi, W, Zhang, J, Yuan, X: Determination of single-kidney glomerular filtration rate (GFR) with CT urography versus renal dynamic imaging Gates method. *Eur Radiol,* 28**:** 1077-1084, 2018.
33. Alazraki, N, Verba, JW, Henry, JE, Becker, R, Taylor, A, Jr., Halpern, SE: Noninvasive determination of glomerular filtration rate using x-ray fluorescence. *Radiology,* 122**:** 183-186, 1977.
34. Bloch, PB, J.: An X-Ray-Fluorescence technique to determine glomerular filtration rate by clearance of iothalamate from plasma. *Medical Physics,* 12**:** 512-512, 1985.
35. Achilefu, S, Dorshow, RB: Dynamic and continuous monitoring of renal and hepatic functions with exogenous markers. *Top Curr Chem,* 222**:** 31-72, 2002.
36. Schwartz, GJ, Furth, SL: Glomerular filtration rate measurement and estimation in chronic kidney disease. *Pediatr Nephrol,* 22**:** 1839-1848, 2007.
37. Yusuf MM, VS, Picascia T, Perciaccante R, Gretz N: An overview of non-invasive methods for transcutaneous measurements of glomerular filtration. *J Exp Nephrol,* 2**:** 7-14, 2021.

38. Frennby, B, Sterner, G: Contrast media as markers of GFR. *Eur Radiol,* 12**:** 475-484, 2002.
39. Schock-Kusch, D, Shulhevich, Y, Xie, Q, Hesser, J, Stsepankou, D, Neudecker, S, Friedemann, J, Koenig, S, Heinrich, R, Hoecklin, F, Pill, J, Gretz, N: Online feedback-controlled renal constant infusion clearances in rats. *Kidney Int,* 82**:** 314-320, 2012.
40. Solomon, R, Goldstein, S: Real-time measurement of glomerular filtration rate. *Curr Opin Crit Care,* 23**:** 470-474, 2017.
41. Schreiber, A, Shulhevich, Y, Geraci, S, Hesser, J, Stsepankou, D, Neudecker, S, Koenig, S, Heinrich, R, Hoecklin, F, Pill, J, Friedemann, J, Schweda, F, Gretz, N, Schock-Kusch, D: Transcutaneous measurement of renal function in conscious mice. *Am J Physiol Renal Physiol,* 303**:** F783-788, 2012.
42. Shmarlouski, A, Schock-Kusch, D, Shulhevich, Y, Buschmann, V, Rohlicke, T, Herdt, D, Radle, M, Hesser, J, Stsepankou, D: A Novel Analysis Technique for Transcutaneous Measurement of Glomerular Filtration Rate With Ultralow Dose Marker Concentrations. *IEEE Trans Biomed Eng,* 63**:** 1742-1750, 2016.
43. Debreczeny, MP, Dorshow, RB: Transdermal optical renal function monitoring in humans: development, verification, and validation of a prototype device. *J Biomed Opt,* 23**:** 1-9, 2018.
44. Hauser-Kawaguchi, A, Milne, M, Li, F, Lee, TY, Luyt, LG: The development of a near infrared inulin optical probe for measuring glomerular filtration rate. *Int J Biol Macromol,* 123**:** 255-260, 2019.
45. Daniele, C, Nardozi, D, Torelli, A, Khan, AUM, Gretz, N: Transcutaneous Measurement of Glomerular Filtration Rate in Rodents. *Methods Mol Biol,* 2067**:** 129-137, 2020.
46. Huang, J, Weinfurter, S, Daniele, C, Perciaccante, R, Federica, R, Della Ciana, L, Pill, J, Gretz, N: Zwitterionic near infrared fluorescent agents for noninvasive real-time transcutaneous assessment of kidney function. *Chem Sci,* 8**:** 2652-2660, 2017.
47. Brigadoi, S, Cooper, RJ: How short is short? Optimum source-detector distance for short-separation channels in functional near-infrared spectroscopy. *Neurophotonics,* 2**:** 025005, 2015.
48. Patil, AV, Safaie, J, Moghaddam, HA, Wallois, F, Grebe, R: Experimental investigation of NIRS spatial sensitivity. *Biomed Opt Express,* 2**:** 1478-1493, 2011.
49. Sood, BG, McLaughlin, K, Cortez, J: Near-infrared spectroscopy: Applications in neonates. *Semin Fetal Neonat M,* 20**:** 164-172, 2015.
50. Hanowell, L, Eisele, JH, Jr., Downs, D: Ambient light affects pulse oximeters. *Anesthesiology,* 67**:** 864-865, 1987.
51. Bauman, LA, Watson, NE, Jr., Scuderi, PE, Peters, MA: Transcutaneous renal function monitor: precision during unsteady hemodynamics. *J Clin Monit Comput,* 14**:** 275-282, 1998.
52. Schock-Kusch, D, Sadick, M, Henninger, N, Kraenzlin, B, Claus, G, Kloetzer, HM, Weiss, C, Pill, J, Gretz, N: Transcutaneous measurement of glomerular filtration rate using FITC-sinistrin in rats. *Nephrol Dial Transplant,* 24**:** 2997-3001, 2009.
53. Wang, K, Kestenbaum, B: Proximal Tubular Secretory Clearance: A Neglected Partner of Kidney Function. *Clin J Am Soc Nephrol,* 13**:** 1291-1296, 2018.
54. Jubran, A: Pulse oximetry. *Crit Care,* 3**:** R11-R17, 1999.
55. Wukitsch, MW, Petterson, MT, Tobler, DR, Pologe, JA: Pulse oximetry: analysis of theory, technology, and practice. *J Clin Monit,* 4**:** 290-301, 1988.

56. Chan, ED, Chan, MM, Chan, MM: Pulse oximetry: understanding its basic principles facilitates appreciation of its limitations. *Respir Med,* 107**:** 789-799, 2013.
57. Schock-Kusch, D, Xie, Q, Shulhevich, Y, Hesser, J, Stsepankou, D, Sadick, M, Koenig, S, Hoecklin, F, Pill, J, Gretz, N: Transcutaneous assessment of renal function in conscious rats with a device for measuring FITC-sinistrin disappearance curves. *Kidney Int,* 79**:** 1254-1258, 2011.
58. IEC: Particular requirements for the safety of ultrasonic medical diagnostic and monitoring equipment. In: IEC (Ed.) *IEC 60601-2-37.* 2004.
59. Meredith, SA, Kusunoki, Y, Connell, SD, Morigaki, K, Evans, SD, Adams, PG: Self-Quenching Behavior of a Fluorescent Probe Incorporated within Lipid Membranes Explored Using Electrophoresis and Fluorescence Lifetime Imaging Microscopy. *J Phys Chem B,* 127**:** 1715-1727, 2023.
60. Trettnak, W: Optical Sensors Based on Fluorescence Quenching. In: *Fluorescence Spectroscopy: New Methods and Applications.* edited by WOLFBEIS, O. S., Berlin, Heidelberg, Springer Berlin Heidelberg, 1993, pp 79-89.
61. Kainan, P, Sinchai, A, Tuwanut, P, Wardkein, P: New pulse oximetry detection based on the light absorbance ratio as determined from amplitude modulation indexes in the time and frequency domains. *Biomed Signal Process Control,* 75**:** 103627, 2022.
62. Friedemann, J, Heinrich, R, Shulhevich, Y, Raedle, M, William-Olsson, L, Pill, J, Schock-Kusch, D: Improved kinetic model for the transcutaneous measurement of glomerular filtration rate in experimental animals. *Kidney Int,* 90**:** 1377-1385, 2016.
63. Scarfe, L, Schock-Kusch, D, Ressel, L, Friedemann, J, Shulhevich, Y, Murray, P, Wilm, B, de Caestecker, M: Transdermal Measurement of Glomerular Filtration Rate in Mice. *J Vis Exp*, 2018.
64. Vajpayee, S: *Development of dyes/tracers for analysis of renal functions.* Med. Dissertation. Medizinische Fakultät Mannheim, Universität Heidelberg, 2024. 10.11588/heidok.000342724
65. Wu, F, Zhang, X, Cheung, JY, Shi, K, Liu, Z, Luo, C, Yin, S, Ruffin, P: Frequency division multiplexed multichannel high-speed fluorescence confocal microscope. *Biophys J,* 91**:** 2290-2296, 2006.
66. Jangampet, VD, Dixit, R, Klotzkin, D, Papautsky, I: Simultaneous, single-detector fluorescence detection of multiple fluorescent dyes. *SENSORS, 2010 IEEE.* 2010 pp 2057-2060.
67. Shultz, K, Debreczeny, M, Dorshow, R, Keating, J, Bechtel, K: *Modeling of transdermal fluorescence measurements from first-in-human clinical trials for renal function determination using fluorescent tracer agent MB-102*, SPIE, 2017.
68. Roudjane, M, Bellemare-Rousseau, S, Khalil, M, Gorgutsa, S, Miled, A, Messaddeq, Y: A Portable Wireless Communication Platform Based on a Multi-Material Fiber Sensor for Real-Time Breath Detection. *Sensors (Basel),* 18, 2018.
69. Yamada, T, Hayamizu, Y, Yamamoto, Y, Yomogida, Y, Izadi-Najafabadi, A, Futaba, DN, Hata, K: A stretchable carbon nanotube strain sensor for human-motion detection. *Nat Nanotechnol,* 6**:** 296-301, 2011.
70. Brooks, TD, Paulus, DA, Winkle, WE: Infrared heat lamps interfere with pulse oximeters. *Anesthesiology,* 61**:** 630, 1984.
71. Alpert, CC, Cooke, JE: Extending the life of oximetry monitoring probes. *Anesth Analg,* 65**:** 826-827, 1986.

72. Lim, CP, J: Wearable transcutaneous oxygen sensor for health monitoring. *Sensors and Actuators A: Physical,* 298**:** 111607, 2019.

8 APPENDIX

LIST OF FIGURES

LIST OF TABLES

9 CURRICULUM VITAE

Name:	Mohammed Mohiuddin Yusuf
Date of birth:	20 December 1990
Place of birth:	Gulbarga, India
Nationality:	Indian
Mobile:	+49 152 1946520
Email:	MohammedMohiuddin.Yusuf@medma.uni-heidelberg.de
	mmyusuf90@gmail.com
Address:	U4 1, 68161 Mannheim
LinkedIn:	https://www.linkedin.com/in/mohammed-yusuf-aa8b8065

ACADEMIC CREDENTIALS

2019-2024	Doctoral Candidate (Marie Curie Fellow- H2020 ETN RenalToolBox) Medical Faculty Mannheim University of Heidelberg
2015-2017	Master of Science in Electrical and Computer Engineering Rochester Institute of Technology, NY
2009-2013	Bachelor of Engineering in Electronics and Communication Ramaiah Institute of Technology, Bangalore, India

WORK EXPERIENCE

2024-Present	Risk Manager (Medical devices) CENTOGENE GmbH
2022- 2024	Scientific Employee Surgical Research Lab, Medical Faculty Mannheim
2019-2022	EU Researcher Center for Medical Research, Medical Faculty Mannheim University of Heidelberg

PUBLICATIONS

Yusuf MM, Vajpayee S, Picascia T, Perciaccante R, Gretz N: *An overview of non-invasive methods for transcutaneous measurements of glomerular filtration.* J Exp Nephrol, 2: 7-14, 2021

10 ACKNOWLEDGEMENTS

I would like to take the opportunity to convey my profound thanks and appreciation to everyone who has supported me towards achieving the completion of this thesis.

Primarily, I am immensely grateful to my supervisor, late Prof. Dr. med. Norbert Gretz for accepting me as a candidate in this prestigious doctoral pathway under Marie Sklodowska-Curie grant offered by the EU's Horizon 2020 research and Innovation program. His invaluable guidance and expertise have been my constant support throughout. His constructive criticism and feedback have been instrumental in shaping this research. The recent loss of my supervisor is deeply felt, and I am profoundly thankful for his indelible impact on this research, leaving an enduring legacy that will be carried forward with the utmost reverence.

I would like to express my heartfelt gratitude to my current supervisor, Prof. Dr. Karen Bieback, who stepped into the role with compassion and dedication following the untimely passing of Prof. Gretz. Prof. Bieback's guidance and support have been invaluable since the start of the project and especially during this transition, and her expertise has contributed significantly to the progression of my doctoral journey. I am truly fortunate to have her as a mentor, and I appreciate her commitment to fostering my academic growth and success.

I am also indebted to the faculty members Prof. Mathias Raedle for his guidance in the initial stages of my research and Prof. Michael Keese for his support and collaboration. I wish to also thank our post-doc, Dr. ing. Arif Khan for providing his expertise and guidance over the years, not to forget our discussions over 'tea breaks' which continue till date.

I am grateful to all the partners of the project RenalToolBox, especially Dr. Arthur Taylor and Dr. Patricia Murray for their overall guidance and efforts in organizing various workshops held in the past few years. I also wish to express my warm regards to all my fellow researchers: Tiziana Picascia, Srishti Vajpayee, and Yinuo Xie for all the productive collaborations we shared.

Special appreciation goes to my dear family members, starting from my parents and my sisters who have supported me and led me through by setting the right examples. My mother has been a constant stone of support and encouragement during this journey. My father has always been the pillar of strength, with his steadfast belief in the power of knowledge, he has been the ultimate source of inspiration to me and my siblings. Last but not least, I express my heartfelt gratitude to my dear wife for her unwavering support and rock-solid patience. Your strength and kindness inspire me daily, and I am truly blessed to have you by my side.

In conclusion, this journey wouldn’t have been possible without the support and encouragement of so many individuals, to you all, I offer my deepest gratitude!